JOURNAL OF PETROLOGY | VOLUME 48 | NUMBER 8 | PAGES 1569–1604 | 2007 | doi:10.1093/petrology/egm030

# Platinum-Group Elements in Sulphide Minerals, Platinum-Group Minerals, and Whole-Rocks of the Merensky Reef (Bushveld Complex, South Africa): Implications for the Formation of the Reef

**BELINDA GODEL[1]*, SARAH-JANE BARNES[1] AND WOLFGANG D. MAIER[2]**

[1]UNIVERSITE DU QUEBEC A CHICOUTIMI, SCIENCES DE LA TERRE, CHICOUTIMI, QC, CANADA, G7H 2B1

[2]CENTRE FOR EXPLORATION TARGETING, UNIVERSITY OF WESTERN AUSTRALIA, CRAWLEY, WA 6009, AUSTRALIA

**RECEIVED NOVEMBER 28, 2006; ACCEPTED MAY 23, 2007**
**ADVANCE ACCESS PUBLICATION JULY 1, 2007**

*The concentrations of platinum-group elements (PGE), Co, Re, Au and Ag have been determined in the base-metal sulphide (BMS) of a section of the Merensky Reef. In addition we performed detailed image analysis of the platinum-group minerals (PGM). The aims of the study were to establish: (1) whether the BMS are the principal host of these elements; (2) whether individual elements preferentially partition into a specific BMS; (3) whether the concentration of the elements varies with stratigraphy or lithology; (4) what is the proportion of PGE hosted by PGM; (5) whether the PGM and the PGE found in BMS could account for the complete PGE budget of the whole-rocks. In all lithologies, most of the PGE (~65 up to ~85%) are hosted by PGM (essentially Pt–Fe alloy, Pt–Pd sulphide, Pt–Pd bismuthotelluride). Lesser amounts of PGE occur in solid solution within the BMS. In most cases, the PGM occur at the contact between the BMS and silicates or oxides, or are included within the BMS. Pentlandite is the principal BMS host of all of the PGE, except Pt, and contains up to 600 ppm combined PGE. It is preferentially enriched in Pd, Rh and Co. Pyrrhotite contains, Rh, Os, Ir and Ru, but excludes both Pt and Pd. Chalcopyrite contains very little of the PGE, but does concentrate Ag and Cd. Platinum and Au do not partition into any of the BMS. Instead, they occur in the form of PGM and electrum. In the chromitite layers the whole-rock concentrations of all the PGE except Pd are enriched by a factor of five relative to S, Ni, Cu and Au. This enrichment could be attributed to BMS in these layers being richer in PGE than the BMS in the silicate layers. However, the PGE content in the BMS varies only slightly as a function of the stratigraphy. The BMS in the chromitites contain twice as much PGE as the BMS in the silicate rocks, but this is not sufficient to explain the strong enrichment of PGE in the chromitites. In the light of our results, we propose that the collection of the PGE occurred in two steps in the chromitites: some PGM formed before sulphide saturation during chromitite layer formation. The remaining PGE were collected by an immiscible sulphide liquid that percolated downward until it encountered the chromitite layers. In the silicate rocks, PGE were collected by only the sulphide liquid.*

KEY WORDS: *Merensky Reef; Rustenburg Platinum Mine; sulphide; platinum-group elements; image analysis; laser ablation ICP-MS*

## INTRODUCTION

Many large mafic and ultramafic layered intrusions, such as the Bushveld Complex (South Africa), contain thin layers enriched in platinum-group elements (PGE) and Au. These are commonly referred to as reefs. The Merensky Reef is one of the PGE-rich layers of the Bushveld Complex and, after the UG2 chromitite, the second largest PGE resource in the world (Cawthorn, 1999). Several processes have been proposed to explain the enrichment of the PGE and the other noble metals in

*Corresponding author. Telephone: +1 418 545-5011 2502. Fax: +1 418 545-5012. E-mail: bgodel@uqac.ca; godelbelinda@yahoo.fr

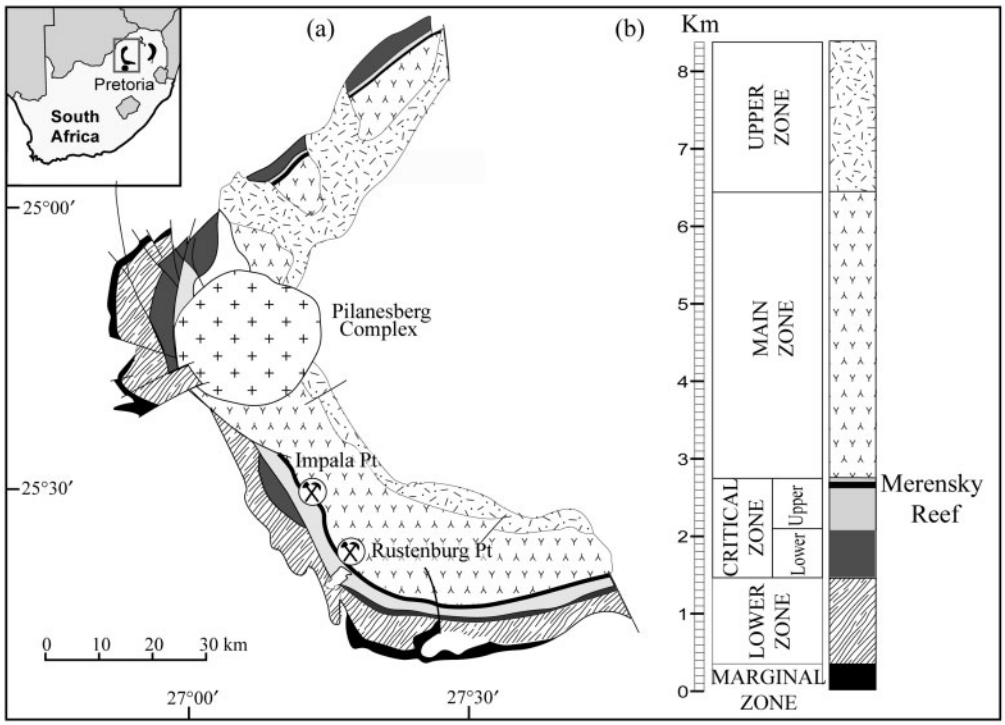


**Fig. 1.** Details of the geology of the western lobe of the Bushveld Complex, South Africa. (a) Simplified geological map, modified after Von Gruenewaldt (1986, 1989). (b) Generalized stratigraphy of the Bushveld Complex, modified after Eales & Cawthorn (1996). The study locality is Rustenburg Platinum Mines, Frank Shaft.

cumulates of layered intrusions. Some workers suggested that the PGE could crystallize from the magma as platinum-group minerals (PGM) that accumulate on the top of the crystal pile (e.g. Hiemstra, 1979). Others have suggested that PGE are collected by a sulphide liquid that segregated from the magma and this sulphide liquid accumulated on the crystal pile (e.g. Campbell *et al.*, 1983; Naldrett *et al.*, 1986). Another process proposed is the collection of PGE by magmatic fluids enriched in Cl (Boudreau & McCallum, 1992; Willmore *et al.*, 2000), which percolated upwards through the cumulate pile and precipitated sulphides and PGE. The cumulate could also have undergone a low-temperature alteration that modified the PGE distribution (Li *et al.*, 2004; Polovina *et al.*, 2004). Although the processes by which PGE collection occurs remain unclear, it is clear that the PGE in the reefs are in many cases found associated with base-metal sulphides (BMS) and/or occur in PGM that are associated with these BMS (Kinloch, 1982; Ballhaus & Sylvester, 2000; Zientek *et al.*, 2002; Prichard *et al.*, 2004). The reef associated with chromitites and magnetites usually contains few visible BMS. However, this is interpreted to be the result of magmatic or post-magmatic BMS resorption (Naldrett & Lehmann, 1988; Maier *et al.*, 2003).

Ballhaus & Sylvester (2000) reported the PGE concentrations in pyrrhotite and pentlandite and the presence of PGM inclusions in olivine, chromite and BMS from four samples of the Merensky Reef at Rustenburg Platinum Mine. They concluded that, apart from Pt, the PGE are largely present in pyrrhotite and pentlandite. However, the presence of PGE-rich inclusions in olivine and chromite, and the presence of PGE-rich zones in the BMS suggested to Ballhaus & Sylvester (2000) that the magma was initially saturated in PGM as minute grains and that these grains were incorporated by the sulphide liquid and other minerals at the stratigraphic layer that is now the Merensky Reef.

Barnes & Maier (2002*a*) examined the PGE, S, Ni and Cu concentrations of each rock type in the reef at Impala Platinum Mines (Fig. 1). They concluded that the PGE concentrations in the silicate rocks could be modelled by collection of the PGE by a base-metal sulphide liquid from the magma followed by percolation of the dense sulphide liquid down through the compacting cumulate pile. They also concluded that this model would not suffice to explain PGE distribution in the chromitite layers and suggested that in addition to the collection of the PGE by sulphide liquid either: (1) some PGM crystallized and settled onto the chromitite layer before the base-metal sulphide liquid percolated down through the cumulate pile; or (2) the BMS that were originally in the chromitite layer had interacted with the chromite (Naldrett & Lehmann, 1988) resulting in loss of S, Cu and Pd from the chromitite layer. Prichard *et al.* (2004) investigated the

PGM present in the Impala Platinum Mines samples to test whether any primary PGM are present in the chromitite layers, which would support the model requiring crystallization of PGM directly from the magma. They found that both in the chromitite layers and the silicate rocks most (~84%) PGM are within the BMS or at the contact between BMS and silicates and appear to have formed by exsolution from the BMS. Thus, the PGM mineralogy does not provide any evidence that primary PGM have crystallized directly from the magma. The close association of the PGE with BMS suggests that they were initially collected by a base-metal sulphide liquid. However, the BMS in the chromitite layers has been depleted in S, Fe and Pd either by dissolution of the original BMS by rising hydrous fluids, or by re-equilibration of the BMS with chromite.

Godel *et al.* (2006), in a 3D textural study on samples from Rustenburg Mine (Fig. 1), showed that the BMS form networks following vertical dilatancies interpreted to be formed during compaction, and that dihedral angles between silicates and BMS are much lower than those between BMS and chromite. These observations suggest that the sulphide liquid wets the silicate minerals more efficiently than chromite. Thus the sulphide liquid could have percolated downwards through the cumulate pile until it encountered the chromitite layer. Because the sulphide liquid could not easily wet the chromite surface it would tend to accumulate at the top of the chromitite layer (Godel *et al.*, 2006).

In the current study we have attempted to establish which minerals host the PGE in order to better constrain these models. The first aim of this study is to determine the concentration of PGE, Re, Ag, Au, Cd and Co in the BMS (pentlandite, pyrrhotite and chalcopyrite) and the whole-rocks, within different lithologies (anorthosite, chromitites, melanorites) of the Merensky Reef at Rustenburg Platinum Mine. This was done to establish: (1) whether the BMS are the principal hosts of these elements; (2) whether these elements preferentially partition into specific BMS; (3) whether PGE and other metal contents of the BMS vary with stratigraphic position and/or lithologies. In addition, detailed image analysis of the PGM distribution has been conducted. Together with the BMS compositional data, this allowed the calculation of a PGE mass balance.

## GEOLOGY AND PETROGRAPHY

The Merensky Reef is one of several layers enriched in PGE in the Upper Critical Zone of the Bushveld Complex, South Africa (Fig. 1). It contains 5–10 ppm PGE (Barnes & Maier, 2002*a*; Cawthorn, 2002). In most cases, the PGE are associated with disseminated BMS (Viljoen & Hieber, 1986). The sample studied in detail in this work is a slab of normal 'narrow' Merensky Reef from Frank Shaft, Rustenburg Platinum Mine (Fig. 1). The sample was previously used for microtomographical and microstructural analyses (Godel *et al.*, 2006). More details on the reef type and its extension have been given by Viljoen & Hieber (1986), Viljoen *et al.* (1986) and Loeb-du Toit (1986).

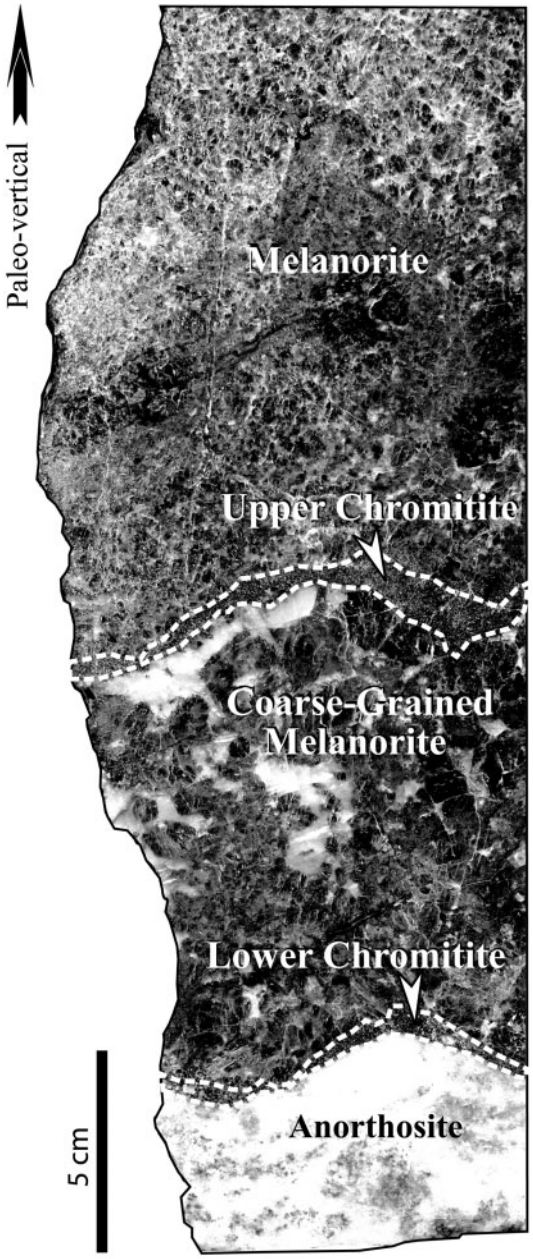


**Fig. 2.** Photograph of the sample of Merensky Reef used in this study.

The petrography of the sample has been described in detail in a previous paper (Godel *et al.*, 2006), and only a summary is presented here. The Merensky Reef sample is composed, from bottom to top, of five layers (Fig. 2): a basal anorthosite overlain by a 0·7–1 cm chromitite, which undulates on a centimetre scale; a coarse-grained

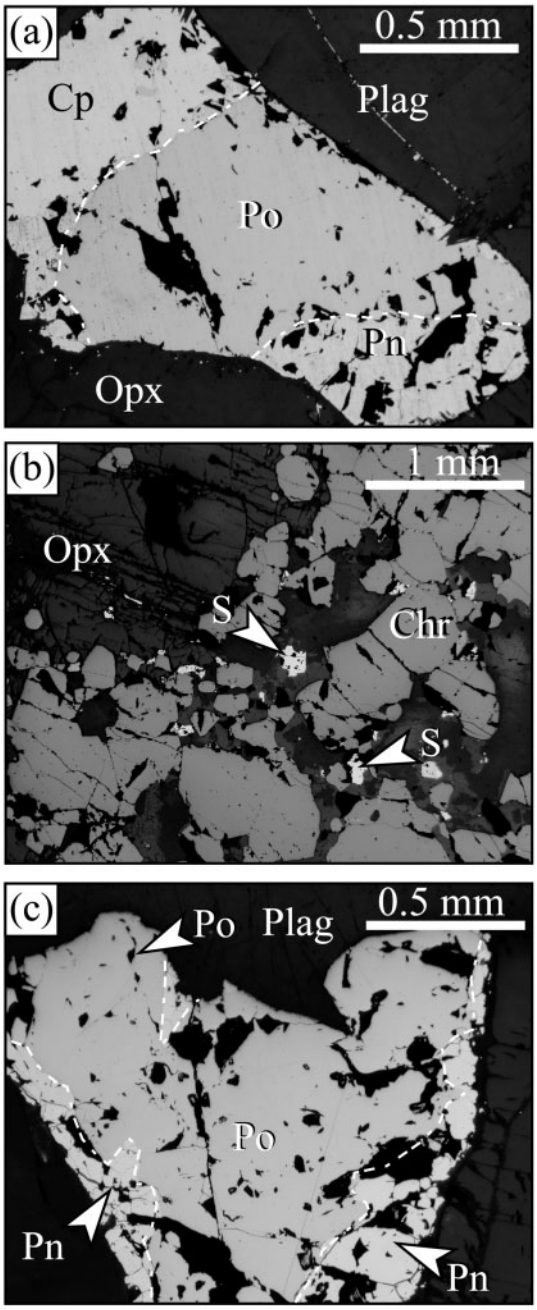


**Fig. 3.** Examples of base-metal sulphides observed in samples of Merensky Reef. (a) Intergrowth of pyrrhotite (Po), pentlandite (Pn) and chalcopyrite (Cp) in coarse-grained melanorite (Opx, orthopyroxene; Plag, plagioclase) (b) Disseminated base-metal sulphides (S) in the chromitite layers (Chr, chromite; Opx, orthopyroxene) (c) Pyrrhotite (Po) surrounded by pentlandite (Pn) in the melanorite.

melanorite of ~10 cm thickness; a second layer of chromitite of ~1 cm thickness; finally, a melanorite. All lithologies contain disseminated BMS (Fig. 3). The BMS content varies (from 0·5 to 8 vol.%) as a function of the stratigraphy of the Merensky Reef (Godel *et al.*, 2006). The BMS are composed of intergrowths of pyrrhotite, pentlandite and chalcopyrite, and in the silicate rocks are located in 3D vertical networks interpreted to have formed during the compaction of the cumulate pile (Godel *et al.*, 2006). In contrast, in the chromitite layers the BMS occur as small droplets.

## ANALYTICAL METHODS

Oriented polished thin sections with a thickness of 100 μm were cut along a vertical section across the slab (Fig. 2). Base-metal sulphides (pyrrhotite, pentlandite and chalcopyrite, Fig. 3) in the thin sections were examined with an optical microscope and sites were then selected for further analysis. To assess the exact position of the analysed BMS in the Reef, thin sections and selected BMS were referenced to the paleovertical. Major elements (S, Ni, Fe and Cu) were determined by electron microprobe analysis at Laval University (Quebec City) using a CAMECA SX100 electron microprobe. The microprobe was operated at 15 kV and 20 nA and a beam diameter of 2–5 μm, with a counting time of 20 s and 10 s on peak and backgrounds. The standards used were from Astimex Microanalysis Standard: hematite for Fe; pentlandite for Ni; skutterudite for Co; marcasite for S. The standard for Cu is the chalcopyrite from P and H Developments Ltd. The results of the microprobe analyses are summarized in Table 1.

The concentration of the PGE, Re, Cd, Co, Au and Ag in BMS was determined at the University of Quebec, Chicoutimi (UQAC) using a laser ablation-inductively coupled plasma-quadrupole mass spectrometer along with an hexapol collision cell (LA-HEX-ICP-MS). The UQAC laser-ablation ICP-MS consists of a Thermo X7 ICP-MS with high-performance interface coupled with a New Wave Research 213 nm Nd:YAG UV laser ablation microprobe. The analyses were conducted using an 80 μm diameter spot, a laser frequency of 20 Hz and a power of 0·8 mJ/pulse. An analysis took 90 s (30 s of analysis of the gas background followed by 60 s of analysis of the minerals). A helium carrier gas mixed with argon was used. The ablated material was then analysed using the Thermo X7 ICP-MS operating in time-resolved mode using peak jumping. $^{34}S$ was used as internal standard to determine concentrations of PGE and other metals. The calibration was carried out using a synthetic FeS standard (Po-52), which had been doped with ~10 ppm of each of the PGE and Au. The exact concentrations of the PGE and Au in Po-52 have been determined by standard solution analysis (Table 2). To verify the accuracy of the calibration the FeS standard LaFlamme-Po727 provided by CANMET has been analysed and the results are within the accepted values (Table 2). The use of the collision cell reduces much of the Ni and Cu argide interferences on PGEs (Mason & Kraan, 2002). Nonetheless there is still some Ni interference on Ru, and some Cu

*Table 1: Average composition of major elements of the sulphide minerals as a function of the stratigraphy*

| Rock type | Sulphide | *n* | | S (wt %) | Fe (wt %) | Cu (wt %) | Ni (wt %) | Co (wt %) | Total |
|---|---|---|---|---|---|---|---|---|---|
| AN | Pyrrhotite | 3 | Average | 38·99 | 59·97 | <0·01 | 0·42 | <0·01 | 99·39 |
| | | | SD | 0·19 | 0·60 | – | 0·19 | – | |
| | Pentlandite | 3 | Average | 32·58 | 31·18 | <0·01 | 34·87 | 0·36 | 98·98 |
| | | | SD | 0·33 | 0·71 | – | 0·36 | 0·14 | |
| | Chalcopyrite | 3 | Average | 34·20 | 30·43 | 33·98 | <0·01 | <0·01 | 98·61 |
| | | | SD | 0·11 | 0·07 | 0·06 | – | – | |
| LC & CGM | Pyrrhotite | 2 | Average | 37·99 | 61·31 | <0·01 | 0·30 | <0·01 | 99·60 |
| | | | SD | 0·28 | 0·01 | – | 0·13 | – | |
| | Pentlandite | 3 | Average | 32·62 | 32·59 | <0·01 | 32·98 | 0·57 | 98·76 |
| | | | SD | 0·06 | 1·58 | – | 1·03 | 0·06 | |
| | Chalcopyrite | 3 | Average | 34·29 | 30·54 | 34·15 | <0·01 | <0·01 | 98·97 |
| | | | SD | 0·07 | 0·10 | 0·21 | – | – | |
| CGM | Pyrrhotite | 4 | Average | 37·26 | 61·45 | <0·01 | 0·12 | <0·01 | 98·83 |
| | | | SD | 0·54 | 0·29 | – | 0·06 | – | |
| | Pentlandite | 2 | Average | 32·39 | 34·81 | <0·01 | 30·53 | 0·66 | 98·40 |
| | | | SD | 0·11 | 0·53 | – | 1·04 | 0·19 | |
| | Chalcopyrite | 4 | Average | 34·10 | 30·59 | 33·84 | <0·01 | <0·01 | 98·52 |
| | | | SD | 0·18 | 0·39 | 0·15 | – | – | |
| UC | Pyrrhotite | 3 | Average | 38·03 | 61·27 | <0·01 | 0·16 | <0·01 | 99·45 |
| | | | SD | 0·16 | 0·56 | – | 0·04 | – | |
| | Pentlandite | 3 | Average | 32·54 | 34·41 | <0·01 | 31·52 | 0·67 | 99·14 |
| | | | SD | 0·02 | 0·44 | – | 0·43 | 0·16 | |
| | Chalcopyrite | 2 | Average | 34·13 | 30·46 | 33·65 | <0·01 | <0·01 | 98·25 |
| | | | SD | 0·00 | 0·03 | 0·13 | – | – | |
| M | Pyrrhotite | 4 | Average | 37·73 | 61·15 | <0·01 | 0·17 | <0·01 | 99·05 |
| | | | SD | 0·13 | 0·52 | – | 0·07 | – | |
| | Pentlandite | 2 | Average | 32·42 | 33·88 | <0·01 | 31·23 | 0·54 | 98·07 |
| | | | SD | 0·13 | 0·69 | – | 0·39 | 0·12 | |
| | Chalcopyrite | 2 | Average | 33·99 | 30·21 | 33·70 | <0·01 | <0·01 | 97·90 |
| | | | SD | 0·05 | 0·17 | 0·20 | – | – | |
| M | Pyrrhotite | 5 | Average | 37·33 | 61·01 | <0·01 | <0·01 | <0·01 | 98·34 |
| | | | SD | 0·88 | 0·75 | – | – | – | |
| | Pentlandite | 6 | Average | 32·12 | 32·69 | <0·01 | 32·36 | 0·53 | 97·70 |
| | | | SD | 0·01 | 1·36 | – | 1·39 | 0·14 | |
| | Chalcopyrite | 4 | Average | 34·03 | 30·26 | 33·69 | <0·01 | <0·01 | 97·98 |
| | | | SD | 0·13 | 0·40 | 0·25 | – | – | |
| M | Pyrrhotite | 4 | Average | 37·95 | 60·58 | <0·01 | 0·51 | <0·01 | 99·04 |
| | | | SD | 0·16 | 0·16 | – | 0·12 | – | |
| | Chalcopyrite | 2 | Average | 34·01 | 30·56 | 33·94 | <0·01 | <0·01 | 98·50 |
| | | | SD | 0·11 | 0·15 | 0·09 | – | – | |
| M | Pyrrhotite | 4 | Average | 38·02 | 60·48 | <0·01 | 0·44 | <0·01 | 98·94 |
| | | | SD | 0·16 | 0·28 | – | 0·14 | – | |
| | Pentlandite | 3 | Average | 32·08 | 31·23 | <0·01 | 33·65 | 0·33 | 97·29 |
| | | | SD | 0·11 | 0·37 | – | 0·20 | 0·12 | |
| | Chalcopyrite | 5 | Average | 33·92 | 30·51 | 33·81 | <0·01 | <0·01 | 98·23 |
| | | | SD | 0·18 | 0·28 | 0·05 | – | – | |

SD, standard deviation for *n* different analyses; AN: anorthosite; LC: lower chromitite; CGM: coarse-grained melanorite; UC: upper chromitite; M: melanorite.

interference on Rh and Pd. These were monitored by using a synthetic $NiFeS_2$ and $CuFeS_2$ blank. On the basis of the blank results 5 ppm Ru, 2 ppm Rh and 2 ppm Pd were subtracted from all chalcopyrite results and 3 ppm Ru was subtracted from all pentlandite results. The Ni and Cu concentrations were calibrated using the synthetic blanks, the concentrations of these elements having been determined by microprobe. Results for Co, Ag, Cd and Re were calculated using semi-quantitative calibration. Details of how the sulphide standards were synthesized have been given by Barnes *et al*. (2006) and Peregoedova *et al*. (2006). Each standard was placed with unknowns (BMS in thin sections) in the ablation chamber and was analysed at the beginning, after each 10 analyses of unknowns and at the end of each analytical session. The reduction of the data was carried out using PlasmaLab software (ThermoElemental) by subtracting gas background from each of the analysed isotopes. The results of calibrations during all analytical sessions are summarized in Table 2. As the analysed BMS are intergrowths of pyrrhotite, pentlandite and chalcopyrite, the concentrations of Ni and Cu were monitored to verify that the signal was generated by only one mineral. The analyses with Ni and/or Cu signals higher than the microprobe concentration (depending on BMS) were not used in further calculations. The detection limits for each BMS are summarized in Table 3.

To compare the PGE content in the BMS with the PGE content in the whole-rocks, the samples (corresponding to the thin sections) were crushed in an Al-ceramic mill at UQAC. Copper and Ni associated with BMS were determined by atomic absorption spectrometry (AAS) at UQAC. Sulphur was also determined at UQAC using an HORIBA EMIA-220V series analyser. The precision of the S analyses based on the relative standard deviation (RDS) is <2·5%. The PGE and Au in the silicate rocks were determined by Ni-sulphide fire assay followed by instrumental neutron activation analysis (INAA) on 10 g of sample using a slightly modified version of the Steele *et al*. (1975) formulae. Because of the difficulty of dissolving chromitites in the standard flux mixtures, the flux mixture for the chromitites was modified using the formula of Bédard & Barnes (2004). Results from our laboratory

*Table 2: Estimation of LA-ICP-MS precision and accuracy based on analysis of FeS standards*

| Sample | Method, laboratory | *n* | $^{101}$Ru (ppm) | $^{103}$Rh (ppm) | $^{105}$Pd (ppm) | $^{108}$Pd (ppm) | $^{192}$Os (ppm) | $^{193}$Ir (ppm) | $^{195}$Pt (ppm) | $^{197}$Au (ppm) |
|---|---|---|---|---|---|---|---|---|---|---|
| PO-52 | Standard addition, UQAC | 6 | 5·32 | 6·53 | 8·67 | 8·67 | 11·60 | 9·71 | 9·01 | 11·28 |
| | SD | | 0·25 | 0·50 | 0·65 | 0·65 | 1·20 | 0·45 | 0·65 | |
| | RSD (%) | | 4·7 | 7·7 | 7·5 | 7·5 | 10·3 | 4·6 | 7·2 | |
| PO-52 | LA-ICP-MS, UQAC | 118 | 5·31 | 6·53 | 8·69 | 8·69 | 11·56 | 9·69 | 8·99 | 10·96 |
| | SD | | 0·29 | 0·40 | 0·40 | 0·34 | 0·92 | 0·72 | 0·57 | 1·96 |
| | RSD (%) | | 5·5 | 6·1 | 4·6 | 3·9 | 8·0 | 7·4 | 6·3 | 17·9 |
| LaFlamme Po727 | Accepted value, CANMET | 43 | 36·50 | 41·60 | 43·40 | 43·40 | 46·70 | 48·00 | 35·50 | 45·80 |
| | SD | | 0·30 | 0·30 | 0·30 | 0·30 | 2·60 | 1·20 | 0·80 | 2·40 |
| | RSD (%) | | 0·8 | 0·7 | 0·7 | 0·7 | 5·6 | 2·5 | 2·3 | 5·2 |
| LaFlamme Po727 | LA-ICP-MS, UQAC | 24 | 36·41 | 41·69 | 43·50 | 43·29 | 46·94 | 48·21 | 35·36 | 45·73 |
| | SD | | 2·72 | 2·86 | 2·80 | 4·11 | 4·21 | 4·21 | 2·78 | 2·90 |
| | RSD (%) | | 7·5 | 6·9 | 6·4 | 9·5 | 9·0 | 8·7 | 7·9 | 6·3 |

SD, standard deviation for *n* different spots; RSD, relative standard deviation (SD × 100/average for *n* different spots).

*Table 3: Detection limit for the analysis of the base-metal sulphides by LA-ICP-MS*

| Element | $^{101}$Ru (ppm) | $^{103}$Rh (ppm) | $^{105}$Pd (ppm) | $^{108}$Pd (ppm) | $^{192}$Os (ppm) | $^{193}$Ir (ppm) | $^{195}$Pt (ppm) | $^{197}$Au (ppm) |
|---|---|---|---|---|---|---|---|---|
| Pyrrhotite | 0·009 | 0·005 | 0·035 | 0·021 | 0·004 | 0·001 | 0·004 | 0·001 |
| Pentlandite | 0·074 | 0·015 | 0·067 | 0·056 | 0·013 | 0·003 | 0·003 | 0·002 |
| Chalcopyrite | 0·150 | 0·060 | 0·350 | 0·090 | 0·030 | 0·020 | 0·100 | 0·030 |

Detection limit $= 3 \times (2 \times BC)^{1/2} \times C/I$, where BC is background counts, $C$ is concentration of analyte in the standard and $I$ is peak intensity for the analyte.

are in agreement with the certified values for the international reference material AMIS0007, which is a sample of Merensky Reef (Table 4).

*Table 4: Comparison of certified values and values obtained in this study for the international reference material AMIS0007*

| Element | Certified values | | UQAC | |
|---|---|---|---|---|
| | (ppm) | ± | (ppm) | ± |
| Cr | 12817 | 2644 | 13438 | 436 |
| Co | 335 | 65 | 315 | 9 |
| Ni | 2072* | 208 | 1774† | 96 |
| Ni | 1669‡ | 200 | 1541‡ | 30 |
| Cu | 1296 | 150 | 1196‡ | 34 |
| Ru | 0·45 | 0·06 | 0·421 | 0·024 |
| Rh | 0·25 | 0·04 | 0·265 | 0·008 |
| Pd | 1·5 | 0·2 | 1·457 | 0·064 |
| Os | n.q. | n.q. | 0·068 | 0·007 |
| Ir | 0·09 | | 0·092 | 0·0004 |
| Pt | 2·48 | 0·28 | 2·633 | 0·045 |
| Au | 0·155 | 0·016 | 0·156 | 0·006 |

*Total acid digestion.
†INAA on rock powder.
‡Aqua regia partial digestion.
n.q., not quantified.

# RESULTS

## Major elements in BMS and proportion of each BMS

Major element (S, Cu, Ni, Fe, Co) contents in the BMS are summarized in Table 1. These concentrations are relatively constant. The proportion of each BMS in each lithology was then calculated using the whole-rock S, Cu and Ni contents (Table 5). The calculation is based on the following assumptions: (1) the BMS are a mixture of pyrrhotite, pentlandite and chalcopyrite; (2) all the Cu is hosted by chalcopyrite; (3) all the Ni is hosted by pentlandite; (4) the remaining sulphur was allocated to pyrrhotite. Whole-rock Ni contents were determined by AAS after aqua regia digestion, and assigning all the Ni to pentlandite assumes that the Ni in the silicates did not dissolve. The total Ni content of the rocks as determined by INAA is generally ~400 ppm higher than the Ni content determined by AAS, which would suggest that ~570 to ~800 ppm Ni is present in the orthopyroxene. These results are in agreement with orthopyroxene analyses of the Merensky Reef (Arndt *et al.*, 2005). The weight

*Table 5: Metal contents of the base-metal sulphides from the Merensky Reef by LA-ICP-MS*

| Rock type | $^{61}$Ni (wt %) | $^{65}$Cu (wt %) | $^{59}$Co (ppm) | $^{185}$Re (ppm) | $^{189}$Os (ppm) | $^{193}$Ir (ppm) | $^{101}$Ru (ppm) | $^{103}$Rh (ppm) | $^{195}$Pt (ppm) | $^{105}$Pd (ppm) | $^{197}$Au (ppm) | $^{107}$Ag (ppm) | $^{111}$Cd (ppm) |
|---|---|---|---|---|---|---|---|---|---|---|---|---|---|
| *Pentlandite* | | | | | | | | | | | | | |
| AN | 34·87 | 0·012 | 8019 | 0·308 | 1·687 | 2·794 | 4·93 | 6·315 | 9·727 | 222·20 | 0·013 | 1·6 | 1·29 |
| AN | 34·87 | 0·450 | 10930 | 0·631 | 7·244 | 6·985 | 10·92 | 26·21 | 14·75 | 226·50 | 0·017 | 0·8 | 1·41 |
| AN | 34·87 | d.l. | 12750 | 0·458 | 4·66 | 8·259 | 13·98 | 13·62 | 36·12 | 165·20 | 0·026 | 0·9 | 0·91 |
| AN | 34·87 | 0·157 | 12140 | 0·075 | 0·486 | 0·218 | 1·24 | 17·89 | 25·49 | 376·70 | 1·362 | 2·0 | 1·45 |
| AN | 34·87 | 0·424 | 8271 | 0·203 | 3·921 | 4·108 | 10·20 | 7·288 | 0·743 | 187·70 | 0·035 | 1·3 | 1·64 |
| LC | 32·98 | 0·003 | 11510 | 0·007 | 0·021 | 47·457 | 9·95 | 648·6 | 5·275 | 19·91 | 0·008 | 7·8 | 1·20 |
| LC | 32·98 | 0·002 | 9917 | 0·084 | 7·14 | 7·119 | 57·75 | 21·66 | 8·58 | 374·50 | 0·008 | 6·5 | 1·17 |
| LC | 32·98 | 0·087 | 11910 | 0·111 | 2·945 | 3·629 | 2·05 | 18·71 | 9·156 | 425·60 | 0·014 | 4·6 | 1·21 |
| LC | 32·98 | 0·003 | 12430 | 0·309 | 5·385 | 5·543 | 11·86 | 34·68 | 10·04 | 497·50 | 0·009 | 3·1 | 1·44 |
| CGM | 30·53 | 0·119 | 10030 | 0·065 | 2·88 | 3·729 | 6·77 | 11·15 | 6·217 | 200·10 | 0·015 | 3·6 | 1·26 |
| CGM | 30·53 | 0·005 | 11610 | 0·14 | 4·701 | 5·098 | 9·79 | 9·811 | 7·731 | 244·70 | 0·091 | 2·9 | 1·30 |
| CGM | 30·53 | 0·038 | 10830 | 1·043 | 2·492 | 1·613 | 2·13 | 14·75 | 3·886 | 191·40 | 0·014 | 2·9 | 1·30 |
| CGM | 30·53 | 0·004 | 12620 | 0·349 | 5·513 | 6·486 | 7·47 | 20·89 | 12·3 | 435·60 | 0·017 | 2·2 | 1·57 |
| UC | 31·52 | 0·003 | 4624 | 0·212 | 2·542 | 2·817 | 2·69 | 202·1 | 1·987 | 599·10 | 0·013 | 1·8 | 1·25 |
| M | 31·52 | 0·247 | 10890 | 0·197 | 8·026 | 6·176 | 3·34 | 34·3 | 7·208 | 305·30 | 0·007 | 9·6 | 1·56 |
| M | 31·52 | 0·399 | 9987 | 0·006 | 0·011 | 0·083 | 0·86 | 10·48 | 3·386 | 259·00 | 0·009 | 8·0 | 1·72 |
| UC | 31·52 | 0·921 | 11250 | 0·041 | 0·673 | 1·963 | 1·29 | 62·1 | 5·87 | 267·00 | 0·011 | 2·3 | 2·07 |

(Continued)

*Table 5: Continued*

| Rock type | $^{61}$Ni (wt %) | $^{65}$Cu (wt %) | $^{59}$Co (ppm) | $^{185}$Re (ppm) | $^{189}$Os (ppm) | $^{193}$Ir (ppm) | $^{101}$Ru (ppm) | $^{103}$Rh (ppm) | $^{195}$Pt (ppm) | $^{105}$Pd (ppm) | $^{197}$Au (ppm) | $^{107}$Ag (ppm) | $^{111}$Cd (ppm) |
|---|---|---|---|---|---|---|---|---|---|---|---|---|---|
| M | 31·52 | 0·007 | 7291 | 0·069 | 2·178 | 2·250 | 2·09 | 11·08 | 9·01 | 179·80 | 0·010 | 2·3 | 1·34 |
| M | 31·52 | 0·009 | 14540 | 0·063 | 3·296 | 1·675 | 4·02 | 25·61 | 20·69 | 461·30 | 0·027 | 16·3 | 2·21 |
| M | 31·52 | 0·010 | 13110 | 0·836 | 4·224 | 3·708 | 5·78 | 44·02 | 7·418 | 310·90 | 0·065 | 3·2 | 2·32 |
| M | 31·52 | 0·022 | 12660 | 0·084 | 0·538 | 3·507 | 3·46 | 14·53 | 25·46 | 307·10 | 0·026 | 2·5 | 1·74 |
| M | 31·52 | 0·116 | 8010 | 0·15 | 1·565 | 2·735 | 1·40 | 28·85 | 7·3 | 146·30 | 0·012 | 3·6 | 2·39 |
| M | 31·23 | 0·003 | 11440 | 0·139 | 11·16 | 17·351 | 56·06 | 65·05 | 2·726 | 233·50 | 0·005 | 5·4 | 1·52 |
| M | 31·23 | 0·002 | 10320 | 0·144 | 2·316 | 3·412 | 1·40 | 24·95 | 5·152 | 219·10 | d.l. | 2·4 | 1·24 |
| M | 31·23 | 0·010 | 12730 | 0·206 | 5·36 | 7·830 | 3·91 | 44·84 | 3·615 | 237·90 | d.l. | 6·5 | 1·69 |
| M | 31·23 | 0·003 | 12190 | 0·163 | 3·666 | 5·934 | 2·45 | 25·44 | 3·021 | 233·20 | 0·004 | 6·5 | 1·64 |
| M | 31·23 | 0·003 | 7917 | 3·752 | 5·9 | 1·879 | 6·56 | 14·12 | 233·3 | 170·20 | 0·114 | 3·6 | 1·69 |
| M | 32·36 | 0·470 | 6505 | 0·012 | 1·963 | 2·186 | 6·56 | 12·34 | 3·535 | 144·80 | d.l. | 41·8 | 1·65 |
| M | 32·36 | 0·005 | 7184 | 0·202 | 3·577 | 3·048 | 7·15 | 8·644 | 0·017 | 147·10 | 0·015 | 8·3 | 1·77 |
| M | 32·36 | 0·086 | 3350 | 0·169 | 2·484 | 3·126 | 6·08 | 19·15 | 0·038 | 79·68 | d.l. | 23·4 | 1·50 |
| M | 32·36 | 0·007 | 7384 | 0·03 | 1·166 | 1·039 | 3·93 | 0·88 | 13·03 | 80·12 | 0·005 | 5·3 | 2·19 |
| M | 32·36 | 0·009 | 6542 | 0·085 | 2·137 | 2·076 | 7·80 | 11·56 | 0·018 | 83·29 | 0·014 | 2·0 | 1·97 |
| M | 32·36 | 0·007 | 8022 | 0·114 | 6·109 | 7·375 | 16·78 | 21·47 | 22·02 | 196·90 | 0·020 | 3·4 | 2·52 |
| M | 32·36 | 0·008 | 9042 | 0·043 | 2·416 | 2·815 | 11·18 | 24·29 | 0·045 | 209·70 | 0·006 | 3·7 | 2·46 |
| M | 32·36 | 0·011 | 10860 | 0·075 | 1·063 | 1·773 | 4·91 | 10·88 | 0·255 | 137·20 | 0·009 | 2·2 | 1·65 |
| M | 32·36 | 0·407 | 11760 | 0·055 | 1·365 | 1·473 | 3·66 | 5·062 | 151 | 194·20 | 0·081 | 2·5 | 1·68 |
| M | 33·65 | 0·002 | 8657 | 0·011 | d.l. | 0·203 | d.l. | 1·267 | 0·058 | 6·64 | 0·009 | 0·9 | 1·02 |
| M | 33·65 | 0·001 | 9096 | 0·025 | 0·398 | 0·870 | 1·99 | 2·729 | 5·76 | 88·70 | 0·007 | 1·0 | 1·04 |
| M | 33·65 | 0·002 | 9784 | 0·18 | 0·892 | 1·099 | 3·29 | 4·372 | 0·043 | 94·85 | 0·005 | 1·0 | 1·05 |
| M | 33·65 | 0·003 | 6855 | 0·162 | 0·673 | 1·197 | 2·25 | 4·802 | 0·231 | 62·47 | 0·079 | 2·9 | 1·61 |
| M | 33·65 | 0·003 | 8598 | 0·119 | 0·365 | 0·675 | 0·99 | 1·343 | 0·021 | 46·11 | 0·008 | 0·8 | 1·04 |
| M | 33·65 | 0·399 | 8869 | 0·277 | 2·263 | 2·165 | 6·37 | 9·539 | 0·198 | 277·40 | 0·006 | 1·5 | 1·19 |
| *Pyrrhotite* | | | | | | | | | | | | | |
| AN | 0·308 | 0·003 | 140·7 | 0·733 | 3·29 | 5·092 | 8·69 | 1·452 | 9·092 | 1·20 | 0·010 | 0·6 | 1·74 |
| AN | 0·486 | 0·002 | 206 | 0·061 | 3·207 | 3·824 | 11·90 | 1·727 | 0·974 | 2·07 | 0·006 | 0·7 | 1·81 |
| AN | 0·396 | 0·000 | 151 | 0·237 | 1·787 | 2·395 | 5·39 | 0·116 | 2·402 | 1·48 | 0·003 | 0·7 | 1·20 |
| AN | 0·382 | 0·004 | 114 | 0·685 | 3·15 | 4·783 | 7·51 | 0·538 | 7·112 | 1·39 | 0·010 | 1·1 | 1·99 |
| AN | 0·532 | 0·001 | 101·5 | 0·007 | 1·269 | 1·130 | 3·06 | 0·096 | 0·405 | 0·32 | 0·057 | 1·0 | 1·22 |
| LC | 0·180 | 0·001 | 68·94 | d.l. | 0·21 | 3·117 | 2·14 | 0·62 | 0·036 | 0·53 | 0·002 | 0·3 | 0·51 |
| LC | 0·097 | 0·001 | 14·55 | 0·125 | 1·809 | 0·419 | 1·18 | 0·29 | 0·117 | 0·48 | 0·008 | 0·5 | 0·62 |
| LC | 0·250 | 0·000 | 38·07 | 0·155 | 7·347 | 8·780 | 12·76 | 0·82 | 0·575 | 0·46 | 0·004 | 0·3 | 0·72 |
| LC | 0·248 | 0·000 | 33·38 | 0·28 | 6·677 | 5·754 | 6·65 | 0·293 | 0·634 | 0·53 | 0·004 | 0·4 | 0·69 |
| LC | 0·286 | 0·000 | 30·37 | 0·27 | 5·539 | 5·538 | 5·87 | 0·252 | 0·894 | 0·47 | 0·004 | 0·4 | 0·62 |
| CGM | 0·528 | 0·002 | 135·3 | d.l. | d.l. | 0·003 | 1·66 | 0·541 | d.l. | 0·74 | 0·001 | 0·5 | 0·58 |
| CGM | 0·576 | 0·000 | 51·95 | 0·27 | 2·939 | 1·412 | 5·29 | 0·541 | 0·693 | 1·11 | 0·006 | 0·9 | 0·55 |
| CGM | 0·715 | 0·000 | 93·63 | 0·41 | 3·705 | 2·168 | 5·87 | 0·418 | 1·073 | 0·83 | 0·002 | 0·7 | 0·66 |
| CGM | 0·505 | 0·000 | 23·6 | 0·584 | 5·734 | 5·748 | 15·26 | 0·471 | 3·742 | 0·57 | 0·006 | 0·4 | 0·76 |
| CGM | 0·503 | 0·000 | 21·39 | 0·379 | 5·381 | 4·361 | 11·78 | 0·44 | 1·617 | 0·66 | 0·004 | 0·4 | 0·83 |
| CGM | 0·711 | 0·001 | 104·8 | 0·234 | 3·637 | 1·286 | 5·09 | 0·318 | 0·579 | 0·79 | 0·003 | 1·4 | 0·66 |
| CGM | 0·422 | 0·000 | 38·37 | 0·183 | 2·399 | 0·951 | 3·77 | 0·343 | 0·342 | 0·69 | 0·009 | 1·2 | 0·82 |
| CGM | 0·683 | 0·003 | 26·14 | d.l. | 0·012 | 0·027 | 1·87 | 0·472 | 0·103 | 2·79 | 0·023 | 1·0 | 0·98 |
| CGM | 0·472 | 0·000 | 24·5 | 0·086 | 3·032 | 2·668 | 3·37 | 0·344 | 0·175 | 0·49 | 0·003 | 0·5 | 0·67 |

(Continued)

*Table 5: Continued*

| Rock type | $^{61}$Ni (wt %) | $^{65}$Cu (wt %) | $^{59}$Co (ppm) | $^{185}$Re (ppm) | $^{189}$Os (ppm) | $^{193}$Ir (ppm) | $^{101}$Ru (ppm) | $^{103}$Rh (ppm) | $^{195}$Pt (ppm) | $^{105}$Pd (ppm) | $^{197}$Au (ppm) | $^{107}$Ag (ppm) | $^{111}$Cd (ppm) |
|---|---|---|---|---|---|---|---|---|---|---|---|---|---|
| CGM | 0·325 | 0·000 | 20·2 | 0·005 | 0·237 | 0·134 | 2·41 | 0·246 | 0·039 | 0·48 | 0·004 | 0·6 | 0·71 |
| CGM | 0·491 | 0·000 | 26·99 | 0·08 | 2·13 | 1·213 | 2·72 | 0·439 | 0·311 | 0·69 | 0·001 | 0·8 | 0·77 |
| CGM | 0·306 | 0·000 | 17·88 | 0·121 | 2·12 | 1·117 | 2·44 | 0·267 | 0·086 | 0·55 | 0·002 | 0·7 | 0·78 |
| CGM | 0·411 | 0·000 | 19·74 | 0·283 | 4·982 | 5·307 | 4·13 | 0·391 | 0·285 | 0·49 | 0·003 | 0·6 | 0·73 |
| CGM | 0·382 | 0·000 | 20·15 | 0·055 | 2·665 | 1·692 | 3·02 | 0·294 | 0·046 | 0·52 | 0·004 | 0·4 | 0·73 |
| CGM | 0·215 | 0·000 | 10·52 | d.l. | d.l. | 0·016 | 1·48 | 0·212 | 0·009 | 0·35 | 0·001 | 0·4 | 0·61 |
| CGM | 0·243 | 0·000 | 11·62 | d.l. | 0·005 | 0·001 | 1·43 | 0·183 | 0·023 | 0·44 | 0·001 | 0·4 | 0·59 |
| CGM | 0·535 | 0·002 | 20·6 | 0·127 | 5·597 | 0·597 | 2·63 | 0·28 | 0·064 | 0·88 | 0·004 | 0·3 | 0·82 |
| CGM | 0·509 | 0·000 | 23·07 | 0·134 | 3·187 | 2·447 | 2·83 | 0·29 | 0·061 | 0·40 | 0·004 | 0·3 | 0·64 |
| UC | 0·297 | 0·002 | 115·7 | 0·217 | 0·772 | 9·966 | 8·34 | 4·487 | 3·109 | 1·46 | 0·006 | 0·7 | 0·98 |
| M | 0·093 | 0·000 | 20·47 | 0·238 | 7·218 | 6·138 | 6·09 | 0·077 | 0·266 | 0·19 | 0·001 | 0·4 | 0·77 |
| M | 0·402 | 0·000 | 231·4 | 0·178 | 3·749 | 1·060 | 1·61 | 0·405 | 0·409 | 3·93 | d.l. | 1·4 | 0·75 |
| M | 0·080 | 0·001 | 17·77 | 0·684 | 2·71 | 0·784 | 1·77 | 0·09 | 0·174 | 0·26 | 0·002 | 0·7 | 0·92 |
| M | 0·315 | 0·001 | 145·3 | 0·143 | 2·543 | 0·991 | 2·34 | 0·108 | 0·119 | 3·65 | 0·001 | 1·0 | 0·91 |
| M | 0·139 | 0·003 | 23·92 | 0·255 | 5·288 | 1·704 | 3·34 | 0·178 | 0·144 | 0·66 | 0·007 | 0·6 | 1·27 |
| UC | 0·085 | 0·001 | 17·69 | 0·256 | 6·959 | 3·199 | 1·58 | 0·897 | 8·004 | 0·21 | 0·004 | 0·3 | 0·80 |
| UC | 0·210 | 0·000 | 32·85 | 0·209 | 4·659 | 4·769 | 4·09 | 0·18 | 0·203 | 0·23 | d.l. | 0·3 | 0·84 |
| M | 0·232 | 0·001 | 35·48 | 0·176 | 6·67 | 5·335 | 6·49 | 0·109 | 0·186 | 0·31 | 0·002 | 0·4 | 0·98 |
| M | 0·370 | 0·002 | 53·83 | 0·126 | 3·618 | 2·945 | 3·44 | 0·176 | 0·179 | 0·53 | 0·018 | 0·6 | 1·19 |
| UC | 0·414 | 0·002 | 217·4 | 0·041 | 3·173 | 15·732 | 4·15 | 32 | 4·818 | 2·56 | 0·008 | 0·6 | 1·20 |
| UC | 0·459 | 0·011 | 330 | 0·149 | 0·534 | 0·086 | 2·34 | 2·964 | 0·249 | 6·63 | 0·029 | 1·5 | 2·05 |
| M | 0·310 | 0·045 | 168·2 | 0·188 | 2·084 | 1·441 | 2·16 | 0·339 | 0·352 | 3·05 | 0·001 | 0·6 | 1·04 |
| M | 0·366 | 0·001 | 162·3 | d.l. | 0·014 | 0·009 | 1·54 | 0·725 | 0·206 | 5·64 | 0·005 | 1·0 | 1·33 |
| M | 0·188 | 0·001 | 34·12 | 0·178 | 3·098 | 1·337 | 3·44 | 0·212 | 0·145 | 0·41 | 0·002 | 0·5 | 1·26 |
| M | 0·182 | 0·007 | 47·89 | 0·155 | 0·595 | 0·088 | 3·19 | 0·156 | 0·082 | 1·15 | 0·006 | 0·8 | 1·33 |
| M | 0·108 | 0·000 | 32·85 | 0·09997 | 3·791 | 4·226 | 2·75 | 0·494 | 0·078 | 0·40 | 0·002 | 0·5 | 1·01 |
| M | 0·163 | 0·000 | 114·2 | 0·1234 | 4·337 | 5·031 | 4·81 | 8·77 | 0·06 | 0·83 | 0·131 | 0·7 | 1·11 |
| M | 0·102 | 0·000 | 32·17 | 0·6581 | 2·835 | 2·233 | 3·27 | 0·613 | 0·074 | 0·54 | 0·006 | 4·0 | 1·10 |
| *Pyrrhotite* | | | | | | | | | | | | | |
| M | 0·104 | 0·000 | 35·59 | 0·1211 | 6·413 | 6·778 | 5·90 | 0·638 | 0·255 | 0·29 | 0·003 | 0·4 | 0·96 |
| M | 0·104 | 0·008 | 33·74 | 0·07354 | 4·584 | 3·933 | 3·62 | 0·579 | 0·06 | 0·44 | d.l. | 0·5 | 0·99 |
| M | 0·089 | 0·000 | 30·72 | 0·1371 | 4·252 | 3·882 | 3·65 | 0·319 | 0·062 | 0·47 | 0·004 | 0·7 | 1·00 |
| M | 0·076 | 0·001 | 25·89 | 0·06152 | 2·038 | 0·810 | 2·67 | 0·283 | 0·016 | 0·47 | 0·002 | 0·6 | 1·11 |
| M | 0·098 | 0·000 | 46·05 | 0·1598 | 6·11 | 3·314 | 5·14 | 0·811 | 0·215 | 0·61 | 0·001 | 0·8 | 1·10 |
| M | 0·067 | 0·001 | 26·38 | 0·3664 | 6·33 | 4·544 | 6·08 | 0·254 | 0·242 | 0·54 | 0·002 | 0·6 | 1·13 |
| M | 0·078 | 0·000 | 37·23 | 0·4119 | 7·575 | 8·789 | 10·99 | 0·331 | 1·215 | 0·56 | 0·004 | 0·6 | 1·15 |
| M | 0·058 | 0·000 | 24·66 | 0·3664 | 6·808 | 5·800 | 5·30 | 0·252 | 0·269 | 0·44 | 0·002 | 0·5 | 1·11 |
| M | 0·058 | 0·001 | 28·79 | 0·4973 | 9·346 | 9·333 | 14·90 | 0·562 | 0·28 | 0·55 | 0·005 | 0·5 | 1·25 |
| M | 0·490 | 0·001 | 611·9 | 0·4054 | 10·86 | 9·270 | 8·76 | 0·259 | 0·493 | 10·13 | 0·001 | 4·0 | 1·19 |
| M | 0·346 | d.l. | 38·31 | d.l. | d.l. | 0·004 | 1·33 | 0·358 | 0·014 | 0·48 | 0·001 | 0·5 | 1·37 |
| M | 0·163 | d.l. | 23·84 | 0·287 | 6·055 | 6·688 | 4·67 | 0·313 | 0·303 | 0·47 | 0·008 | 0·5 | 1·39 |
| M | 0·156 | d.l. | 22·22 | 0·197 | 5·247 | 5·078 | 5·03 | 0·33 | 0·366 | 0·26 | 0·002 | 0·5 | 1·38 |
| M | 0·139 | d.l. | 18·96 | 0·169 | 3·687 | 3·086 | 3·21 | 0·297 | 0·046 | 0·54 | d.l. | 0·5 | 1·44 |
| M | 0·148 | d.l. | 22·44 | 0·121 | 3·4 | 1·661 | 3·15 | 0·357 | 0·026 | 0·60 | d.l. | 0·8 | 1·68 |
| M | 0·147 | d.l. | 20·76 | 0·284 | 4·018 | 2·217 | 2·70 | 0·344 | 0·283 | 0·54 | d.l. | 0·6 | 1·76 |

(Continued)

*Table 5: Continued*

| Rock type | $^{61}$Ni (wt%) | $^{65}$Cu (wt%) | $^{59}$Co (ppm) | $^{185}$Re (ppm) | $^{189}$Os (ppm) | $^{193}$Ir (ppm) | $^{101}$Ru (ppm) | $^{103}$Rh (ppm) | $^{195}$Pt (ppm) | $^{105}$Pd (ppm) | $^{197}$Au (ppm) | $^{107}$Ag (ppm) | $^{111}$Cd (ppm) |
|---|---|---|---|---|---|---|---|---|---|---|---|---|---|
| M | 0·108 | 0·799 | 43·4 | 0·168 | 2·23 | 1·003 | 6·02 | 0·919 | 0·848 | 1·72 | 0·016 | 2·9 | 1·55 |
| M | 0·215 | 0·004 | 103 | 0 | 4·063 | 4·567 | 9·17 | 1·125 | 0·389 | 2·16 | 0·019 | 2·4 | 1·31 |
| M | 0·250 | 0·136 | 120·3 | 0·004 | 1·738 | 0·630 | 6·19 | 0·854 | 0·553 | 2·12 | 0·001 | 4·4 | 1·73 |
| M | 0·089 | 0·002 | 29·2 | 0·206 | 2·79 | 2·524 | 8·01 | 1·329 | 0·345 | 1·42 | 0·003 | 1·3 | 1·67 |
| M | 0·310 | 0·002 | 144·9 | 0·207 | 3·944 | 3·663 | 11·35 | 0·982 | 0·074 | 1·92 | 0·004 | 2·5 | 1·71 |
| M | 0·406 | 0·003 | 206·8 | 0·195 | 4·153 | 3·749 | 11·03 | 0·915 | 0·063 | 2·77 | 0·008 | 2·6 | 1·97 |
| M | 0·217 | 0·008 | 44·56 | 0·283 | 4·365 | 3·338 | 10·90 | 1·226 | 0·131 | 2·75 | 0·013 | 1·4 | 3·33 |
| M | 0·167 | 0·003 | 32·79 | 0·252 | 4·811 | 3·208 | 10·20 | 1·326 | 0·192 | 1·69 | 0·012 | 1·5 | 2·61 |
| *Ni-rich pyrrhotite* | | | | | | | | | | | | | |
| M | 1·097 | 0·001 | 40·11 | d.l. | 0·347 | 0·046 | 2·93 | 0·147 | 0·016 | 0·51 | d.l. | 0·7 | 1·96 |
| M | 1·619 | 0·002 | 69·17 | 0·666 | 7·81 | 9·970 | 25·81 | 2·179 | 14·34 | 0·78 | 0·016 | 0·7 | 2·27 |
| M | 1·349 | 0·002 | 66·72 | 0·258 | 1·474 | 9·192 | 12·56 | 0·513 | 3·049 | 0·90 | d.l. | 0·9 | 2·21 |
| M | 1·076 | 0·003 | 50·53 | 0·249 | 2·173 | 2·002 | 7·27 | 0·33 | 0·661 | 1·35 | 0·005 | 1·0 | 2·57 |
| M | 1·170 | 0·002 | 58·67 | 0·914 | 7·107 | 7·114 | 19·96 | 0·397 | 7·572 | 0·78 | 0·007 | 0·9 | 2·39 |
| M | 1·389 | 0·001 | 87·45 | 0·053 | 0·444 | 0·462 | 1·80 | 0·291 | 0·459 | 1·33 | 0·001 | 0·9 | 2·20 |
| M | 1·328 | 0·002 | 66·95 | 0·362 | 7·006 | 6·290 | 23·03 | 0·325 | 2·103 | 1·06 | 0·009 | 0·8 | 2·44 |
| M | 1·627 | 0·002 | 49·52 | 0·331 | 3·035 | 1·364 | 11·33 | 0·101 | 0·556 | 0·22 | 0·003 | 0·3 | 0·67 |
| M | 1·366 | 0·001 | 41·55 | 0·141 | 3·805 | 0·794 | 8·89 | 0·114 | 0·545 | 0·27 | d.l. | 0·4 | 0·73 |
| M | 1·321 | 0·002 | 40·52 | 0·153 | 0·335 | 0·086 | 1·45 | 0·127 | 0·017 | 0·32 | d.l. | 0·4 | 0·85 |
| M | 1·082 | 0·001 | 38·34 | 0·232 | 0·548 | 0·231 | 1·46 | 0·133 | 0·121 | 0·26 | 0·006 | 0·4 | 0·83 |
| M | 1·246 | 0·001 | 67·86 | 0·034 | 7·501 | 1·879 | 27·26 | 0·156 | 0·595 | 0·37 | 0·004 | 0·4 | 0·82 |
| M | 1·192 | 0·000 | 66·12 | 0·279 | 2·439 | 0·644 | 5·33 | 0·116 | 0·078 | 0·38 | d.l. | 0·3 | 0·92 |
| *Chalcopyrite* | | | | | | | | | | | | | |
| AN | 0·151 | 33·98 | 79·48 | 0·007 | 0·069 | 0·074 | d.l. | d.l. | 0·313 | 5·79 | 0·008 | 77·0 | 5·91 |
| AN | 0·303 | 33·98 | 223·9 | 0·007 | 0·082 | 0·033 | d.l. | d.l. | 0·718 | 7·96 | 0·035 | 17·4 | 6·72 |
| AN | 0·493 | 33·98 | 235·2 | d.l. | d.l. | 0·007 | d.l. | d.l. | 0·995 | 12·00 | 0·07 | 17·5 | 8·90 |
| AN | 0·003 | 33·98 | 3·496 | d.l. | d.l. | d.l. | d.l. | d.l. | 0·046 | 5·61 | d.l. | 7·9 | 7·77 |
| AN | 0·009 | 33·98 | 3·851 | d.l. | d.l. | d.l. | d.l. | d.l. | 0·016 | 5·49 | d.l. | 4·6 | 14·60 |
| AN | 0·023 | 33·98 | 5·628 | d.l. | 0·005 | d.l. | d.l. | d.l. | 0·047 | 6·22 | 0·018 | 5·7 | 16·34 |
| LC | d.l. | 34·15 | 0·79 | d.l. | d.l. | d.l. | d.l. | d.l. | 0·019 | 2·24 | d.l. | 6·0 | 10·64 |
| LC | 0·004 | 34·15 | 2·085 | d.l. | 0·005 | 0·010 | d.l. | d.l. | 0·124 | 1·77 | 0·151 | 6·6 | 10·15 |
| LC | 0·016 | 34·15 | 12·13 | d.l. | 0·008 | 0·092 | d.l. | d.l. | 0·057 | 4·49 | 0·041 | 14·1 | 10·27 |
| LC | 0·007 | 34·15 | 5·397 | d.l. | 0·006 | 0·109 | d.l. | d.l. | 0·452 | 2·81 | 0·011 | 34·7 | 14·01 |
| CGM | 0·044 | 33·84 | 32·71 | d.l. | 0·008 | d.l. | d.l. | d.l. | 0·014 | 7·02 | d.l. | 19·8 | 4·27 |
| CGM | d.l. | 33·84 | 1·234 | d.l. | d.l. | 0·005 | d.l. | d.l. | 0·01 | 6·94 | 0·007 | 3·6 | 4·75 |
| CGM | 0·178 | 33·84 | 19·25 | 0·005 | d.l. | 0·007 | d.l. | d.l. | 0·017 | 7·23 | 0·01 | 4·1 | 5·77 |
| CGM | d.l. | 33·84 | 3·246 | 0·004 | 0·011 | d.l. | d.l. | d.l. | 0·011 | 6·97 | 0·006 | 5·2 | 7·44 |
| UC | 0·027 | 33·65 | 8·274 | 0·003 | 0·008 | 0·008 | d.l. | d.l. | 0·071 | 6·33 | 0·006 | 5·8 | 13·05 |
| UC | 0·139 | 33·65 | 125·9 | 0·005 | 0·028 | 0·102 | d.l. | 1·265 | 0·261 | 11·85 | 0·281 | 6·7 | 3·33 |
| UC | 0·011 | 33·65 | 8·981 | 0·002 | 0·021 | 0·023 | d.l. | d.l. | 15·72 | 2·95 | 0·097 | 3·7 | 3·42 |
| M | 0·281 | 33·65 | 192·8 | 0·009 | 0·112 | 0·085 | d.l. | d.l. | 0·291 | 7·93 | 0·062 | 46·0 | 4·60 |
| M | 0·117 | 33·65 | 73·26 | d.l. | 0·022 | 0·034 | d.l. | d.l. | 0·107 | 4·87 | 0·03 | 6·3 | 5·46 |
| M | 0·004 | 33·65 | 4·132 | d.l. | d.l. | d.l. | d.l. | d.l. | d.l. | 4·42 | 0·02 | 9·3 | 5·17 |
| M | 0·036 | 33·65 | 25·67 | d.l. | 0·005 | 0·007 | d.l. | d.l. | 0·112 | 4·40 | 0·006 | 4·9 | 13·49 |
| M | 0·028 | 33·65 | 9·651 | d.l. | d.l. | 0·008 | d.l. | d.l. | 0·495 | 3·55 | 0·013 | 4·1 | 13·89 |

(Continued)

*Table 5: Continued*

| Rock type | $^{61}$Ni (wt %) | $^{65}$Cu (wt %) | $^{59}$Co (ppm) | $^{185}$Re (ppm) | $^{189}$Os (ppm) | $^{193}$Ir (ppm) | $^{101}$Ru (ppm) | $^{103}$Rh (ppm) | $^{195}$Pt (ppm) | $^{105}$Pd (ppm) | $^{197}$Au (ppm) | $^{107}$Ag (ppm) | $^{111}$Cd (ppm) |
|---|---|---|---|---|---|---|---|---|---|---|---|---|---|
| M | 0·171 | 33·65 | 102·3 | 0·006 | 0·01 | 0·044 | d.l. | d.l. | 0·246 | 6·57 | d.l. | 4·8 | 9·38 |
| M | 0·067 | 33·65 | 223·4 | 0·004 | 0·01 | d.l. | d.l. | d.l. | d.l. | 5·00 | 0·006 | 9·2 | 11·79 |
| M | 0·321 | 33·70 | 108·1 | 0·185 | 1·405 | 0·628 | 2·74 | d.l. | 0·254 | 11·43 | 0·006 | 5·0 | 4·46 |
| M | 0·406 | 33·70 | 125·2 | d.l. | 0·01 | 0·037 | d.l. | d.l. | 0·167 | 12·82 | 0·006 | 8·7 | 7·29 |
| M | d.l. | 33·94 | d.l. | d.l. | d.l. | d.l. | d.l. | d.l. | 0·009 | 2·46 | d.l. | 2·4 | 3·09 |
| M | 0·050 | 33·94 | 14·57 | 0·115 | 0·047 | 0·094 | d.l. | d.l. | 0·15 | 3·13 | 0·006 | 65·2 | 19·03 |
| M | d.l. | 33·94 | d.l. | d.l. | d.l. | d.l. | d.l. | d.l. | 0·01 | 2·45 | 0·008 | 2·6 | 3·06 |
| M | d.l. | 33·94 | d.l. | d.l. | d.l. | d.l. | d.l. | d.l. | 0·083 | 2·41 | 0·005 | 2·7 | 4·27 |
| M | 0·301 | 33·81 | 21·56 | d.l. | 0·011 | 0·088 | d.l. | d.l. | 0·201 | 4·01 | 0·052 | 4·6 | 3·95 |
| M | 0·540 | 33·81 | 27·24 | 0·009 | 0·009 | 0·124 | d.l. | d.l. | 0·577 | 5·83 | 0·098 | 7·2 | 4·96 |
| M | 0·173 | 33·81 | 10·72 | d.l. | 0·017 | 0·122 | d.l. | d.l. | 0·293 | 4·52 | 0·072 | 5·4 | 6·34 |
| M | 0·139 | 33·81 | 14·93 | 0·005 | 0·012 | 0·088 | d.l. | d.l. | 0·081 | 3·76 | 0·018 | 4·0 | 5·22 |
| M | 0·304 | 33·81 | 20·7 | 0·189 | 2·897 | 4·035 | 2·90 | d.l. | 1·747 | 5·80 | d.l. | 5·9 | 4·98 |
| M | 0·300 | 33·81 | 19·52 | d.l. | d.l. | 0·008 | d.l. | d.l. | 0·024 | 6·54 | 0·017 | 10·2 | 8·18 |

d.l., value under the detection limit.

fraction of chalcopyrite ($F_{Cp}$) is given by ($Cu_{WR}/Cu_{Cp}$), where $Cu_{WR}$ is the concentration of Cu in the whole-rock and $Cu_{Cp}$ is the average concentration of Cu in the chalcopyrite. The weight fraction of pentlandite ($F_{Pn}$) is given by ($Ni_{WR}/Ni_{Pn}$), where $Ni_{WR}$ is the concentration of Ni in the whole-rock and $Ni_{Pn}$ is the average concentration of Ni in the pentlandite. The weight fraction of pyrrhotite ($F_{Po}$) is calculated by $(S_{WR} - S_{Cp} \times F_{Cp} - S_{Pn} \times F_{Pn})/S_{Po}$, where $S_{WR}$ is the sulphur content in the whole-rock, $S_{Cp}$ is the average sulphur concentration in the chalcopyrite, $S_{Pn}$ is the average sulphur concentration in the pentlandite and $S_{Po}$ is the average sulphur concentration in the pyrrhotite. On average the BMS component of the rocks (Fig. 4) consists of ~44 wt% pentlandite, ~37 wt% pyrrhotite and ~19 wt% chalcopyrite. These results are in agreement with those obtained by Vermaak (1976) and Barnes & Maier (2002*a*) on other Merensky Reef samples. In our samples of Merensky Reef, BMS in the chromitite layers and the rock immediately below each chromitite layer are richer in chalcopyrite (25–30 wt%) than the silicate rocks overlying the chromitite layers (9–14 wt%).

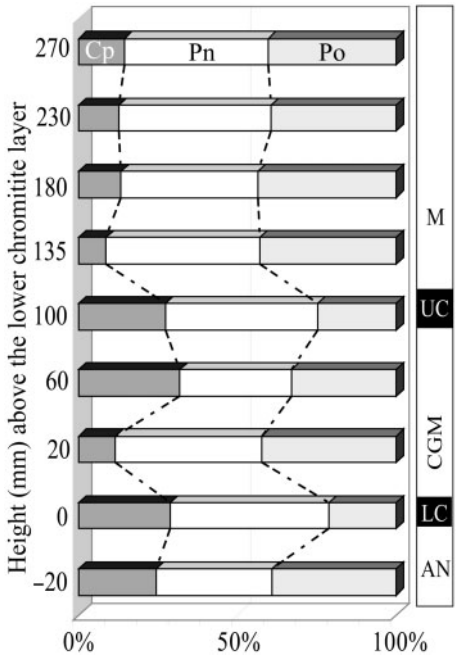


**Fig. 4.** Proportions of each base-metal sulphide as a function of the stratigraphy. Po, pyrrhotite; Pn, pentlandite; Cp, chalcopyrite.

## PGE and other metals in BMS

All the BMS analysed (pyrrhotite, pentlandite and chalcopyrite) (Table 6) contain some PGE, Re, Ag, Au, Cd, Co, Cu and Ni in solid solution. Pentlandite is the BMS that contains the highest PGE concentrations, mostly (in 80% of cases) between 200 and 500 ppm of PGE (Fig. 5). These values are similar to those observed by Ballhaus & Ryan (1995) and Ballhaus & Sylvester (2000). On average, 90% of the pyrrhotite analyses contain between 10 and 40 ppm PGE (Table 6, Fig. 5). Chalcopyrite has the lowest PGE contents, with 85% of grains containing 4–10 ppm (Fig. 5).

*Table 6: Whole-rock analysis and recalculation to 100% sulphides*

| Sample | Height (mm) | S (wt %) | Ni (wt %) | Cu (wt %) | Co (ppm) | Re (ppm) | Os (ppm) | Ir (ppm) | Ru (ppm) | Rh (ppm) | Pt (ppm) | Pd (ppm) | Au (ppm) | Ag (ppm) | All PGE (ppm) | Se (ppm) |
|---|---|---|---|---|---|---|---|---|---|---|---|---|---|---|---|---|
| *Whole-rock* | | | | | | | | | | | | | | | | |
| AN | −20 | 0·37 | 0·13 | 0·09 | 24 | d.l. | 0·10 | 0·12 | 0·50 | 0·42 | 5·34 | 4·03 | 0·33 | d.l. | 10·5 | 1·3 |
| LC | 0 | 0·47 | 0·22 | 0·13 | 211 | d.l. | 0·73 | 1·11 | 5·41 | 3·80 | 33·10 | 4·40 | 0·34 | d.l. | 48·6 | d.l. |
| CGM-1 | 20 | 3·07 | 1·31 | 0·35 | 273 | 0·01 | 0·58 | 0·58 | 2·53 | 1·34 | 42·08 | 16·29 | 2·56 | 2·54 | 63·4 | 13·7 |
| CGM-2 | 60 | 1·39 | 0·44 | 0·43 | 147 | d.l. | 0·14 | 0·14 | 0·60 | 0·40 | 8·84 | 5·94 | 4·64 | 1·64 | 16·1 | 4·3 |
| UC | 100 | 0·53 | 0·23 | 0·14 | 167 | d.l. | 0·26 | 0·35 | 1·70 | 1·00 | 13·45 | 4·27 | 0·31 | d.l. | 21·0 | d.l. |
| M-1 | 135 | 3·21 | 1·37 | 0·28 | 291 | 0·02 | 0·49 | 0·63 | 2·78 | 1·69 | 16·55 | 11·90 | 1·27 | 3·07 | 34·0 | 15·4 |
| M-2 | 180 | 0·74 | 0·29 | 0·10 | 117 | 0·01 | 0·09 | 0·10 | 0·36 | 0·21 | 3·14 | 2·22 | 0·34 | d.l. | 6·1 | 3·0 |
| M-3 | 230 | 0·89 | 0·41 | 0·11 | 137 | 0·01 | 0·09 | 0·10 | 0·64 | 0·20 | 2·48 | 2·36 | 0·42 | d.l. | 5·9 | 4·0 |
| M-4 | 270 | 0·98 | 0·42 | 0·14 | 137 | 0·01 | 0·07 | 0·07 | 0·32 | 0·17 | 5·21 | 2·16 | 0·22 | d.l. | 8·0 | 4·6 |

| Sample | S (wt %) | Ni (wt %) | Cu (wt %) | Co (ppm) | Re (ppm) | Os (ppm) | Ir (ppm) | Ru (ppm) | Rh (ppm) | Pt (ppm) | Pd (ppm) | Au (ppm) | Ag (ppm) | Pt/Pd (ppm) | Pd/Ir (ppm) | All PGE (ppm) |
|---|---|---|---|---|---|---|---|---|---|---|---|---|---|---|---|---|
| *Recalculation to 100% sulphide** | | | | | | | | | | | | | | | | |
| AN | 36·1 | 12·7 | 8·4 | 2300 | d.l. | 9·4 | 11·4 | 48·1 | 40·7 | 515 | 389 | 31·4 | d.l. | 1·3 | 34·2 | 1013 |
| LC | 35·1 | 16·6 | 10·0 | 15872 | d.l. | 54·7 | 84·0 | 408·0 | 286·7 | 2495 | 332 | 25·3 | d.l. | 7·5 | 3·9 | 3660 |
| CGM-1 | 36·1 | 15·5 | 4·1 | 3216 | 0·142 | 6·9 | 6·8 | 29·9 | 15·8 | 496 | 192 | 30·1 | 29·9 | 2·6 | 28·3 | 747 |
| CGM-2 | 36·0 | 11·3 | 11·1 | 3790 | d.l. | 3·7 | 3·6 | 15·4 | 10·4 | 228 | 153 | 119·8 | 42·4 | 1·5 | 42·1 | 415 |
| UC | 35·5 | 15·2 | 9·4 | 11243 | d.l. | 17·5 | 23·6 | 114·8 | 67·1 | 906 | 288 | 20·6 | d.l. | 3·1 | 12·2 | 1417 |
| M-1 | 36·3 | 15·5 | 3·1 | 3292 | 0·224 | 5·5 | 7·1 | 31·4 | 19·1 | 187 | 135 | 14·4 | 34·7 | 1·4 | 18·9 | 385 |
| M-2 | 36·3 | 14·3 | 4·7 | 5743 | 0·246 | 4·3 | 5·0 | 17·6 | 10·5 | 154 | 109 | 16·7 | d.l. | 1·4 | 21·9 | 300 |
| M-3 | 35·9 | 16·4 | 4·4 | 5507 | 0·218 | 3·8 | 4·1 | 25·7 | 8·2 | 100 | 95 | 17·1 | d.l. | 1·0 | 23·0 | 237 |
| M-4 | 36·0 | 15·5 | 5·0 | 5022 | 0·192 | 2·7 | 2·7 | 11·6 | 6·2 | 191 | 79 | 7·9 | d.l. | 2·4 | 29·0 | 294 |

*$C_{(100\%\ \text{sulphide})} = C_{WR} \times 100/(2{\cdot}527S + 0{\cdot}3408Cu + 0{\cdot}4715Ni)$, Barnes & Lightfoot (2005). AN, anorthosite; LC, lower chromitite; CGM-1 and CGM-2, coarse-grained melanorites; UC, upper chromitite; M1, M2, M3 and M4, melanorite; d.l., value under the detection limit.

## Controls on trace elements in the BMS

During the evolution of a Fe–Ni–Cu sulphide liquid, a monosulphide solid solution enriched in Fe (Mss) and a liquid enriched in Cu form (Kullerud *et al.*, 1969; Naldrett, 1989). Osmium, Ir, Ru, Rh and Re preferentially partition into the Fe-rich Mss whereas Cu, Pt, Pd, Ag, Au, Cd and Zn concentrate in the Cu-rich fractionated liquid (Li *et al.*, 1996; Barnes *et al.*, 2001; Mungall *et al.*, 2005). Nickel partitions almost equally between Mss and the liquid. The Cu-rich fractionated liquid crystallizes as intermediate solid solution (Iss) and minor Ni-rich Mss. At temperature <600°C, the Mss exsolves into pyrrhotite ($Fe_{1-x}S$), and pentlandite [$(Ni, Fe)_9S_8$] and the Iss exsolves to form chalcopyrite ($CuFeS_2$) ± cubanite ($CuFe_2S_3$). If the trace elements have not been redistributed during the exsolution of the BMS, one would expect pyrrhotite and pentlandite to be enriched in Os, Ir, Ru, Rh and Re, and chalcopyrite to be enriched in the remaining elements.

## Iridium, osmium, ruthenium and rhenium

Osmium, Ru and Re show a positive correlation with Ir and are largely present in pentlandite and pyrrhotite with no preference for either of the two minerals (Fig. 6a–c and Table 5). As explained above, this co-variance probably reflects the control of these elements by Mss and only a limited redistribution of the elements during exsolution. Osmium and Ir contents (Fig. 6a) in both pentlandite and pyrrhotite cover a similar range (~0·1 to ~15 ppm). Iridium and Os contents of chalcopyrite (Fig. 6a) are <1 ppm. Pentlandite (Fig. 6b) contains ~4 to 20 ppm Ru (two values are higher, ~60 ppm Ru). The Ru content in the pyrrhotite (Fig. 6b) is slightly lower, from ~1 to ~15 ppm. In the chalcopyrite Ru contents are below the detection limit (i.e. <0·2 ppm). Pentlandite and pyrrhotite (Fig. 6c) contain 0·002–2 ppm Re, with most values <0·5 ppm. Rhenium contents are lower in chalcopyrite, with values ranging from 0·003 to 0·02 ppm (Fig. 6c).

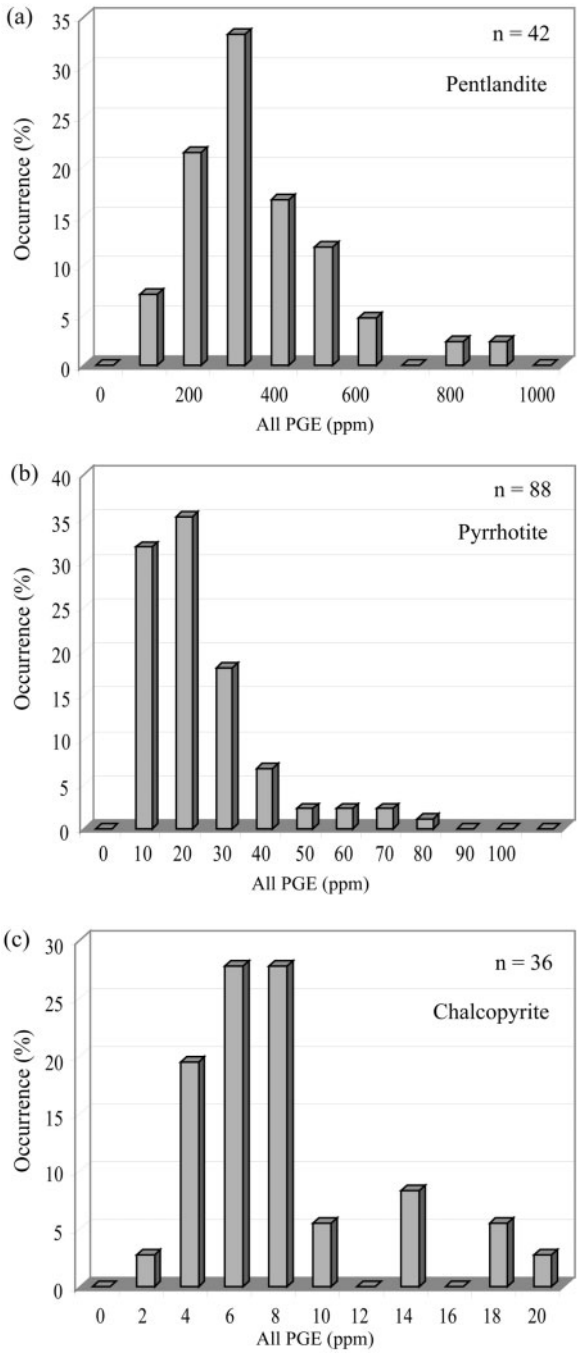


**Fig. 5.** Total PGE content in base-metal sulphide minerals (a) in pentlandite; (b) in pyrrhotite; (c) in chalcopyrite.

## Copper, cadmium, silver, platinum and gold

As would be predicted by the Mss fractionation model, Ag and Cd show a positive correlation with Cu and are concentrated in chalcopyrite (Fig. 7a, b and Table 6). Chalcopyrite contains more Ag than pentlandite and pyrrhotite, with values ranging from ~3 to ~80 ppm,

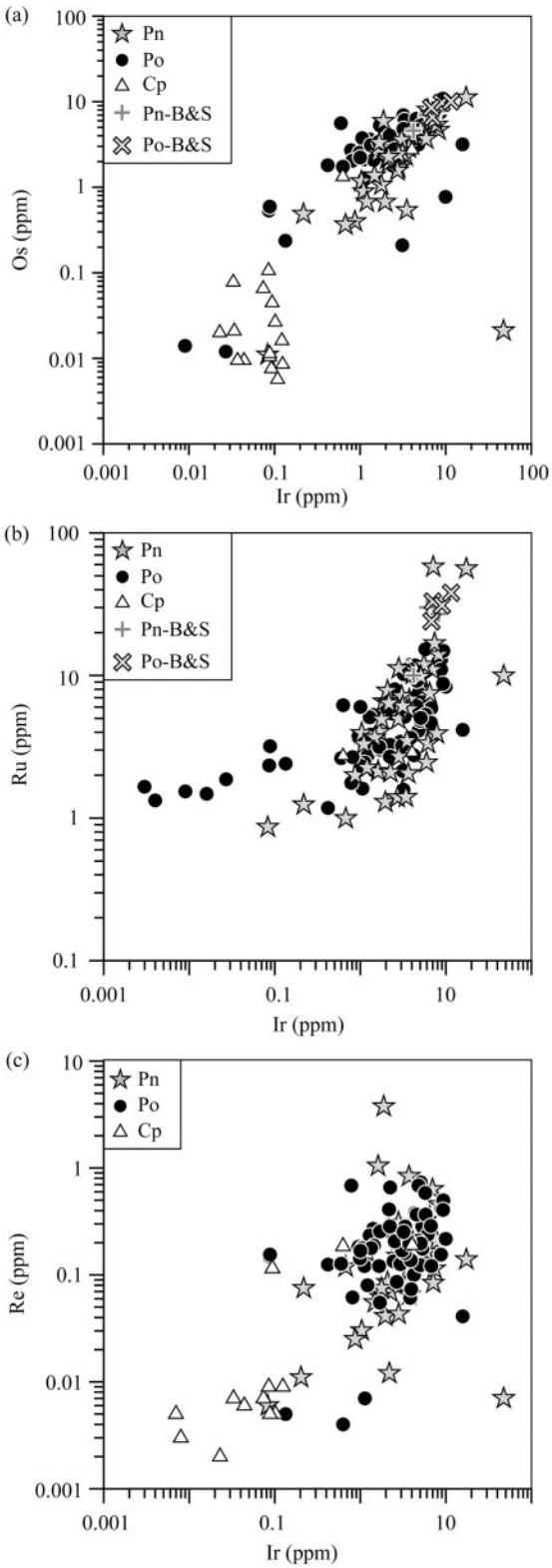


**Fig. 6.** Binary variation diagrams, plotting (a) Os vs Ir, (b) Ru vs Ir, and (c) Re vs Ir. Results obtained by Ballhaus & Sylvester (2000) were added for comparison (Pn-B&S for pentlandite and Po-B&S for pyrrhotite).

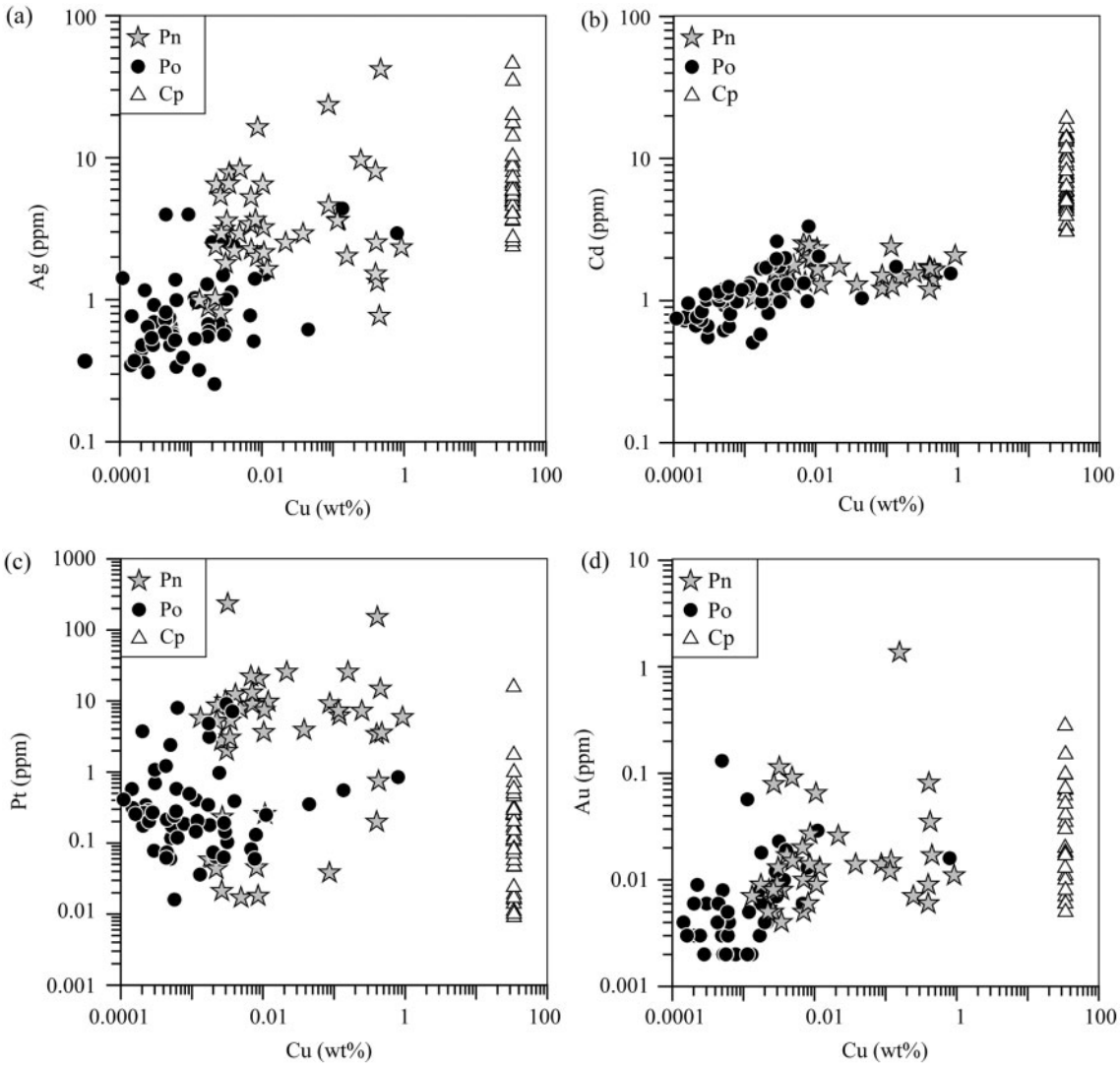


**Fig. 7.** Binary variation diagrams of (a) Ag vs Cu, (b) Cd vs Cu, (c) Pt vs Cu, (d) Au vs Cu.

but most of the values are <20 ppm (Fig. 7a and Table 6). Silver contents in most pentlandite analyses are ~1 to ~7 ppm (three values were found between 15 and 40 ppm). In pyrrhotite, Ag values are ~0·3 to ~3 ppm (Fig. 7a and Table 6). Silver also occurs as inclusions, both in BMS and at the contact between BMS and silicate minerals (see description below). Chalcopyrite contains 3–20 ppm Cd (Fig. 7b and Table 6). Pentlandite and pyrrhotite contain ~0·5 to ~3 ppm Cd (Fig. 7b and Table 5).

In contrast to Cd and Ag, Pt and Au are not partitioned into specific BMS (Fig, 7c, d and Table 6). These results are in agreement with those of Ballhaus & Sylvester (2000). Platinum concentrations in pentlandite are 0·02–30 ppm (Fig. 7c). Pyrrhotite and chalcopyrite contain 0·01–10 ppm Pt (Fig. 7c). There are no significant correlations between Pt and other metals. During the laser ablation several inclusions enriched in platinum were observed in the BMS or at the contact between BMS and silicate (see description below). Gold is not partitioned into any particular BMS (Fig. 7d and Table 6). Gold contents in most pentlandite, pyrrhotite and chalcopyrite analyses are ~0·01 to ~0·3 ppm (Fig. 7d). Minor amounts of Au are associated with Ag in inclusions that are probably composed of palladian electrum (see description below).

## Nickel, cobalt, palladium and rhodium

These four elements are largely concentrated in pentlandite. Nickel, Rh, Pd and Co all show a positive correlation with each other (Fig. 8 and Table 6). The Co content in pentlandite (Fig. 8a, b and Table 6) varies from ~0·5 to ~1·4 wt%, similar to the values determined by electron microprobe and to the values reported by Ballhaus & Sylvester (2000). Pyrrhotite contains between 10 and 200 ppm Co (Fig. 8a, b and Table 6). Chalcopyrite contains

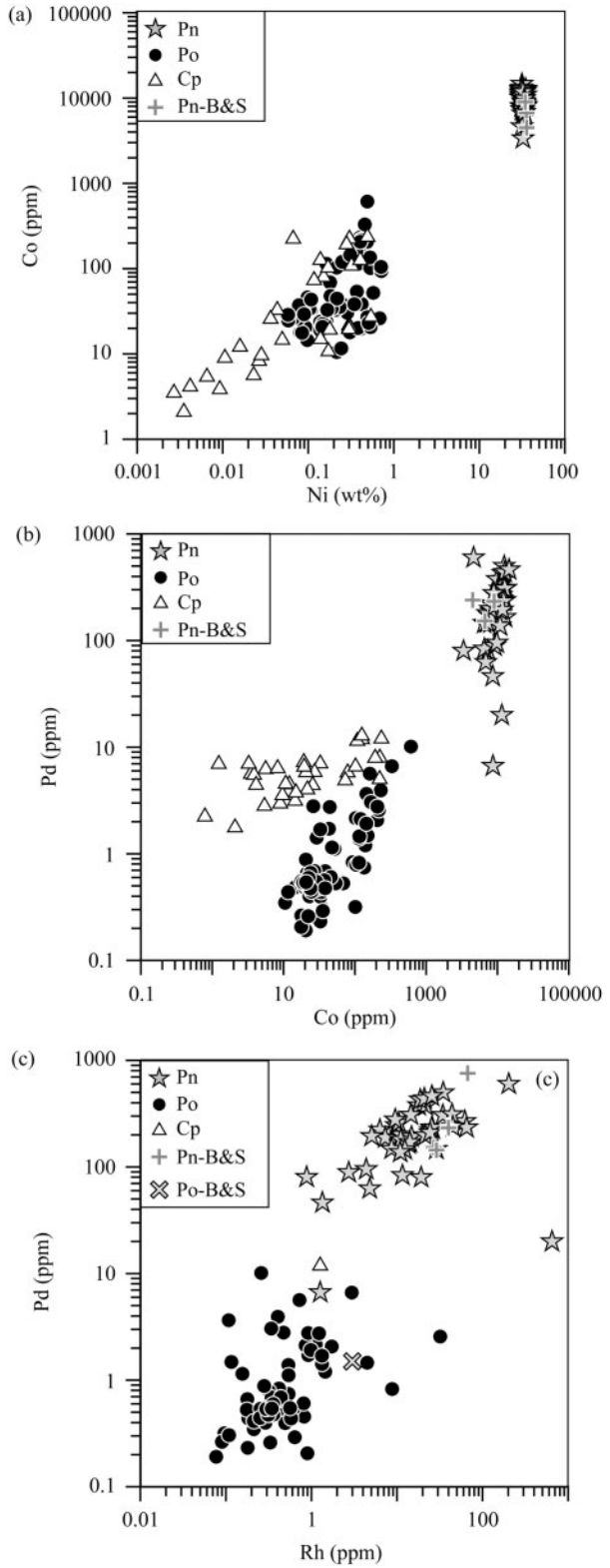


**Fig. 8.** Binary variation diagrams of (a) Co vs Ni, (b) Pd vs Co, and (c) Pd vs Rh. Results obtained by Ballhaus & Sylvester (2000) were added as comparison (Pn-B&S for pentlandite and Po-B&S for pyrrhotite).

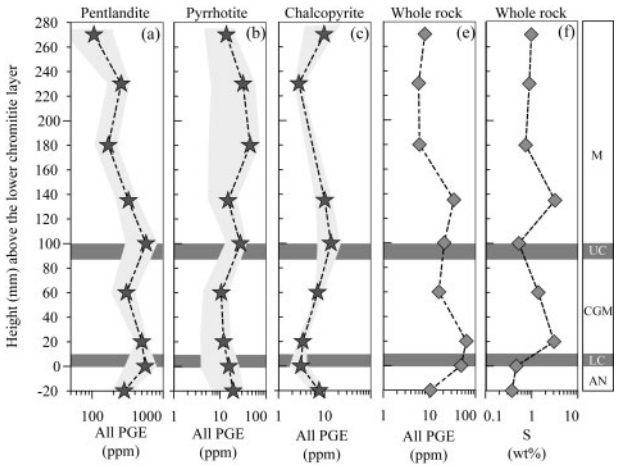


**Fig. 9.** Stratigraphic variation of PGE contents in the base-metal sulphide minerals and in the whole-rock.

~1 to ~235 ppm of Co, with most values in the 1–30 ppm level (Fig. 8a, b and Table 6).

Palladium contents of pentlandite are in the 50–600 ppm range (Fig. 8b and Table 6). Pyrrhotite and chalcopyrite contain less Pd, with values of ~0·1 to ~10 ppm and ~3 to ~15 ppm, respectively.

Most of the Rh was found to be present in pentlandite (Fig. 8c and Table 6), with most grains containing 1–100 ppm Rh. In contrast, most pyrrhotites contain ~0·3 to ~1 ppm Rh. The concentration of Rh in chalcopyrite is generally <0·2 ppm.

The available data thus suggest that, during exsolution of pentlandite from Mss, Ni, Co and Pd partitioned into pentlandite. The lack of correlation between Ir and Rh and the high concentration of Rh in pentlandite suggest that Rh also diffused into the pentlandite rather than into the pyrrhotite. The Pd content in the product of Mss exsolution (pentlandite and pyrrhotite) increases with the Co content. This feature is not observed for chalcopyrite (derived from Cu-rich sulphide liquid).

## Stratigraphic variation of the PGE in the BMS

In addition to variation in PGE content between different BMS there is also some systematic variation in the PGE content of individual BMS depending on their stratigraphic position. The total PGE and more particularly the Pd content in pentlandite and pyrrhotite are highest at the level of the chromitite layers, mirroring the pattern of the whole-rocks (Fig. 9).

## Mass balance of PGE in BMS calculation

To determine what percentages of PGE are present in BMS, the whole-rock concentrations of Ni, Cu, S, Co, PGE and Au have been determined (Table 5).

The percentage ($P_{Sul}i$) of each PGE ($i$) in a given BMS was calculated as follows:

$$(P_{Sul}i) = (F_{Sul}C_{Sul}{}^{i}/C_{WR}{}^{i}) \times 100$$

where $F_{Sul}$ is the weight fraction of the BMS considered (the same as the calculation for the proportion of each BMS above), $C_{Sul}{}^{i}$ is the concentration of the element $i$ in the BMS considered, and $C_{WR}{}^{i}$ is the concentration of the element $i$ in the whole-rock. The results obtained for each BMS in each lithology are summarized in Table 7.

In all lithologies relatively little (0·1 to ~10 wt%) Au and Pt are present in BMS (Table 7 and Fig. 10). In most rock types Pd and Rh are predominantly (50–100%) present in BMS (Table 7 and Fig. 10). A large proportion (35–72%) of the Os, Ir and Ru in the silicate rocks is present in BMS. However, in the chromitite layers a far smaller proportion (0·2 to ~12%) of Os, Ir, Ru, Pt and Au is found in BMS (Table 7 and Fig. 10). If we considered all the PGE, only ~15% (in the chromitites) to ~40% (in the silicate rocks) of these elements are present in BMS. This indicates that phases other than the BMS accommodate the PGE.

It is well known that there are numerous platinum-group minerals (PGM) present in the Merensky Reef (Vermaak & Hendriks, 1976; Kinloch, 1982; Kinloch & Peyerl, 1990; Prichard *et al.*, 2004) and during the laser ablation we observed PGE inclusions in the BMS. To investigate whether the PGM and inclusions may account for the 'missing' PGE we studied the PGM and PGE-rich inclusions present in our samples.

## Platinum-group minerals

Backscattered electron (BSE) image analysis of four sections representing different lithologies (lower chromitite, coarse-grained melanorite, upper chromitite and melanorite) was carried out using the scanning electron microprobe at Laval University (Quebec City). A total of 222 PGM (Table 8) and myrmekitic-like structures (Fig. 11) of isoferroplatinum ($Pt_3Fe$) were found. As these PGM are very small, quantitative analysis was carried out only on a few grains (Table 9). The other PGM were characterized using energy-dispersive spectra. Only the PGM with a diameter >0·5 μm are visible in the BSE images and are taken into account for the further calculations. Six types of PGM were found (Table 10): (1) Pt sulphide; (2) Pt–Pd sulphide; (3) Pt–Pd telluride; (4) Ru–Ir-Os sulphide; (5) Pt–Fe alloy; (6) Pt. The distribution of the PGM varies as a function of lithology and they are found in five different textural modes (Tables 8 and 10): at the BMS–silicate boundaries; included in BMS; included in silicate; at the chromite–BMS contact; included in chromite.

In the silicate rocks, most of the PGM (~83%) are Pt–Pd tellurides or bismuthotellurides (Fig. 11c), the majority of which are included in BMS (~53%) or located at the contact between silicate and BMS (~32%). The others (~14%) are included in silicates. In the chromitite layers Pt–Pd tellurides represent only a minority (~12%) of the PGM. Most of them are located at silicate–BMS boundaries (~63%). The remainder are included in BMS (~25%) or associated with alteration silicates (~13%).

Pt–Fe alloy (isoferroplatinum) occurs in two forms: (1) as a myrmekitic-like structure associated with pyrrhotite (Fig. 11a); (2) as euhedral grains (Fig. 11b). The myrmekitic-like structure is composed of small (~1–2 μm) ragged grains of isoferroplatinum, of vertical networks of isoferroplatinum of ~4 μm width in the central part of the structure and of euhedral grains (up to 10 μm) near the border of the myrmekitic-like structure. Euhedral grains of Pt–Fe alloy with a composition similar to those of the myrmekitic-like structure have also been observed in other parts of the silicate and chromite-rich rocks. In both melanorites, Pt–Fe grains are located at the contact between silicates and BMS (pyrrhotite in general). In the chromitite layers, the few Pt–Fe grains that were found are included in BMS or located at the contact between chromite and BMS.

Pt–Pd sulphides (Fig. 11f) were found in the all rock types. In the silicate rocks, they represent only ~5% of the PGM observed. Most of them are located at the boundaries between BMS and silicate (~50%). The others are surrounded by silicates (~38%) or included in BMS (~12%). In contrast, in the chromitite layers, Pt–Pd sulphides represent ~63% of the PGM which are essentially (~63%) located at the contact between the BMS and the chromites. The other grains are included in BMS (~21%) or located between BMS and silicates. Only one grain was found included in a chromite grain.

Other types of PGM were also observed, but they represent only a minor proportion of the total PGM content. Several grains of rustenburgite (Pt–Pd–Sn-rich PGM, Fig. 11e) were observed in the chromitites (in total 10 grains located at silicate–BMS or BMS–chromite boundaries) and in the melanorite (three grains associated with or included in BMS). Two grains of laurite (Ru–Ir-Os sulphide, Fig. 11d) were found in the lower chromitite layer: a euhedral grain, which is included in a chromite grain, and ragged grain, which is associated with alteration silicates. Two small grains of platinum were also observed.

## Inclusions of PGE-rich phases

During laser ablation, signals from 30 micro-inclusions enriched in PGE were observed in the BMS (~20% of grains contain inclusions) or at the contact between the BMS and the silicates. The inclusions are found in all lithologies (anorthosite, chromitites and melanorites). Pentlandite and pyrrhotite are the principal hosts of the inclusions; however, some inclusions have been observed in chalcopyrite.

*Table 7: Calculated proportions of each PGE in the base-metal sulphides*

| Sample | Sulphide | Os (%) | Ir (%) | Ru (%) | Rh (%) | Pt (%) | Pd (%) | Au (%) | All PGE (%) |
|---|---|---|---|---|---|---|---|---|---|
| AN | Pyrrhotite | 10·4 | 11·7 | 5·8 | 0·7 | 0·3 | 0·1 | 0·0 | 0·7 |
| | Pentlandite | 13·9 | 14·4 | 6·3 | 12·8 | 1·2 | 22·1 | 0·3 | 10·2 |
| | Chalcopyrite | 0·1 | 0·0 | 0·0 | 0·0 | 0·0 | 0·5 | 0·0 | 0·2 |
| | All sulphide | 23·7 | 25·3 | 11·8 | 13·0 | 1·5 | 21·8 | 0·4 | 10·7 |
| LC | Pyrrhotite | 1·7 | 1·2 | 0·3 | 0·0 | 0·0 | 0·0 | 0·0 | 0·1 |
| | Pentlandite | 3·6 | 9·6 | 2·5 | 31·8 | 0·2 | 50·0 | 0·0 | 7·7 |
| | Chalcopyrite | 0·0 | 0·0 | 0·0 | 0·0 | 0·0 | 0·2 | 0·1 | 0·0 |
| | All sulphide | 5·2 | 10·8 | 2·8 | 31·8 | 0·2 | 50·2 | 0·1 | 7·8 |
| CGM-1 | Pyrrhotite | 25·4 | 13·3 | 7·3 | 1·2 | 0·1 | 0·2 | 0·0 | 0·8 |
| | Pentlandite | 35·3 | 37·6 | 37·5 | 74·2 | 0·9 | 105·7 | 0·0 | 31·5 |
| | Chalcopyrite | 0·0 | 0·2 | 0·0 | 0·0 | 0·0 | 0·2 | 0·0 | 0·1 |
| | All sulphide | 60·7 | 51·1 | 44·9 | 75·4 | 1·0 | 106·1 | 0·0 | 32·3 |
| CGM-2 | Pyrrhotite | 26·7 | 18·3 | 9·4 | 1·1 | 0·1 | 0·2 | 0·0 | 0·9 |
| | Pentlandite | 38·5 | 43·0 | 15·7 | 50·3 | 1·2 | 64·6 | 0·0 | 27·1 |
| | Chalcopyrite | 0·1 | 0·0 | 0·0 | 0·0 | 0·0 | 1·5 | 0·0 | 0·6 |
| | All sulphide | 65·3 | 61·3 | 25·2 | 51·4 | 1·3 | 66·3 | 0·0 | 28·6 |
| UC | Pyrrhotite | 5·2 | 8·1 | 1·0 | 3·4 | 0·1 | 0·2 | 0·0 | 0·6 |
| | Pentlandite | 4·4 | 4·9 | 0·8 | 95·3 | 0·2 | 72·8 | 0·0 | 19·6 |
| | Chalcopyrite | 0·0 | 0·1 | 0·0 | 0·5 | 0·2 | 0·7 | 0·2 | 0·3 |
| | All sulphide | 9·7 | 13·1 | 1·9 | 99·2 | 0·5 | 73·7 | 0·2 | 20·5 |
| M1 | Pyrrhotite | 40·1 | 24·1 | 6·7 | 1·6 | 0·1 | 0·5 | 0·0 | 1·8 |
| | Pentlandite | 25·2 | 19·9 | 4·7 | 62·1 | 3·0 | 102·8 | 0·1 | 41·6 |
| | Chalcopyrite | 0·4 | 0·1 | 0·8 | 0·0 | 0·0 | 0·5 | 0·0 | 0·2 |
| | All sulphide | 65·7 | 44·2 | 12·2 | 63·7 | 3·1 | 103·8 | 0·1 | 43·7 |
| M2 | Pyrrhotite | 69·3 | 40·7 | 53·2 | 16·5 | 0·6 | 4·4 | 0·1 | 7·3 |
| | Pentlandite | 28·9 | 27·5 | 21·3 | 59·3 | 1·6 | 54·6 | 0·0 | 24·8 |
| | Chalcopyrite | 0·0 | 0·0 | 0·0 | 0·0 | 0·0 | 0·0 | 0·0 | 0·0 |
| | All sulphide | 98·2 | 68·2 | 74·5 | 75·8 | 2·2 | 59·0 | 0·1 | 32·1 |
| M3 | Pyrrhotite | 45·8 | 56·6 | 23·4 | 3·3 | 1·9 | 0·4 | 0·0 | 5·3 |
| | Pentlandite | 16·2 | 19·9 | 8·4 | 49·2 | 38·3 | 88·0 | 0·1 | 54·7 |
| | Chalcopyrite | 0·2 | 0·2 | 0·0 | 0·0 | 0·0 | 0·4 | 0·0 | 0·2 |
| | All sulphide | 62·1 | 76·6 | 31·8 | 52·4 | 40·2 | 88·8 | 0·2 | 60·2 |
| M4 | Pyrrhotite | 43·7 | 12·5 | 32·8 | 0·8 | 0·1 | 0·2 | 0·0 | 1·9 |
| | Pentlandite | 15·4 | 17·5 | 11·8 | 29·9 | 0·3 | 55·8 | 0·1 | 16·6 |
| | Chalcopyrite | 3·2 | 4·0 | 3·7 | 0·0 | 0·0 | 0·9 | 0·1 | 0·5 |
| | All sulphide | 62·3 | 33·9 | 48·3 | 30·7 | 0·4 | 56·9 | 0·2 | 19·0 |
| Average CGM | Pyrrhotite | 26·0 | 15·8 | 8·4 | 1·2 | 0·1 | 0·2 | 0·0 | 0·8 |
| | Pentlandite | 36·9 | 40·3 | 26·6 | 62·3 | 1·0 | 85·2 | 0·0 | 29·3 |
| | Chalcopyrite | 0·0 | 0·1 | 0·0 | 0·0 | 0·0 | 0·8 | 0·0 | 0·3 |
| | All sulphide | 63·0 | 56·2 | 35·0 | 63·4 | 1·1 | 86·2 | 0·0 | 30·4 |
| Average M | Pyrrhotite | 49·7 | 33·5 | 29·0 | 5·6 | 0·7 | 1·4 | 0·0 | 4·1 |
| | Pentlandite | 21·4 | 21·2 | 11·6 | 50·1 | 10·8 | 75·3 | 0·1 | 34·4 |
| | Chalcopyrite | 0·9 | 1·1 | 1·1 | 0·0 | 0·0 | 0·4 | 0·0 | 0·2 |
| | All sulphide | 72·1 | 55·7 | 41·7 | 55·6 | 11·5 | 77·1 | 0·2 | 38·8 |
| Average chromitite | Pyrrhotite | 3·4 | 4·7 | 0·7 | 1·7 | 0·1 | 0·1 | 0·0 | 0·3 |
| | Pentlandite | 4·0 | 7·2 | 1·7 | 63·5 | 0·2 | 61·4 | 0·0 | 13·7 |
| | Chalcopyrite | 0·0 | 0·0 | 0·0 | 0·3 | 0·1 | 0·5 | 0·1 | 0·1 |
| | All sulphide | 7·5 | 11·9 | 2·3 | 65·5 | 0·3 | 62·0 | 0·2 | 14·1 |

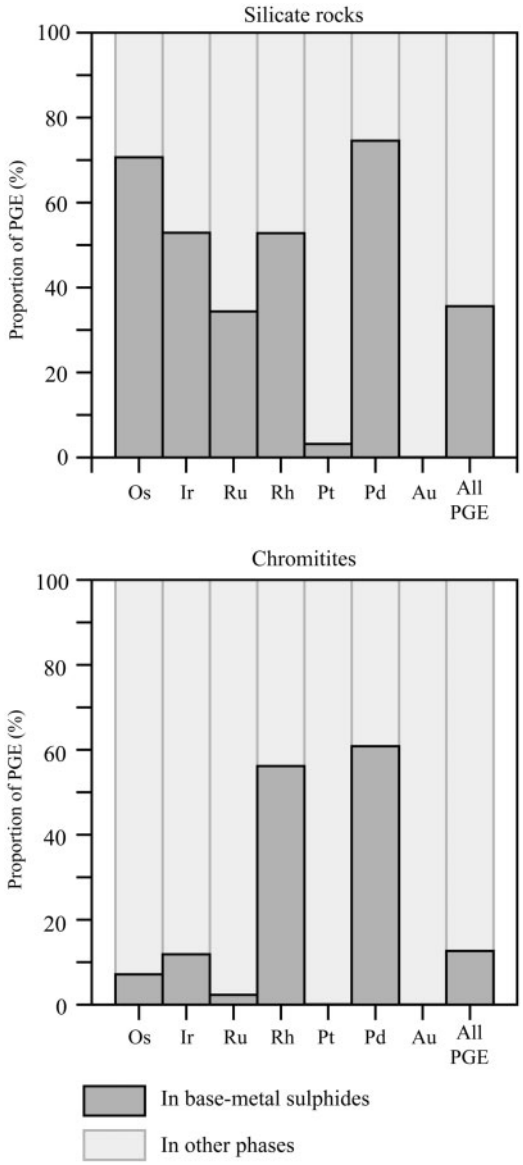


**Fig. 10.** Proportion of PGE in base-metal sulphides and other phases.

The most common inclusions are Pt-rich. In many cases, Pt is associated with other PGE (Ir, Os, Re, Ru and Rh). Typical Pt-rich inclusions are: (1) Pt (Fig. 12b); (2) Pt–Ir with minor Os–Rh–Re (Fig. 12d). Pt may also occur in minor amounts in inclusions dominated by Ir or Re (Fig. 12c, e and f). Most Pt inclusions are found at the contact between the BMS and the silicate minerals. Iridium in Ir-rich inclusions is found associated with Ru, Os and in some cases with Rh (Fig. 12e and f). These inclusions are most common in the chromitite layers. In the melanorite, one inclusion enriched in Re was found. In that case, Re was associated with minor Ir, Os and Pt (Fig. 12c). Another common type of inclusion consists of Ag inclusions. Silver can be found associated with Au and Pd (Fig. 12a). No other inclusion enriched in Pd was observed. By considering the PGM described above and relative abundances of PGM reported from the Merensky Reef by other workers (Kinloch, 1982; Viljoen & Hieber, 1986; Prichard *et al.*, 2004), we can infer some of the possible PGM found in the observed inclusions. The Pt-rich inclusions could be Pt–Fe alloy, Pt sulphide, Pt telluride and/or Pt arsenide commonly observed in the Merensky Reef (Vermaak & Hendriks, 1976; Kinloch, 1982; Viljoen & Hieber, 1986; Prichard *et al.*, 2004). Iridium, Ru and Os inclusions could be laurite, Pt–Ir–Rh inclusions could be the unknown Pt–Cu–Ir–Rh–S PGM of Viljoen & Hieber (1986) and Ag–Pd–Au could be palladian electrum.

The size of the inclusions (assumed to be cubic in shape; see Appendix B) observed in the time-resolved analysis was roughly estimated using ablation rates in BMS and time-resolved analysis (Fig. 13 and Appendix B). Details of the methods and results are given in Appendix B. Most (~80%) of the inclusions observed during laser ablation are ~1 to ~4 μm in length. These results are similar to the size of the PGM observed in the BSE image analysis of the 222 PGM described above (Fig. 13). The size of our inclusions is considerably larger than those reported by Ballhaus & Sylvester (2000). Inspection of their data suggests to us that a calculation error was made in their paper, and applying the method outlined in Appendix B to their data we find that the size of their inclusions is similar to ours. This is important in the interpretation of the inclusions, as we suggest that they represent exsolution of PGM from the BMS, whereas Ballhaus & Sylvester (2000) suggested that they represent PGE clusters or micronuggets captured by sulphide liquid.

## Estimation of the contribution of the PGM

### *Principle*

The goal of the following calculation is to use the PGM (as determined by BSE images and geochemical analysis) to evaluate the possible PGE mass balance between these PGM, the PGE contents in the BMS and the whole-rock data. The details of the method for image analysis are given in Appendix A. The results of the calculations are given in Tables 11 and 12.

### *Results*

The results of the mass balance calculations are summarized in Table 13. For all rock types Pt and Pd concentrations in the whole-rock can be accounted for by combination of Pd and Pt in the BMS and PGM associated with the BMS, with most Pt present in PGM and most of the Pd present in BMS (Table 13). For the coarse-grained melanorite, the results do not take into account the myrmekitic-like structure. The calculation was also made including this structure and this considerably overestimates the amount of Pt present in the whole-rock, which probably reflects

*Table 8: Type of association of the PGM in the analysed rock types*

| | Sulphide–silicate contact | Included in sulphide | Included in silicate | Chromite–sulphide contact | Included in chromitite | Total |
|---|---|---|---|---|---|---|
| *Melanorite (M1)* | | | | | | |
| PGM BiTe | 33 | 53 | 6 | | | 92 |
| PGM sulphide | 1 | | | | | 1 |
| Pt–Fe | 1 | | | | | 1 |
| Pt | 1 | | | | | 1 |
| All PGM | 36 | 53 | 6 | | | 95 |
| *Upper chromitite* | | | | | | |
| PGM sulphide | 5 | 6 | | 6 | | 17 |
| Pt–Pd–Sn–S | 10 | | | | | 10 |
| All PGM | 15 | 6 | | 6 | | 27 |
| *Coarse-grained melanorite* | | | | | | |
| PGM BiTe | 8 | 16 | 12 | | | 36 |
| PGM sulphide | 1 | 1 | | | | 2 |
| Pt–Fe* | 13 | | | | | 13 |
| Pt–Pd–Sn–S | 2 | 1 | | | | 3 |
| All PGM | 24 | 18 | 12 | | | 54 |
| *Lower chromitite* | | | | | | |
| PGM BiTe | 5 | 2 | 1 | | | 8 |
| PGM sulphide | 1 | 3 | | 21 | 1 | 26 |
| Pt–Fe | | 1 | | 1 | | 2 |
| Pt–Pd–Sn–S | | | | 2 | | 2 |
| Ru–Ir–Os–S | | | 1 | | 1 | 2 |
| Pt | | | | | 1 | 1 |
| All PGM | 6 | 6 | 2 | 24 | 3 | 41 |
| *Anorthosite* | | | | | | |
| PGM sulphide | 2 | | 3 | | | 5 |
| All PGM | 2 | | 3 | | | 5 |
| *All rock types* | | | | | | |
| PGM BiTe | 46 | 71 | 19 | | | 136 |
| PGM sulphide | 10 | 10 | 3 | 27 | 1 | 51 |
| Pt–Fe | 14 | 1 | | 1 | | 16 |
| Pt–Pd–Sn–S | 12 | 1 | | 2 | | 15 |
| Ru–Ir–Os–S | | | 1 | | 1 | 2 |
| Pt | 1 | | | | 1 | 2 |
| All PGM | 83 | 83 | 23 | 30 | 3 | 222 |

*The myrmekitic-like structure (Fig. 10a) was not taken into account in this calculation.

the fact that this kind of structure is rarely observed in thin section in the Merensky Reef (Kingston & El-Dosuky, 1982).

Although in some rocks the Os, Ir, Ru and Rh present in BMS and associated PGM accounts for most of these elements, there is a persistent tendency for a shortfall (Table 13). The worse case for this is the upper chromitite for Os, Ir and Ru and the lower chromitite for Rh. Some experimental work (Righter *et al.*, 2004) suggested that iridium-like platinum-group element (IPGE) partition into chromite.

If we consider this possibility, the amount of Ir, Os, Ru and Rh required to be present in the chromite to achieve a mass balance is ~0·1 to ~0·5 ppm Ir, ~0·3 to ~0·4 ppm Os, ~2·7 to ~2·9 ppm Ru and ~4·1 to ~4·35 ppm Rh (calculation made using both chromitite layers).

*Table 9: Composition of platinum-group minerals found in the Merensky Reef at Rustenburg Platinum Mine*

| Point* | Mineral | Sulphide host | Ni (wt %) | Fe (wt %) | Pt (wt %) | Cu (wt %) | Te (wt %) | Pd (wt %) | Bi (wt %) | Total (wt %) | Ni (at. %) | Fe (at. %) | Pt (at. %) | Cu (at. %) | Te (at. %) | Pd (at. %) | Bi (at. %) |
|---|---|---|---|---|---|---|---|---|---|---|---|---|---|---|---|---|---|
| 1 | Pt–Fe alloy | Pyrrhotite | 0·03 | 9·61 | 90·61 | 0·10 | n.d. | 0·01 | n.d. | 100·4 | 0·09 | 26·94 | 72·70 | 0·26 | n.d. | 0·01 | n.d. |
| 2 | Pt–Fe alloy | Pyrrhotite | 0·11 | 9·02 | 91·05 | 0·25 | n.d. | n.d. | 0·02 | 100·4 | 0·29 | 25·48 | 73·61 | 0·61 | n.d. | n.d. | 0·02 |
| 3 | Pt–Fe alloy | Pyrrhotite | 0·23 | 10·41 | 91·14 | 0·11 | n.d. | 0·09 | n.d. | 102·0 | 0·60 | 28·24 | 70·77 | 0·27 | n.d. | 0·13 | n.d. |
| 4 | Pt–Fe alloy | Pyrrhotite | 0·14 | 10·51 | 89·45 | 0·15 | n.d. | 0·06 | n.d. | 100·3 | 0·36 | 28·86 | 70·34 | 0·35 | n.d. | 0·09 | n.d. |
| | Pt–Fe alloy | Pyrrhotite | n.d. | 9·13 | 91·14 | 0·14 | n.d. | 0·02 | n.d. | 100·4 | n.d. | 25·83 | 73·79 | 0·36 | n.d. | 0·03 | n.d. |
| | Pt–Fe alloy | Pyrrhotite | 0·18 | 9·74 | 91·47 | 0·39 | n.d. | 0·04 | 0·00 | 101·8 | 0·47 | 26·72 | 71·81 | 0·94 | n.d. | 0·05 | 0·00 |
| | Pt–Pd–Bi–Te | Pyrrhotite | 0·19 | 0·01 | 18·60 | n.d. | 50·01 | 13·93 | 14·29 | 97·0 | 0·46 | 0·03 | 13·82 | n.d. | 56·81 | 18·97 | 9·91 |
| | Pt–Pd–Bi–Te | Pyrrhotite | n.d. | 0·05 | 0·48 | n.d. | 33·91 | 37·22 | 24·56 | 96·2 | n.d. | 0·11 | 0·34 | n.d. | 36·09 | 47·50 | 15·96 |
| | Pt–Pd–Bi–Te | Pyrrhotite | 0·29 | 0·34 | 34·27 | n.d. | 45·94 | 2·80 | 14·86 | 98·6 | 0·76 | 0·95 | 27·20 | n.d. | 55·76 | 4·07 | 11·01 |
| | Pt–Pd–Bi–Te | Pentlandite | 0·23 | 0·49 | 37·22 | n.d. | 42·10 | n.d. | 18·41 | 98·5 | 0·64 | 1·40 | 30·63 | n.d. | 52·96 | n.d. | 14·14 |
| | Pt–Pd–Bi–Te | Pyrrhotite | 0·21 | 0·03 | 18·25 | n.d. | 49·26 | 13·82 | 14·34 | 95·9 | 0·51 | 0·08 | 13·71 | n.d. | 56·60 | 19·05 | 10·06 |

n.d., not detected.
*Position shown in Fig. 10a.

*Table 10: Type of association of the PGM as percentages of the total of PGM in the silicate rocks and the chromitites*

| | Sulphide–silicate contact | Included in sulphide | Included in silicate | Chromite–sulphide contact | Included in chromitite | Total |
|---|---|---|---|---|---|---|
| *Silicate rocks** | | | | | | |
| PGM Bi-Te | 32 | 54 | 14 | 0 | 0 | 100 |
| PGM sulphide | 50 | 13 | 38 | 0 | 0 | 100 |
| Pt-Fe | 100 | 0 | 0 | 0 | 0 | 100 |
| Pt-Pd-Sn-S | 67 | 33 | 0 | 0 | 0 | 100 |
| Pt | 100 | 0 | 0 | 0 | 0 | 100 |
| All PGM | 40 | 46 | 14 | 0 | 0 | 100 |
| *Chromitites*† | | | | | | |
| PGM Bi-Te | 63 | 25 | 13 | 0 | 0 | 100 |
| PGM sulphide | 14 | 21 | 0 | 63 | 2 | 100 |
| Pt-Fe | 0 | 50 | 0 | 50 | 0 | 100 |
| Pt-Pd-Sn-S | 83 | 0 | 0 | 17 | 0 | 100 |
| Ru-Ir-Os-S | 0 | 0 | 50 | 0 | 50 | 100 |
| Pt | 0 | 0 | 0 | 0 | 100 | 100 |
| All PGM | 31 | 18 | 3 | 44 | 4 | 100 |

*Anorthosite, coarse-grained melanorite and melanorite.
†Lower and upper chromitites.

Assuming that the magma from which the Merensky Reef formed contained ~0·3 ppb Os and Ir, 1·8 ppb Ru and 1 ppb Rh (Barnes & Maier, 2002*a*) then these values imply partition coefficients between silicate liquid and chromite of 1000–2000 for Os, Ir and Ru, and ~4200 for Rh. These partition coefficients are 10 times greater than those determined both experimentally (Righter *et al.*, 2004) and empirically (Puchtel *et al.*, 2004). This seems too large a discrepancy to us to accept and thus we do not consider that the 'missing' IPGE are present in the chromite structure (Puchtel *et al.*, 2004).

In the lower chromitite layer two grains of laurite were observed and these could account for the balance of IPGE in this sample. However, no phases highly enriched in Ru,

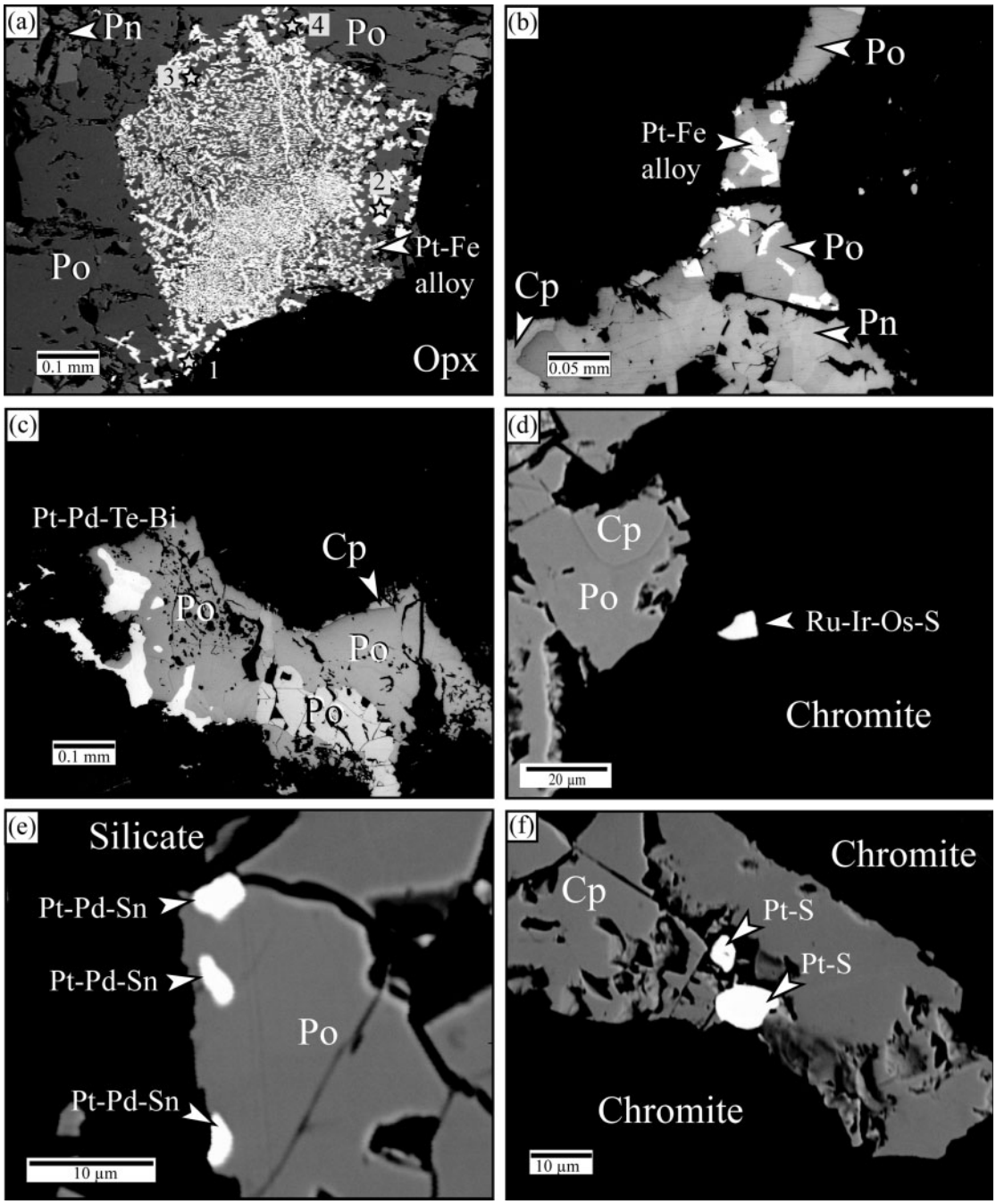


**Fig. 11.** Backscattered electron images of platinum-group minerals observed in Merensky Reef samples at Rustenburg Platinum Mine. (a) Myrmekitic and euhedral Pt–Fe alloy (isoferroplatinum) found associated with pyrrhotite (Po) and also developed at the contact between pyrrhotite and orthopyroxene (Opx). Stars represent the location of the microprobe analysis (Table 8). (b) Euhedral isoferroplatinum (Pt3Fe) included in pyrrhotite. (c) Platinum-group bismuthotellurides found at the contact between silicate and pyrrhotite. (d) Laurite (Ru–Ir–Os–S) included in chromite grains. (e) Rustenburgite (Pt–Pd–Sn) included in pyrrhotite or located at the contact between pyrrhotite and silicate. (f) Pt sulphide (Pt–S) included in chalcopyrite or located at the contact between chromite and sulphide. Opx, orthopyroxene; Po, pyrrhotite; Pn, pentlandite; Cp, chalcopyrite.

Ir, Os, Rh or Au (PGM or alloys) were observed in the other three rocks. Nonetheless, several zones enriched in these elements (Fig. 12) were observed during the laser ablation of the BMS. We interpret these zones to represent laurite inclusions. Laurite has been observed in Merensky Reef samples by many workers (Kingston & El-Dosuky, 1982; Kinloch, 1982; Viljoen & Hieber, 1986; Kinloch & Peyerl, 1990; Prichard *et al.*, 2004) and only a small

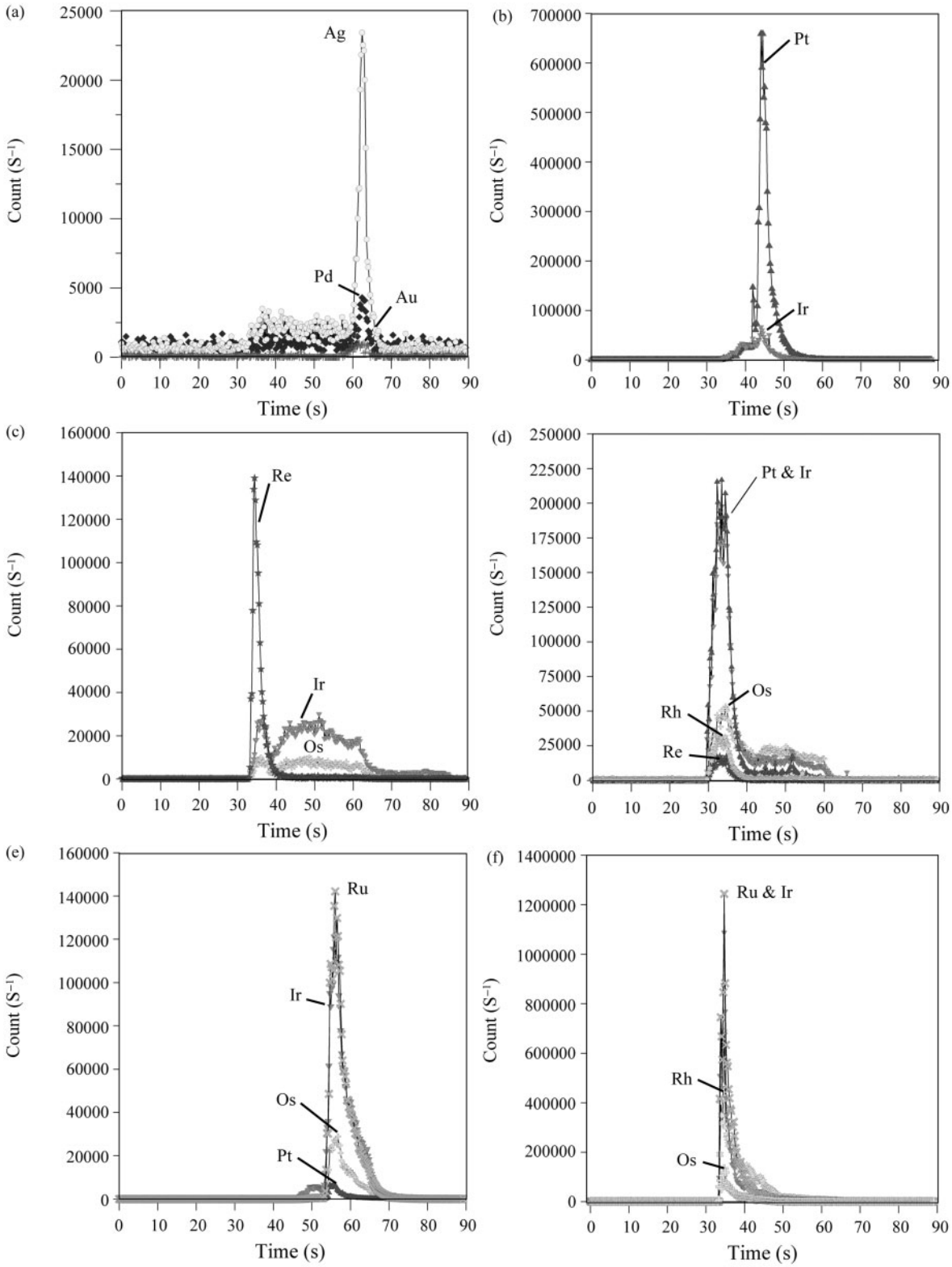


**Fig. 12.** Types of PGE-rich inclusion phases found associated with the base-metal sulphide minerals. (a) Inclusion of Ag, Pd and Au in pyrrhotite. (b) Inclusion of platinum associated with pentlandite. (c) Inclusion of Re, Ir and minor Os and Pt associated with pyrrhotite. (d) Inclusion of Pt–Ir, Os, Rh and Re associated with pyrrhotite. (e) Inclusion of Ir, Ru, Os and minor Pt associated with pyrrhotite. (f) Inclusion of Ir, Ru, Rh with minor Os associated with pyrrhotite.

quantity (~65 μg) is needed to satisfy our mass balance. This represents in our samples about 10 grains of laurite of 10 μm diameter.

The mass balance for Au indicates that only a very small quantity is accounted by the BMS. Furthermore, only one grain of Au was observed in thin section. However, zones enriched in Pd, Ag and Au were observed during laser ablation, suggesting that palladian electrum is present. Kingston & El-Dosuky (1982) in their study of PGM mineralogy of the Rustenburg Mine reported 1 vol.% of this mineral. Our mass balance requires ~50 μg of electrum (Au–Ag alloy), equivalent in our samples to three grains of 10 μm diameter.

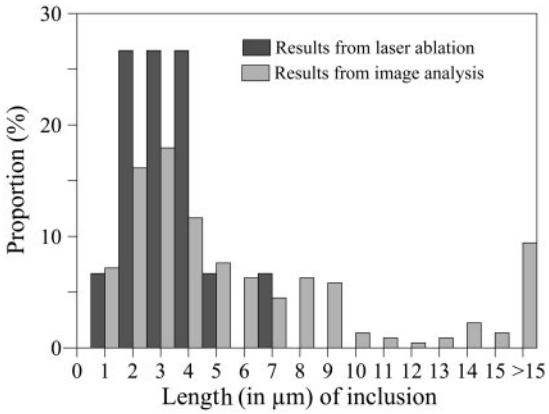


**Fig. 13.** Comparison between the size of inclusions observed during laser ablation and the size of the platinum-group mineral observed on thin sections.

In summary, 88% by volume of the PGM are included in or at the contact with BMS. The mass balance works considering the PGM and the BMS accounts for most Pt, Pd and Rh. To account for the Os, Ru, Ir and Au requires that some laurite and palladian electrum is present but rarely observed in thin section. There is evidence for these minerals in the time-resolved analysis from the laser ablation of the BMS. However, as the thin sections scanned for PGM analyses are not necessarily those that were used for the laser ablation and that we have probably not 'ablated' all the inclusions, we cannot conclude on their exact influence on mass balance.

## Modelling the role of sulphide liquid on PGE distribution

### *Principle*

The model of collection of the PGE by a sulphide liquid presented by Campbell & Naldrett (1979) is based on the assumption that PGE and others metals have a large partition coefficient with respect to the sulphide liquid and that the PGE concentration in sulphides is dependent on the relative volume of magma that interacted with the sulphide liquid. In a closed system, the concentration of an element

*Table 11: Summary of calculated parameters for the estimation of the PGM contribution*

| Lithology | $V_{Litho}$ ($cm^3$) | Proportion of major phases (vol.%) | | | | Volume of each PGM ($\times 10^{-6} cm^3$) | | | | | | | |
|---|---|---|---|---|---|---|---|---|---|---|---|---|---|
| | | Px | Plg | Chr | S | Pt-Pd sulphide | Pt sulphide | Pt-Pd-Te | Ru-Ir-Os-S | Pt-Fe | Pt-Sn-S | Pt | Gold |
| LC | 1·24 | 8·8 | 40 | 50 | 1·2 | 7·17 | 10·96 | 1·98 | 9·68 | 1·5 | 0·2 | 0·07 | |
| CGM | 4·86 | 70 | 20 | 6·5 | 3·5 | 0·13 | 0·3 | 14·91 | | 33·5 | 0·3 | | 0·5 |
| UC | 3·96 | 23·5 | 25 | 50 | 1·5 | 30·68 | 2·55 | | | | 0·53 | | |
| M1 | 7·01 | 69 | 20 | 6 | 5 | 0·11 | | 94·4 | | 0·04 | | 0·6 | |

*Table 12: Calculated PGM and PGE mass from the BSE image analysis*

| Lithology | Calculated PGM mass (μg) | | | | | | | | Calculated PGE mass (μg) | | | | | |
|---|---|---|---|---|---|---|---|---|---|---|---|---|---|---|
| | Pt-Pd-S | Pt-S | Pt-Pd-Te | Ru-Ir-Os-S | Pt-Fe | Pt-Sn-S | Pt | Au | Pt | Pd | Ru | Ir | Os | Au |
| LC | 147·6 | 243·5 | 44·2 | 136·9 | 60·1 | 8 | 2·9 | | 384·9 | 20·8 | 62·0 | 7·5 | 8·2 | |
| CGM | 0·8 | 1·9 | 94·4 | | 380·4 | 3·4 | | 5·5 | 388·8 | 0·3 | | | | 5·5 |
| UC | 192·4 | 17·25 | | | | 6·4 | | | 146·6 | 24·8 | | | | |
| M1 | 0·4 | | 429·7 | | 0·3 | | 4·9 | | 190·3 | 0·9 | | | | |

*Table 13: Mass balance calculation between PGM image analysis,* in situ *and whole-rock PGE analysis*

| Data | Unit | Os | Ir | Ru | Rh | Pt | Pd | Au |
|---|---|---|---|---|---|---|---|---|
| *Lower chromitite* | | | | | | | | |
| Whole-rock content | μg | 7·30 | 11·10 | 54·10 | 38·00 | 331·00 | 44·00 | 3·40 |
| | error | 0·37 | 0·56 | 2·71 | 1·90 | 16·55 | 2·20 | 0·17 |
| *In situ* sulphide* | μg | 0·36 | 1·17 | 1·48 | 11·77 | 0·55 | 21·52 | 0·00 |
| | error | 0·04 | 0·12 | 0·15 | 1·18 | 0·06 | 2·15 | 0·00 |
| | % WR | 5·0 | 10·5 | 2·7 | 31·0 | 0·2 | 48·9 | 0·1 |
| PGE due to PGM analysis | μg | 8·21 | 7·53 | 62·00 | | 385·00 | 20·86 | |
| | error | 1·64 | 1·51 | 12·40 | | 77·00 | 4·17 | |
| | % WR | 112·5 | 67·8 | 114·6 | | 116·3 | 47·4 | |
| *In situ* sulphide and PGM analysis | μg | 8·57 | 8·70 | 63·48 | 11·77 | 385·55 | 42·38 | 0·00 |
| | error | 1·40 | 1·21 | 12·55 | 1·18 | 77·06 | 6·32 | 0·00 |
| | % WR | 117·4 | 78·3 | 117·3 | 31·0 | 116·5 | 96·3 | 0·1 |
| | error% | 19 | 11 | 23 | 3 | 23 | 14 | 0 |
| *Upper chromitite* | | | | | | | | |
| Whole-rock content | μg | 2·60 | 3·50 | 17·00 | 10·00 | 134·50 | 42·70 | 3·10 |
| | error | 0·13 | 0·18 | 0·85 | 0·50 | 6·73 | 2·14 | 0·16 |
| *In situ* sulphide* | μg | 0·11 | 0·17 | 0·14 | 9·31 | 0·49 | 30·64 | 0·01 |
| | error | 0·01 | 0·02 | 0·01 | 0·93 | 0·05 | 3·06 | 0·00 |
| | % WR | 4·4 | 4·8 | 0·8 | 93·1 | 0·4 | 71·8 | 0·2 |
| PGE due to PGM analysis | μg | | | | | 146·60 | 24·80 | |
| | error | | | | | 29·32 | 4·96 | |
| | % WR | | | | | 109·0 | 58·1 | |
| *In situ* sulphide and PGM analysis | μg | 0·11 | 0·17 | 0·14 | 9·31 | 146·49 | 54·64 | 0·01 |
| | error | 0·14 | 0·19 | 0·86 | 1·43 | 35·97 | 10·00 | 0·16 |
| | % WR | 4·4 | 4·8 | 0·8 | 93·1 | 109·4 | 129·8 | 0·2 |
| | error | 5 | 5 | 5 | 14 | 27 | 23 | 5 |
| *Coarse-grained melanorite* | | | | | | | | |
| Whole-rock content | μg | 5·8 | 5·8 | 25·3 | 13·4 | 420·8 | 162·9 | 25·6 |
| | error | 0·29 | 0·29 | 1·265 | 0·67 | 21·04 | 8·145 | 1·28 |
| *In situ* sulphide* | μg | 3·34 | 2·83 | 11·03 | 9·96 | 3·94 | 170·32 | 0·01 |
| | error | 0·33 | 0·28 | 1·10 | 1·00 | 0·39 | 17·03 | |
| | % WR | 57·5 | 48·8 | 43·6 | 74·4 | 0·9 | 104·6 | |
| PGE due to PGM analysis | μg | | | | | 388·80 | 0·29 | |
| | error | | | | | 77·76 | 0·06 | |
| | % WR | | | | | 92·4 | 0·2 | |
| *In situ* sulphide and PGM analysis | μg | 3·34 | 2·83 | 11·03 | 9·96 | 391·94 | 170·61 | 0·01 |
| | error | 0·33 | 0·28 | 1·10 | 1·00 | 77·99 | 17·09 | 0·00 |
| | % WR | 57·5 | 48·8 | 43·6 | 74·4 | 93·3 | 104·7 | 0·0 |
| | error | 6 | 5 | 4 | 7 | 19 | 10 | 0 |
| *Melanorite* | | | | | | | | |
| Whole-rock content | μg | 4·9 | 6·3 | 27·8 | 16·9 | 165·5 | 119 | 12·7 |
| | error | 0·25 | 0·32 | 1·39 | 0·85 | 8·28 | 5·95 | 0·64 |
| *In situ* sulphide* | μg | 3·04 | 2·64 | 3·22 | 10·65 | 5·06 | 122·37 | 0·01 |
| | error | 0·30 | 0·26 | 0·32 | 1·06 | 0·51 | 12·24 | 0·00 |
| | % WR | 62·0 | 42·0 | 11·6 | 63·0 | 3·1 | 102·8 | 0·1 |

(Continued)

*Table 13: Continued*

| Data | Unit | Os | Ir | Ru | Rh | Pt | Pd | Au |
|---|---|---|---|---|---|---|---|---|
| PGE due to PGM analysis | µg | | | | | 190·30 | 0·91 | |
| | error | | | | | 38·06 | 0·18 | |
| | % WR | | | | | 115·0 | 0·8 | |
| *In situ* sulphide and PGM analysis | µg | 3·04 | 2·64 | 3·22 | 10·65 | 195·36 | 123·28 | 0·01 |
| | error | 0·30 | 0·26 | 0·32 | 1·06 | 38·57 | 12·42 | 0·00 |
| | % WR | 62·0 | 42·0 | 11·6 | 63·0 | 118·0 | 103·6 | 0·1 |
| | error | 6 | 4 | 1 | 6 | 23 | 10 | 0 |

*Recalculated to whole-rock sulphur content.
All calculation are made on the basis of 10 g of sample. Details of the calculation are given in Appendix A.

in the sulphide ($C_{Sul}$) is given by the following equation (Campbell & Naldrett, 1979):

$$C_{Sul} = C_{Sil} D^{Sul/Sil}(R+1)/\left(R + D^{Sul/Sil}\right)$$

where $C_{Sil}$ is the concentration in the silicate liquid, $D^{Sul/Sil}$ is the partition coefficient (for each metal) between the sulphide and the silicate liquids, and $R$ is the ratio of silicate to sulphide liquid.

As sulphide liquid sinks throughout the magma column, Brügmann *et al.* (1993) have proposed that the sulphide liquid composition may be adequately modelled using the zone-refining equation. In this case, the concentration of an element in the sulphide ($C_{Sul}$) is given by Brügmann *et al.* (1993):

$$C_{Sul} = C_{Sil}\left\{D^{Sul/Sil} - \left(D^{Sul/Sil}\right)\exp\left[-\left(1/D^{Sul/Sil}N\right)\right]\right\}$$

where $N$ is the ratio of silicate to sulphide liquid (similar to $R$-factor).

These two equations can be applied to our data as follows: if the PGE were initially in the sulphide liquid, the contents of the PGE and others metal in the whole-rock can be modelled with the equation above. In the case where PGE crystallized directly as PGM, the PGE content would not be well modelled with these equations and, consequently, other processes are needed to explain the observed features.

### *Initial magma*

The Merensky Reef occurs in the Upper Critical Zone of the Bushveld Complex. According to Davis & Tredoux (1985) and Harmer & Sharpe (1985), the rocks from the Merensky Reef can be formed from two possible silicate liquids: a Mg-rich basaltic andesite and a tholeiitic basalt. The composition of magma used for the calculation is the mixed magma proposed by Barnes & Maier (2002*a*). This composition is given in Table 14.

### *Results of the modelling*

The two equations described above give relatively similar results. Parameters and results of the modelling using the equations proposed by Brügmann *et al.* (1993) are summarized in Table 14. The composition of the BMS in the silicate rocks of the Rustenburg Merensky Reef sample can be modelled using an $N$-factor of 45 000 and by considering that these rocks contain 1–8% sulphides (Fig. 13a and Table 14). These sulphide contents are consistent with whole-rock data (Table 6) and the results of X-ray tomography (Godel *et al.*, 2006).

In contrast to the silicate rocks, the PGE budget of the chromitite layers cannot be modelled by sulphide segregation alone. Using an $N$-factor of 45 000 and 1·5% sulphides (as observed in the whole-rocks), there is a mismatch between the model composition and the composition of the chromitites (Fig. 14a and b). The calculated composition contains lower Pt, Os, Ir, Ru, and Rh than the observed composition. It is possible to model the composition of the chromitite layers to contain 1·5 % sulphide liquid (with $N = 45\,000$) and 0·4 PGM% for the lower chromitite layer and 0·1 PGM% for the upper chromitite layer (Table 14). The assemblage of PGM used in the calculation consists of cooperite, laurite and malanite (Table 14). These PGM have to crystallize before an immiscible sulphide liquid has formed. Barnes & Maier (2002*a*) found a similar problem in matching the PGE content of the chromitite from the Impala Platinum Mine.

## DISCUSSION

In the light of our results any model for the formation of the reef needs to consider: (1) the association of the PGE and PGM with BMS; (2) the tendency of the BMS to distribute preferentially in the direction of the paleovertical; (3) the enrichment of IPGE, Rh and Pt relative to S, Ni, Pd and Au in the chromitite layers.

*Table 14: Results of sulphide liquid modelling*

| Parameters | Ni (ppm) | Os (ppb) | Ir (ppb) | Ru (ppb) | Rh (ppb) | Pt (ppb) | Pd (ppb) | Au (ppb) | Cu (ppb) |
|---|---|---|---|---|---|---|---|---|---|
| Initial magma† | 249 | 0·29 | 0·28 | 1·8 | 1·08 | 16·6 | 9·8 | 3 | 60 |
| $D^{Sil/Sul}$ | 550 | 40000 | 40000 | 40000 | 40000 | 40000 | 40000 | 20000 | 1000 |
| Modelled compositions for the silicate rocks | Ni (wt %) | Os (ppb) | Ir (ppb) | Ru (ppb) | Rh (ppb) | Pt (ppb) | Pd (ppb) | Au (ppb) | Cu (wt %) |
| $R = 45\,000$ | 13·70 | 7834 | 7564 | 48626 | 29175 | 448436 | 264739 | 81043 | 6 |
| Modelled compositions for the chromitite layers | Ni (wt %) | Os (ppb) | Ir (ppb) | Ru (ppb) | Rh (ppb) | Pt (ppb) | Pd (ppb) | Au (ppb) | Cu (wt %) |
| *Lower chromitite* | | | | | | | | | |
| $R = 45\,000$ sulphide + 0·4 PGM%* | 13·70 | 69434 | 84844 | 577266 | 191095 | 2478676 | 278739 | 53676 | 6·11 |
| *Upper chromitite* | | | | | | | | | |
| $R = 45\,000$ sulphide + 0·1 PGM%* | 13·70 | 23234 | 26884 | 180786 | 69655 | 955996 | 268239 | 53676 | 6·03 |

*Composition of the platinum-group minerals used in the calculation

| | Ni (wt %) | Os (wt %) | Ir (wt %) | Ru (wt %) | Rh (wt %) | Pt (wt %) | Pd (wt %) | Au (wt %) | Cu (wt %) | Proportion (%) |
|---|---|---|---|---|---|---|---|---|---|---|
| Cooperite‡ | 0·7 | | | | | 84 | 0·7 | | | 50 |
| Laurite‡ | | 5·5 | 6·9 | 47·2 | | | | | | 28 |
| Malanite§ | | | | | 18·4 | 39·8 | | | 12·4 | 22 |

†Mixed magma (Barnes & Maier, 2002).
‡Kingston & El-Dosuky (1982).
§Cabri (2002).
$D^{Sil/Sul}$, partition coefficient between silicate and sulphide liquids.

Five possible processes, which are not necessarily mutually exclusive, could be considered as important in the origin of the Merensky Reef: (1) collection of the PGE by an immiscible sulphide liquid; (2) partitioning of the IPGE into chromite; (3) crystallization of the PGM directly from the magma; (4) loss of S, Pd and base metals from the BMS in the chromitite layer; (5) redistribution of the PGE by a fluid rising from the underlying cumulate pile. The implication of each of these processes will be considered and a possible model for the formation of the Merensky Reef will then be proposed.

## Collection of the PGE by an immiscible sulphide liquid

The model is based on the suggestion that when a new magma enters the chamber, it mixes with the resident magma to form a mixed magma, which becomes saturated in an immiscible sulphide liquid (Campbell & Naldrett, 1979; Li & Ripley, 2005). As PGE have a large partition coefficient into sulphide liquid the immiscible sulphide liquid collects the PGE then settles onto the cumulate pile (Campbell *et al.*, 1983; Naldrett *et al.*, 1986). The BMS occur as interstitial phases in vertical networks developed along the silicate grain boundaries in the melanorites and as droplets in the chromitite layers (Godel *et al.*, 2006). Based on our modelling, the PGE in the silicate rocks can all be accommodated in a sulphide liquid that interacted with a large volume of silicate magma ($N$-factor = 45 000).

In contrast, in the chromitite layers, as previously described by Barnes & Maier (2002*a*) at Impala Platinum Mine, it is not possible to explain the PGE content by considering only the model of collection of the PGE by a sulphide liquid.

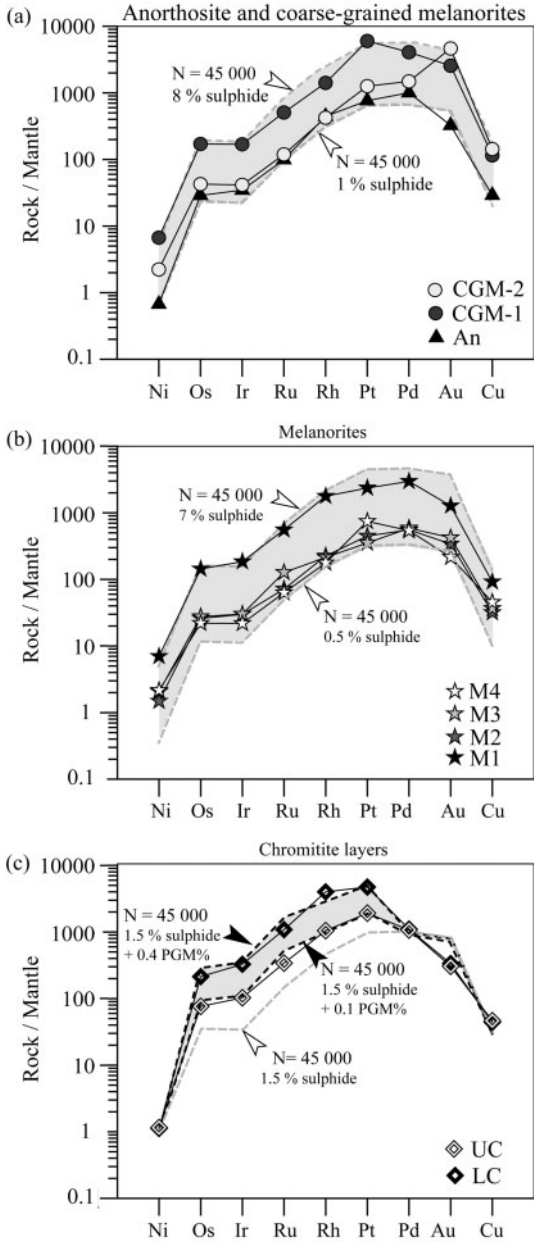


**Fig. 14.** Comparison of observed and modelled mantle-normalized metal concentrations of rock types in the Merensky Reef (a) and (b). The PGE contents of the silicate rocks can be modelled by assuming that they are hosted by base-metal sulphide that segregated at an *N*-factor of 45 000. (c) The PGE contents of the chromitite layers are mostly too high to be explained by base-metal sulphide collection alone, but can be modelled by assuming crystallization of 0·1–0·4% PGM (see text for explanation).

## Partitioning of PGE in the Cr-spinel

Another possibility is that the IPGE and Rh partitioned into chromite during crystallization. Experimental studies on partitioning of Ir, Ru, Rh and Pd between spinel and silicate melt (Capobianco & Drake, 1990; Capobianco *et al.*, 1994; Sattari *et al.*, 2002; Righter *et al.*, 2004) have shown that Ir, Rh and Ru could partition into spinel phases. Applying this to our dataset the mass balance calculations for this model require that the partition coefficients for the IPGE and Rh are considerable higher than those that have been determined experimentally, although it should be mentioned that the experimental data are sparse and the possibility of collection of IPGE and Rh by chromite cannot be entirely ruled out. The main problem with this model is that it does not account for the high Pt values in the chromite layer.

## Crystallization of the PGM directly from the magma

Some workers (e.g. Hiemstra, 1979) have suggested that PGM could have crystallized directly from the Bushveld magma and been precipitated from the magma by minerals on the liquidus such as chromite. Because of the low concentration of the PGE, the grains would be very small, and to collect them in the cumulate pile they would have to be incorporated in the other crystallizing phases such as chromite or olivine. Empirical evidence for the formation of PGM directly from mafic magmas has been provided by many workers from Keays & Campbell (1981) to Fiorentini *et al.* (2004). Barnes (1993) has suggested that the PGE could be included in BMS liquid. However, because of the very low concentrations of PGE in the magma at the time of saturation (0·1–0·5 ppb for IPGE to 10–20 ppb for Pt) and the presence of BMS, some debate has arisen as to how this could occur. To overcome the kinetic problem that arises in nucleating PGM in a magma with such low PGE concentrations a model whereby PGE and metalloid atoms form clusters of 100–1000 atoms in the silicate magma was proposed by Tredoux *et al.* (1995). The clusters have no structure and are not minerals or nuclei. These clusters are then physically captured by whatever phase is crystallizing. This is not an equilibrium process and partition coefficients are not applicable. A variation of this model has been applied to formation of the Merensky Reef by Ballhaus & Sylvester (2000).

The crystallization of PGM from the silicate magma has remained controversial because it is difficult to determine the solubility of PGE in mafic magma at an $fO_2$ approaching that of natural systems. Early experiments were plagued by the formation of micronuggets (e.g. Borisov & Palme, 1997). The presence of the micronuggets has been used as evidence that clusters exist. However, recent experimental work suggests that micronuggets are an experimental artefact (Fortenfant *et al.*, 2003; Pruseth & Palme, 2004; Blaine *et al.*, 2005; Brenan *et al.*, 2005). Based on the experimental database and thermodynamic calculations, Borisov & Palme (1997) calculated that at an $fO_2$ at or just below fayalite–magnetite–quartz (FMQ), Fe-bearing mafic magmas become saturated in Pt–Ru and Ir–Fe alloys at 0·4–14 ppb. These concentrations are

similar to those observed in the Bushveld magma and many other mafic magmas. If the magmas are saturated in Fe–PGE alloys then clusters are no longer required. It could be argued that the high values of these elements in the chromitite layers are due to the crystallization of the Fe–PGE alloys that have been incorporated into the chromite and collected onto the crystal pile with chromite. This model has a difficulty in that our PGM study has shown that the PGM contained in the chromitite layers are commonly associated with the BMS and only few PGM are included in chromite grains. This observation is in agreement with other PGM studies of the Merensky Reef samples (e.g. Kinloch, 1982; Lee & Parry, 1988; Prichard *et al.*, 2004), in all of which it was suggested that the PGM exsolved from BMS. The association of the PGM sulphides is also problematic because Brenan & Andrews (2001) calculated that at the $fO_2$ and $fS_2$ at which a BMS liquid segregates from a mafic magma Fe–PGE alloys are not stable. They suggested that the PGM crystallized and were subsequently absorbed by the infiltration of the BMS liquid.

## Sulphur, Pd and base-metal loss from the chromitite layers

Naldrett & Lehmann (1988) suggested that the Fe-sulphide could react with chromite producing an Fe-rich chromite and removing S from the system, thereby triggering PGM crystallization by lowering the $fS_2$. This suggestion could explain the fact that BMS in the chromitite layers of the Bushveld Complex have a high PGE/S ratio and are generally rich in Cu and Ni (Fig. 4). By this argument, the chromitite layers originally contained five times more BMS than they do now and the PGE were originally collected by these BMS. However, it does not explain why the chromitite layers are not as rich in Pd as the other PGE or Au.

Peregoedova *et al.* (2004) have shown that the desulphidization of Mss results in the formation of an IPGE-rich mss, Fe–Pt alloys and a Cu–Pd (±) Au sulphide liquid. Applying this process to our data, we could suggest that a cumulate pile formed consisting of a semi-consolidated chromitite layer and melanorite. The silicate magma became saturated in base-metal sulphide liquid, which collected the PGE. The sulphide liquid percolated downwards through the cumulate pile. The highest concentration of the sulphide liquid collected in the chromitite layer. During cooling Fe from the BMS was lost to the chromite and S was released (Naldrett & Lehmann, 1988). This resulted in the formation of PGM-alloys, MSS and Cu–Pd–Au sulphide melt (Peregoedova *et al.*, 2004). The loss of S may be evaluated by using the S/Se ratios of the whole-rock (e.g. Lorand *et al.*, 2003). Selenium substitutes for S in BMS and primary magmas have S/Se ratios of ~3000. During alteration, S is more mobile during alteration than Se and consequently the S/Se decreases strongly (e.g. ~1400 for the J-M reef samples of the Stillwater complex (Godel & Barnes, in preparation). In our samples of Merensky Reef, the S/Se ratios (Table 6) are ~2500–3000, which implies that no extensive S removal has occurred. These S/Se results are similar to those calculated from data of Barnes & Maier (2002*a*) for the Merensky Reef at Impala Platinum Mine; thus S loss does not seem probable.

## Redistribution of the PGE by a fluid rising from the underlying cumulate pile

Some workers have proposed that PGE enrichment in some portions of layered intrusions was caused by upward migration of fluid enriched in Cl (Boudreau & McCallum, 1992; Boudreau & Meurer, 1999; Willmore *et al.*, 2000). In this model, the fractionated intercumulus liquid became saturated in hydrous Cl-rich fluid and PGE partitioned into the fluid, which migrated upward in the cumulate pile. The fluid (enriched in S, base metals and possibly some PGE) migrated upward until it encountered a layer where the intercumulate silicate liquid was fluid undersaturated. The fluid then dissolved in the silicate liquid and the metals and S that the fluid was transporting precipitated as BMS among the silicate grains.

If we apply this model to our data, we would have to argue that the rising fluid started to dissolve into the interstitial silicate liquid at the level of the chromitite layer and deposited most of its Cu, IPGE, Rh and Pt at this point. Not all the fluid dissolved in the chromitite layer, and the remainder continued to rise through the melanorite and encouraged grain growth, resulting in the layer being coarse grained. As more fluid dissolved into the interstitial silicate liquid, the S and metals it was carrying were deposited along the fluid pathways, and the amount of PGE and Au deposited decreased as the fluid became depleted upsection.

This model has a number of weaknesses. It is possible to argue that this occurred for the first chromitite layer and overlying melanorite, assuming that the cumulate pile below the chromitite is depleted in PGE. For the second chromitite layer and the overlying melanorite, however, it is not clear to us where the metals and S come from, as the fluid should have been depleted in these elements by the time it reached the second chromitite layer and yet the chromitite is enriched in PGE. It is also impossible to test the model numerically because experimental work determining the solubility of the PGE in magmatic fluids is sparse and only values for Pt and Au are available (Hanley *et al.*, 2005). Barnes & Maier (2002*b*) considered this model on a much larger scale for the Bushveld and concluded that it is the rocks above the reefs that are depleted in PGE and not the rocks below the reef. Therefore it seems more likely that the PGE were collected from the magma above the reef than the cumulate pile below.

## Proposed model of formation for the Merensky Reef

Integration of the above considerations allows us to propose the following model for the formation of the Merensky Reef at the Rustenburg Platinum mine. A crystal pile consisting of plagioclase and trapped melt (proto-anorthosite) overlain by a fractionated silicate liquid formed. A new injection of magma (possibly high-Mg basalt) entered the chamber and mixed with the resident magma, bringing chromite, orthopyroxene and PGE alloys onto the liquidus (Fig. 15a). These minerals settled onto the protoanorthosite. Chromite grains and associated PGM were concentrated immediately above the protoanorthosite to form a layer consisting of chromite, PGM and trapped melt (protochromite layer), and the orthopyroxene was concentrated immediately above this to form a layer consisting mainly of orthopyroxene and trapped melt (protomelanorite). The fractionated melt become saturated in a base-metal sulphide liquid (Fig. 15b), and immiscible sulphide droplets formed and collected the remaining PGE by extensive interaction with the silicate magma ($N$-factor = 45 000).

During the evolution of the sulphide liquid, a monosulphide solid solution enriched in Fe (Mss) and a fractionated sulphide liquid enriched in Cu formed. The Fe–Ni–Cu–PGE sulphide liquid collected along vertical networks along the dilatancies formed during the compaction (Barnes & Maier, 2002*a*; Godel *et al.*, 2006) of the cumulate pile (Fig. 15c). Magma chamber instabilities may improve the downward migration of the sulphide liquid. As Cu-rich sulphide liquid has an higher wettability against silicate and oxides than low-Cu sulphide liquid (Ebel & Naldrett, 1996, 1997), some of the Cu-rich liquid migrated through the chromitite. The liquid dissolved some of the PGE alloys that had earlier crystallized and collected in the chromitite layer when the silicate liquid was sulphide undersaturated. The BMS now observed in the chromitite layer occur as droplets, thus the sulphides that escape downward into the silicate rocks below the chromitites were probably not interconnected and were trapped rapidly in the silicate matrix as temperature decreased (Fig. 15d). This phenomenon would explain the BMS in the chromitite layers and the observation that the rocks immediately below each chromitite layer are richer in chalcopyrite. Magma chamber instabilities may also trigger fluid (magmatic, aqueous or even vapour) migration. This fluid may react with the BMS and lead to their partial desulphurization, triggering formation of Pt–Fe alloy (isoferroplatinum), as in experiments (e.g. Peregoedova *et al.*, 2004).

A second magma injection entered into the magma chamber, similarly triggering the formation of the upper chromitite. The magma chamber was heated by this new influx of magma so that the orthopyroxenes in the protomelanorite were maintained close to their solidus temperature and could recrystallize to form large grains (Cawthorn & Boerst, 2006). Furthermore, compaction appears to have forced some orthopyroxene grains together, resulting in a fusion of the grains, with small chromite grains marking the old grain boundaries (Barnes & Maier, 2002a). The combination of these processes could have resulted in coarsening of grain size and the formation of the coarse-grained melanorite (Merensky pegmatoid).

As the temperature fell, the Mss exsolved to pyrrhotite and pentlandite and the Iss exsolved to chalcopyrite. Most of the PGM (e.g. sulphides or bismutho-tellurides) exsolved from the BMS. Pentlandite and pyrrhotite are preferentially enriched in IPGE and Rh as would be expected if these minerals exsolved from Mss. However, pentlandite is also enriched in Pd and this requires that during exsolution of sulphides Pd diffused into the pentlandite from the Cu-rich minerals.

## CONCLUSION

The majority (~65 to ~85%) of the PGE in the Merensky Reef at Rustenburg Platinum Mine are not found in solid solution within the BMS, but are essentially found as PGM closely associated with the BMS (included in BMS or located at the BMS–silicate or oxide grain boundaries). Amongst the BMS, pentlandite is the principal host of Pd, Rh, Os, Ir and Ru. Platinum and gold are not partitioned in sulphide minerals, but occur as PGM or electrum. The BMS in the chromitite layers are slightly enriched in PGE (by a factor of two), but this cannot explain the strong (by a factor of five) enrichment of the chromitite in PGE. The data suggest that some PGE are hosted by BMS (principally pentlandite), but the majority is hosted by PGM. Our modellings have shown that the PGM found in the chromitite layers are unlikely to be solely the results of exsolution from a sulphide liquid. A primary (i.e. before immiscible sulphide formed) crystallization of PGM is needed to account for the PGE mass balance.

Thus, in light of our results, the collection of the PGE in chromitite layers of the Merensky Reef at Rustenburg Platinum Mine may have happened in two steps: (1) some PGM (essentially laurite, cooperite and malanite) crystallized from the magma during the formation of chromite and before sulphide saturation; (2) an immiscible sulphide liquid formed and the remaining PGE were collected by this liquid, which then percolated downward in the crystal pile until it encountered the chromitite layers. In the silicate rocks, only one step is needed; the PGE are collected by an immiscible sulphide liquid, which percolated in the silicate rocks. On cooling, some PGMs exsolve from the Mss and Iss in both chromitites and silicate rocks.

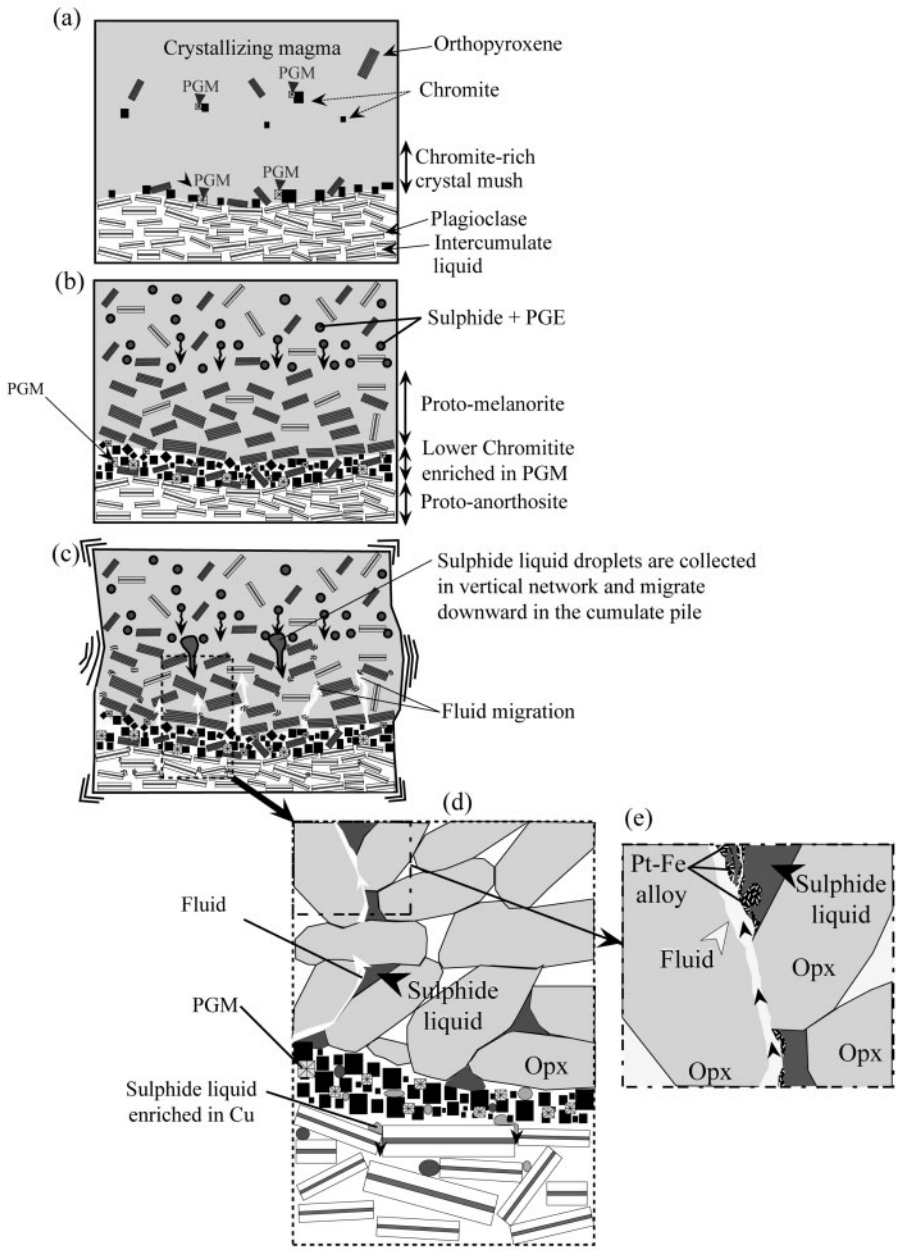


**Fig. 15.** Proposed model of formation for the Merensky Reef at Rustenburg Platinum Mine. (a) A new injection of magma entered the chamber and mixed with the resident magma. Chromite associated with PGM and orthopyroxene crystallized and settled on the top of the underlying proto-anorthosite overlain by proto-melanorite. (b) After chromite and orthopyroxene crystallization, the magma became saturated in an immiscible sulphide liquid, which collected the remaining PGE. (c) Magma chamber instabilities (possibly movements as a result of earthquakes) triggered the collection of the sulphide droplets to networks, facilitating downward migration of the sulphide liquid along vertical dilatancies formed during compaction. The downward migration of the sulphide liquid is slowed as it reaches the chromitite layer (as a result of a change in sulphide liquid wetting properties in chromitite). (d) As temperature decreases, fluid interacts with the base-metal sulphides, triggering their partial desulphurization. (e) Pt–Fe alloy forms by partial desulphurization of the system. The fluid triggers locally a disequilibrium of the base-metal sulphide, leading to crystallization of myrmekitic Pt–Fe alloy.

## ACKNOWLEDGEMENTS

Rustenburg Platinum Mine is thanked for allowing access to its properties and allowing sampling of the Merensky Reef. Dr Richard Cox (UQAC) is thanked for his assistance with the LA-ICP-MS analysis. Dr Paul Bédard and Mr Dany Savard (UQAC) are thanked for their advice and assistance during the whole-rock analysis. Dr Marc Choquette (Laval University) is thanked for his assistance with the microprobe analysis. Pr Christian Ballhaus, Dr Stephen Barnes, and Pr James Mungall are thanked

for their constructive reviews. This work was funded by a Discovery Grant from the Natural Science and Engineering Research Council of Canada and the Canadian Research Chair in Magmatic Metallogeny.

## REFERENCES


Arndt, N., Jenner, G., Ohnenstetter, M., Deloule, E. & Wilson, A. (2005). Trace elements in the Merensky Reef and adjacent norites, Bushveld Complex, South Africa. *Mineralium Deposita* **40**(5), 550–575.

Ballhaus, C. & Ryan, C. G. (1995). Platinum-group elements in the Merensky reef. I. PGE in solid solution in base metal sulfides and the down-temperature equilibration history of Merensky ores. *Contributions to Mineralogy and Petrology* **122**(3), 241–251.

Ballhaus, C. & Sylvester, P. (2000). Noble metal enrichment processes in the Merensky Reef, Bushveld Complex. *Journal of Petrology* **41**(4), 545–561.

Barnes, S. J. (1993). Partitioning of the Platinum Group Elements and gold between silicate and sulfide magmas in the Munni-Munni Complex, Western Australia. *Geochimica et Cosmochimica Acta* **57**(6), 1277–1290.

Barnes, S.-J. & Lightfoot, P. C. (2005). Formation of magmatic nickel sulfide deposits and processes affecting their copper and Platinum Group Element contents. *Economic Geology 100th Anniversary Volume*, 179–213.

Barnes, S.-J. & Maier, W. D. (2002*a*). Platinum-group elements and microstructures of Normal Merensky Reef from Impala Platinum Mines, Bushveld Complex. *Journal of Petrology* **43**(1), 103–128.

Barnes, S.-J. & Maier, W. D. (2002*b*). Platinum-Group Element distributions in the Rustenburg Layered Suite of the Bushveld Complex, South Africa. In: Cabri, L. J. (ed.) *Geology, Geochemistry, Mineralogy and Mineral Benefication of Platinum Group Element. Canadian Institute of Mining, Metallurgy and Petroleum, Special Volume* **54**, 553–580.

Barnes, S.-J., van Achterbergh, E., Makovicky, E. & Li, C. (2001). Proton microprobe results for the partitioning of platinum-group elements between monosulphide solid solution and sulphide liquid. *South African Journal of Geology* **104**(4), 275–286.

Barnes, S.-J., Cox, R. & Zientek, M. (2006). Platinum-group element, gold, silver and base metal distribution in compositionally zoned sulfide droplets from the Medvezky Creek Mine, Noril'sk, Russia. *Contributions to Mineralogy and Petrology* **152**(2), 187–200.

Bédard, L. P. & Barnes, S. J. (2004). Improved Platinum-Group Element extraction by NiS fire assay from chromitite ore samples using a flux containing sodium metaphosphate. *Geostandards and Geoanalytical Research* **28**(2), 311–316.

Blaine, F. A., Linnen, R. L., Holtz, F. & Brugmann, G. E. (2005). Platinum solubility in a haplobasaltic melt at 1250°C and 0·2 GPa: the effect of water content and oxygen fugacity. *Geochimica et Cosmochimica Acta* **69**(5), 1265–1273.

Borisov, A. & Palme, H. (1997). Experimental determination of the solubility of platinum in silicate melts. *Geochimica et Cosmochimica Acta* **61**(20), 4349–4357.

Boudreau, A. E. & McCallum, I. S. (1992). Infiltration metasomatism in layered intrusions—an example from the Stillwater Complex, Montana. *Journal of Volcanology and Geothermal Research* **52**(1–3), 171–183.

Boudreau, A. E. & Meurer, W. P. (1999). Chromatographic separation of the platinum-group elements, gold, base metals and sulfur during degassing of a compacting and solidifying igneous crystal pile. *Contributions to Mineralogy and Petrology* **134**(2–3), 174–185.

Brenan, J. M. & Andrews, D. R. A. (2001). High-temperature stability of laurite and Ru–Ir–Os alloy and their role on PGE fractionation in mafic magmas. *Canadian Mineralogist* **39**, 341–360.

Brenan, J. M., McDonough, W. F. & Ash, R. (2005). An experimental study of the solubility and partitioning of iridium, osmium and gold between olivine and silicate melt. *Earth and Planetary Science Letters* **237**(3–4), 855–872.

Brügmann, G. E., Naldrett, A. J., Asif, M., Lightfoot, P. C., Gorbachev, N. S. & Fedorenko, V. A. (1993). Siderophile and chalcophile metals as tracers of the evolution of the Siberian Trap in the Noril'sk region, Russia. *Geochimica et Cosmochimica Acta* **57**(9), 2001–2018.

Cabri, L. J. (2002). The Platinum-Group Minerals. In: Cabri, L. J. (ed.) *Geology, Geochemistry, Mineralogy and Mineral Benefication of Platinum Group Element. Canadian Institute of Mining, Metallurgy and Petroleum, Special Volume* **54**, 13–129.

Campbell, I. H. & Naldrett, A. J. (1979). The influence of silicate silicate:sulphide ratios on the geochemistry of magmatic sulphides. *Economic Geology* **74**, 1503–1505.

Campbell, I. H., Naldrett, A. J. & Barnes, S. J. (1983). A model for the origin of the platinum-rich sulfide horizons in the Bushveld and Stillwater Complexes. *Journal of Petrology* **24**(2), 133–165.

Capobianco, C. J. & Drake, M. J. (1990). Partitioning of ruthenium, rhodium, and palladium between spinel and silicate melt and implications for platinum group element fractionation trends. *Geochimica et Cosmochimica Acta* **54**(3), 869–874.

Capobianco, C. J., Hervig, R. L. & Drake, M. J. (1994). Experiments on crystal/liquid partitioning of Ru, Rh and Pd for magnetite and hematite solid solutions crystallized from silicate melt. *Chemical Geology* **113**(1–2), 23–43.

Cawthorn, R. G. (1999). The platinum and palladium resources of the Bushveld Complex. *South African Journal of Science* **95**(11–12), 481.

Cawthorn, R. G. (2002). Platinum-Group Element deposits in the Bushveld Complex, South Africa. In: Cabri, L. J. (ed.) *Geology, Geochemistry, Mineralogy and Mineral Benefication of Platinum Group Element. Canadian Institute of Mining, Metallurgy and Petroleum, Special Volume* **54**, 389–429.

Cawthorn, R. G. & Boerst, K. (2006). Origin of the pegmatitic pyroxenite in the Merensky Unit, Bushveld Complex, South Africa. *Journal of Petrology* **47**, 1509–1530.

Davies, G. & Tredoux, M. (1985). The platinum-group element and gold contents of the marginal rocks and sills of the Bushveld Complex. *Economic Geology* **80**, 838–848.

Eales, H. V. & Cawthorn, R. G. (1996). The Bushveld Complex. In: Cawthorn, R. G. (ed.) *Layered Intrusions*. Amsterdam: Elsevier, pp. 181–230.

Ebel, D. S. & Naldrett, A. J. (1996). Fractional crystallisation of sulfide ore liquids at high temperature. *Economic Geology* **91**, 607–621.

Ebel, D. S. & Naldrett, A. J. (1997). Crystallization of sulfide liquids and the interpretation of ore composition. *Canadian Journal of Earth Sciences* **34**(4), 352–365.

Fiorentini, M. L., Stone, W. E., Beresford, S. W. & Barley, M. E. (2004). Platinum-group element alloy inclusions in chromites from Archaean mafic–ultramafic units: evidence from the Abitibi and the Agnew–Wiluna Greenstone Belts. *Mineralogy and Petrology* **82**(3–4), 341–355.

Fortenfant, S. S., Gunther, D., Dingwell, D. B. & Rubie, D. C. (2003). Temperature dependence of Pt and Rh solubilities in a haplobasaltic melt. *Geochimica et Cosmochimica Acta* **67**(1), 123–131.

Godel, B. & Barnes, S.-J. (2007). Platinum-group elements in sulfide minerals and whole rocks of the J-M reef (Stillwater Complex, U.S.A.): implication for the formation of the reef. *Chemical Geology* , doi:10.1016/j.chemgeo.2007.05.006.

Godel, B., Barnes, S.-J. & Maier, W. D. (2006). 3-D distribution of sulphide minerals in the Merensky Reef (Bushveld Complex, South Africa) and the J-M Reef (Stillwater Complex, USA) and their relationship to microstructures using X-ray computed tomography. *Journal of Petrology* **47**, 1853–1872.

Hanley, J. J., Pettke, T., Mungall, J. E. & Spooner, E. T. C. (2005). The solubility of platinum and gold in NaCl brines at 1·5 kbar, 600 to 800°C: a laser ablation ICP-MS pilot study of synthetic fluid inclusions. *Geochimica et Cosmochimica Acta* **69**(10), 2593–2611.

Harmer, R. E. & Sharpe, M. R. (1985). Field relations and strontium isotope systematic of the marginal rocks of the eastern Bushveld Complex. *Economic Geology* **80**, 813–837.

Hiemstra, S. A. (1979). The role of collectors in the formation of the platinum deposits in the Bushveld Complex. *Canadian Mineralogist* **17**, 469–482.

Keays, R. R. & Campbell, I. H. (1981). Precious metals in the Jimberlana Intrusion, Western Australia: implications for the genesis of platiniferous ores in layered intrusions. *Economic Geology* **76**, 1118–1141.

Kingston, G. A. & El-Dosuky, B. T. (1982). A contribution on the Platinum-Group mineralogy of the Merensky Reef at the Rustenburg Platinum Mine. *Economic Geology* **77**(6), 1367–1384.

Kinloch, E. D. (1982). Regional trends in the Platinum-Group mineralogy of the Critical Zone of the Bushveld Complex, South Africa. *Economic Geology* **77**(6), 1328–1347.

Kinloch, E. D. & Peyerl, W. (1990). Platinum-Group Minerals in various rock types of the Merensky Reef: genetic implications. *Economic Geology* **85**, 537–555.

Kullerud, G., Yund, R. A. & Moh, G. H. (1969). Phase relations in the Cu–Fe–S, Cu–Ni–S and Fe–Ni–S systems. *Economic Geology, Monograph* **4**, 323–343.

Lee, C. A. & Parry, S. J. (1988). Platinum-Group Element geochemistry of the lower and middle group chromitites of the eastern Bushveld Complex. *Economic Geology* **83**(6), 1127–1139.

Li, C. & Ripley, E. M. (2005). Empirical equations to predict the sulfur content of mafic magmas at sulfide saturation and applications to magmatic sulfide deposits. *Mineralium Deposita* **40**, 218–230.

Li, C., Barnes, S.-J., Makovicky, E., Rose-Hansen, J. & Makovicky, M. (1996). Partitioning of Ni, Cu, Ir, Rh, Pt, and Pd between monosulfide solid solution and sulfide liquid: effects of composition and temperature. *Geochimica et Cosmochimica Acta* **60**(7), 1231–1238.

Li, C., Ripley, E. M., Merino, E. & Maier, W. D. (2004). Replacement of base metal sulfides by actinolite, epidote, calcite, and magnetite in the UG2 and Merensky Reef of the Bushveld Complex, South Africa. *Economic Geology* **99**(1), 173–184.

Loeb-Du Toit, A. (1986). The Impala Platinum Mines. In: Anhaeusser, C. R. & Maske, S. (eds) *Mineral Deposits of Southern Africa, I and II*. Johannesburg: Geological Society of South Africa, pp. 1901–1106.

Lorand, J. P., Alard, O., Luguet, A. & Keays, R. R. (2003). Sulfur and selenium systematics of the subcontinental lithospheric mantle: inferences from the Massif Central xenolith suite (France). *Geochimica et Cosmochimica Acta* **67**(21), 4137–4151.

Maier, W. D., Barnes, S. J., Gartz, V. & Andrews, G. (2003). Pt–Pd reefs in magnetites of the Stella layered intrusion, South Africa: a world of new exploration opportunities for platinum group elements. *Geology* **31**(10), 885–888.

Mason, P. R. D. & Kraan, W. J. (2002). Attenuation of spectral interferences during laser ablation inductively coupled plasma mass spectrometry (LA-ICP-MS) using an rf only collision and reaction. *Journal of Analytical Atomic Spectrometry* **17**(8), 858–867.

Mungall, J. E., Andrews, D. R. A., Cabri, L. J., Sylvester, P. J. & Tubrett, M. (2005). Partitioning of Cu, Ni, Au, and platinum-group elements between monosulfide solid solution and sulfide melt under controlled oxygen and sulfur fugacities. *Geochimica et Cosmochimica Acta* **69**(17), 4349–4360.

Naldrett, A. J. (ed.) (1989). *Magmatic Sulfide Deposits*. Oxford: Oxford University Press, 189 pp.

Naldrett, A. J. & Lehmann, J. (1988). Spinel non-stoichiometry as an explanation for Ni-, Cu-, and PGE-enriched sulphides in chromitites. In: Prichard, H. M., Potts, P. J., Bowles, J. F. W. & Cribb, S. J. (eds) *Geo-Platinum 87*. Amsterdam: Elsevier, pp. 113–143.

Naldrett, A. J., Gasparrini, E. C., Barnes, S. J., Von Gruenewaldt, G. & Sharpe, M. R. (1986). The Upper Critical Zone of the Bushveld Complex and the origin of Merensky-type ores. *Economic Geology* **81**(5), 1105–1117.

Peregoedova, A., Barnes, S.-J. & Baker, D. R. (2004). The formation of Pt–Ir alloys and Cu–Pd-rich sulfide melts by partial desulfurization of Fe–Ni–Cu sulfides: results of experiments and implications for natural systems. *Chemical Geology* **208**(1–4), 247–264.

Peregoedova, A., Barnes, S.-J. & Baker, D. R. (2006). An experimental study of mass transfer of platinum-group elements, gold, nickel and copper in sulfur-dominated vapor at magmatic temperatures. *Chemical Geology* **235**(1–2), 59–75.

Polovina, J. S., Hudson, D. M. & Jones, R. E. (2004). Petrographic and geochemical characteristics of postmagmatic hydrothermal alteration and mineralization in the J-M Reef, Stillwater Complex, Montana. *Canadian Mineralogist* **42**, 261–277.

Prichard, H. M., Barnes, S.-J., Maier, W. D. & Fisher, P. C. (2004). Variations in the nature of the platinum-group minerals in a cross-section through the Merensky Reef at Impala Platinum: implications for the mode of formation of the reef. *Canadian Mineralogist* **42**, 423–437.

Pruseth, K. L. & Palme, H. (2004). The solubility of Pt in liquid Fe-sulfides. *Chemical Geology* **208**(1–4), 233–245.

Puchtel, I. S., Humayun, M., Campbell, A. J., Sproule, R. A. & Lesher, C. M. (2004). Platinum group element geochemistry of komatiites from the Alexo and Pyke Hill areas, Ontario, Canada. *Geochimica et Cosmochimica Acta* **68**(6), 1361–1383.

Righter, K., Campbell, A. J., Humayun, M. & Hervig, R. L. (2004). Partitioning of Ru, Rh, Pd, Re, Ir, and Au between Cr-bearing spinel, olivine, pyroxene and silicate melts. *Geochimica et Cosmochimica Acta* **68**(4), 867–880.

Sattari, P., Brenan, J. M., Horn, I. & McDonough, W. F. (2002). Experimental constraints on the sulfide– and chromite–silicate melt partitioning behavior of rhenium and Platinum-Group Elements. *Economic Geology* **97**(2), 385–398.

Steele, T. W., Levin, J. & Copelowitz, I. (1975). Preparation and certification of a reference sample of a precious metal ore. *National Institute for Metallurgy Report*, 1696–1975.

Tredoux, M., Lindsay, N. M., Davies, G. & McDonald, I. (1995). The fractionation of platinum-group elements in magmatic systems, with the suggestion of a novel causal mechanism. *South African Journal of Geology* **98**, 157–167.

Vermaak, C. F. (1976). Merensky Reef—thoughts on its environment and genesis. *Economic Geology* **71**(7), 1270–1298.

Vermaak, C. F. & Hendriks, L. P. (1976). Review of mineralogy of Merensky Reef, with specific reference to new data on precious metal mineralogy. *Economic Geology* **71**(7), 1244–1269.

Viljoen, M. J. & Hieber, R. (1986). The Rustenburg section of the Rustenburg Platinum Mines Limited, with reference to the Merensky Reef. In: Anhaeusser, C. R. & Maske, S. (eds) *Mineral Deposits of Southern Africa, II*. Johannesburg: Geological Society of Southern Africa, pp. 1107–1034.

Viljoen, M. J., Theron, J., Underwood, B. M., Walters, J. & Peyerl, W. (1986). The Amandelbult section of Rustenburg Platinum Mines

Limited, with reference to the Merensky Reef. In: Anhaeusser, C. R. & Maske, S. (eds) *Mineral Deposits of Southern Africa, II*. Johannesburg: Geological Society of Southern Africa, pp. 1041–1060.

Von Gruenewaldt, G. (1986). Platinum-group element–chromitite associations in the Bushveld Complex. *Economic Geology* **81**, *A third issue devoted to platinum deposits*, 1067–1079.

Von Gruenewaldt, G. (1989). Contrasting platinum-group element concentration patterns in cumulates of the Bushveld Complex. *Mineralium Deposita* **24**(3), 219–229.

Willmore, C. C., Boudreau, A. E. & Kruger, F. J. (2000). The halogen geochemistry of the Bushveld Complex, Republic of South Africa: implications for chalcophile element distribution in the lower and critical zones. *Journal of Petrology* **41**(10), 1517–1539.

Zientek, M. L., Cooper, R. W., Corson, S. R. & Geraghty, E. P. (2002). Platinum-Group Element mineralization in the Stillwater Complex, Montana. In: Cabri, L. J. (ed.) *Geology, Geochemistry, Mineralogy and Mineral Benefication of Platinum Group Element. Canadian Institute of Mining, Metallurgy and Petroleum, Special Volume* **54**, 459–481.

# APPENDIX A: METHOD OF CALCULATION OF PGM CONTRIBUTION ON THE PGE CONTENT

## Image analysis

BSE images were collected for all the PGM described previously. The first step is to determine the area represented by each PGM. Automated PGM boundaries extraction from BSE images was done using homemade IDL (ITT Visual Information Solutions) code and new 8-bit images of the PGM were created. The scales on the BSE images were used to calculate the real image sizes. These new images of the PGM were then imported into ImageJ software (a PC version of NIH image) and were analysed using a particle measurement function which calculates many parameters such as the area, the major and minor axis, the orientation and the position of each PGM. The summary of the results are given in Tables 11 and 12. In a second step, the area represented by each lithology ($V_{\mathrm{Litho}}$) was calculated using high-resolution scans of corresponding thin sections. A mask image of each lithology was created and then analysed using the same method as for the PGM. The proportion of each non-sulphide mineral was also determined by image analysis, and the proportions of each sulphide mineral (pyrrhotite, pentlandite and chalcopyrite) used in the further calculation are given in Fig. 4. As no information is available on the 3D distribution or size of the PGM, in the further calculation we made the assumption that the volume represented by each phase or lithology can be approximated by the area calculated from the 2D images. In other words, the thickness considered to calculate a volume from an area is regarded as infinitely small, so that area and volume are almost identical.

## Equations for the calculation

### *Mass of each lithology*

The first step of the calculation is to calculate the mass of each lithology by taking into account the volume of each lithology, the proportions of each mineral, the volume of PGM and the densities of each phase. All the parameters, their abbreviations, the units and the constant used in the further calculation are summarized in Table A1.

The mass of the non-PGM phase ($m_{\mathrm{Oth}}$) is given by the following equations:

$$m_{\mathrm{Oth}} = m_{\mathrm{Px}} + m_{\mathrm{Plg}} + m_{\mathrm{Chr}} + m_{\mathrm{Sul}}$$

with

$$\begin{aligned} V_{\mathrm{Oth}} &= (V_{\mathrm{Litho}} - V_{\mathrm{PGM}}) \\ m_{\mathrm{Px}} &= V_{\mathrm{Oth}} \times X_{\mathrm{Px}} \times D_{\mathrm{Px}} \\ m_{\mathrm{Plg}} &= V_{\mathrm{Oth}} \times X_{\mathrm{Plg}} \times D_{\mathrm{Plg}} \\ m_{\mathrm{Chr}} &= V_{\mathrm{Oth}} \times X_{\mathrm{Chr}} \times D_{\mathrm{Chr}} \\ m_{\mathrm{Sul}} &= V_{\mathrm{Oth}} \times X_{\mathrm{Sul}} \times D_{\mathrm{Sul}}. \end{aligned}$$

The mass of the PGM ($M_{\mathrm{PGM}}$) is given by the following equations:

$$\begin{aligned} m_{\mathrm{PGM}} = {} & m_{\mathrm{Braggite}} + m_{\mathrm{Cooperite}} + m_{\mathrm{Moncheite}} + m_{\mathrm{Laurite}} \\ & + m_{\mathrm{Isoferroplatinum}} + m_{\mathrm{Rustenburgite}} + m_{\mathrm{Pt}} \end{aligned}$$

with

$$\begin{aligned} m_{\mathrm{Braggite}} &= V_{\mathrm{Braggite}} \times D_{\mathrm{Braggite}} \\ m_{\mathrm{Cooperite}} &= V_{\mathrm{Cooperite}} \times D_{\mathrm{Cooperite}} \\ m_{\mathrm{Moncheite}} &= V_{\mathrm{Moncheite}} \times D_{\mathrm{Moncheite}} \\ m_{\mathrm{Laurite}} &= V_{\mathrm{Laurite}} \times D_{\mathrm{Laurite}} \\ m_{\mathrm{Isoferroplatinum}} &= V_{\mathrm{Isoferroplatinum}} \times D_{\mathrm{Isoferroplatinum}} \\ m_{\mathrm{Rustenburgite}} &= V_{\mathrm{Rustenburgite}} \times D_{\mathrm{Rustenburgite}} \\ m_{\mathrm{Pt}} &= V_{\mathrm{Pt}} \times D_{\mathrm{Pt.}} \end{aligned}$$

The total mass of the sample ($m_{\mathrm{Sam}}$) is given by

$$m_{\mathrm{Sam}} = m_{\mathrm{PGM}} + m_{\mathrm{Oth}}.$$

### *Calculation of the PGM content*

The second step is to calculate the content (in ppm) of each PGM in a mass of sample equal to the mass of sample used for the geochemical analysis (i.e. 10 g).

For example, for the braggite content ($C_{\mathrm{Braggite}}$) is given by the equation

$$C_{\mathrm{Braggite}} = \left[(m_{\mathrm{Braggite}} \times 10^6)/m_{\mathrm{Sam}}\right] \times 10.$$

The $10^6$ corresponds to the conversion from g to μg

The structure of the equation is similar for the other PGM. The results of the calculation are given in Table 12.

### *Calculation of each PGE content*

The final step is to calculate the total mass of each PGE due to the PGM using the PGM composition (Table A2) and the PGM content calculated above.

*Table A1: Parameters used in the calculation, with their abbreviations and units*

| Abbreviation | Description | Unit |
|---|---|---|
| Px | Pyroxene | |
| Plg | Plagioclase | |
| Chr | Chromite | |
| Po | Pyrrhotite | |
| Pn | Pentlandite | |
| Cp | Chalcopyrite | |
| $V_z$ | Volume of $z$ | $cm^3$ |
| $X_z$ | Fraction of the phase $z$ | |
| $X_{yz}$ | Fraction of $y$ in $z$ | |
| $D_z$ | Density of phase $z$ | $g/cm^3$ |
| $D_{Sul}$ | Density of sulphides: | |
| | $D_{Sul} = (D_{Po} \times X_{Po}) + (D_{Pn} \times X_{Pn}) + (D_{Cp} \times X_{Cp})$ $g/cm^3$ | |
| $m_z$ | Mass of the phase $z$: | |
| | $m_z = D_z \times V_z$ | g |

*Table A2: Composition of PGM and density of PGM and other minerals used in the calculation*

| PGM | Mineral | Density ($g/cm^3$) | Pt (wt%) | Pd (wt%) | Ru (wt%) | Ir (wt%) | Os (wt%) | Au (wt%) |
|---|---|---|---|---|---|---|---|---|
| Pt-Pd-S | Braggite | 9·4 | 66·5 | 12·4 | | | | |
| PtS | Cooperite | 10·1 | 84 | 0·6 | | | | |
| Pt-Te | Moncheite | 10·2 | 43 | 0·2 | | | | |
| Ru-Ir-Os-S | Laurite | 6·4 | | | 47·2 | 5·5 | 6·9 | |
| Pt-Fe | Isoferroplatinum | 18·2 | 91 | | | | | |
| Pt-Sn-S | Rustenburgite | 18·2 | 69 | 12·5 | | | | |
| Pt | Platinum | 19·1 | 100 | | | | | |
| | Gold | 17·6 | | | | | | 100 |
| | Chromite | 4·5 | | | | | | |
| | Pyroxene | 3·3 | | | | | | |
| | Plagioclase | 2·7 | | | | | | |
| | Pentlandite | 4·8 | | | | | | |
| | Pyrrhotite | 4·6 | | | | | | |
| | Chalcopyrite | 4·2 | | | | | | |

The Pt content due to PGM ($Pt_{Rec}$) is given by

$$Pt_{Rec} = (C_{Braggite} \times X_{PtBraggite}) + (C_{Cooperite} \times X_{PtCooperite}) + (C_{Moncheite} \times X_{PtMoncheite}) + (C_{Isoferroplatinum} \times X_{PtIsoferroplatinum}) + (C_{Rustenburgite} \times X_{PtRustenburgite}) + (C_{Pt} \times X_{PtPt}).$$

The Pd content due to PGM ($Pd_{Rec}$) is given by

$$Pd_{Rec} = (C_{Braggite} \times X_{PdBraggite}) + (C_{Cooperite} \times X_{PdCoopertite}) + (C_{Moncheite} \times X_{PdMoncheite}) + (C_{Rustenburgite} \times X_{PdRustenburgite}.)$$

The Ru content due to PGM ($Ru_{Rec}$) is given by

$$Ru_{Rec} = C_{Laurite} \times X_{RuLaurite.}$$

The Os content due to PGM ($Os_{Rec}$) is given by

$$Os_{Rec} = C_{Laurite} \times X_{OsLaurite}.$$

The Ir content due to PGM ($Ru_{Rec}$) is given by

$$Ru_{Rec} = C_{Laurite} \times X_{IrLaurite}.$$

The results are summarized in Table 12.

## APPENDIX B: ESTIMATION OF THE SIZE OF THE INCLUSIONS OBSERVED DURING LASER ABLATION

During laser ablation, signals from 30 micro-inclusions enriched in PGE were observed in the base-metal sulphides (BMS) or at the contact between the BMS and the silicates in our samples of the Merensky Reef at Rustenburg Platinum Mine. The precise volumes of these inclusions are difficult to calculate, as their shapes and orientation relative to the laser beam remain unknown. However, we can try to estimate the size (or length) of these inclusions making some assumptions or estimations. Thus, if we considered that these inclusions are cubic, we can estimate the minimal and maximal size of the inclusions using: minimal, maximal and average ablation rates, two different (Fig. B1) grain orientations (relative to laser beam), and the laser ablation spectra (time resolved).

### Estimation of ablation rates

As pointed out by Ballhaus & Sylvester (2000), the ablation rate may be calculated using the depths of the ablation pits (in μm) and the duration (in s) of the ablation. Our analyses indicate that the ablation rate varies as a function of the composition of the BMS ablated. Calculation based on 48 measurements gives as ablation rate averaging $2{\cdot}5 \pm 1$ μm/s. Consequently, to more closely consider this variation and its implications on the calculation of inclusion sizes, we will use in the following three ablation rates: 1·5, 2·5 and 3·5 μm/s.

### Grain orientations

Laser ablation allows us to assess the distribution of elements in three dimensions and to detect inclusions (PGM, for example). Nevertheless, it remains difficult to infer the orientation or size of the grains and it is

impossible to know whether the whole of the inclusion was ablated. However, by approximating the shape of the inclusions to a cube and by considering that the whole grains are ablated, one can consider two 'extreme' cases to calculate minimal and maximal inclusion diameters.

*Case 1*

The laser strikes the grains perpendicular to the crystal faces. Consequently, the distance (in μm) covered by the laser throughout the inclusion (DI) corresponds to the distance AB (Fig. B1). This represents the length of the inclusion (LI).

*Case 2*

The laser strikes the grains along the diagonal of the cube. Consequently, DI corresponds to the distance CE (Fig. B1); this represents the diagonal of the cube and is given by the formula

$$CE^2 = 3 \times LI^2$$

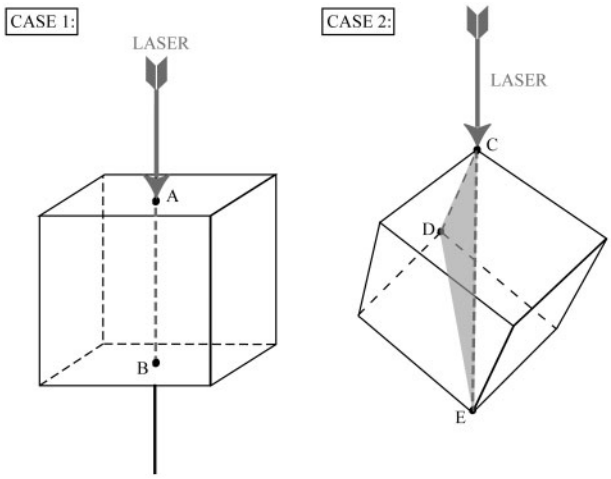


**Fig. B1.** Orientation of inclusions (cubic) relative to laser beam

where LI is the length of the inclusion.

The length of the inclusion is inferred as follows:

$$LI = (1/3 \times CE^2)^{1/2}.$$

The estimation of the distances covered by the laser throughout an inclusion (distance AB and CE) is detailed below.

## Estimation of the length of grains ablated

The distance covered by the laser throughout the inclusion (DI) can be calculated using the ablation rates and the time of the inclusion ablation deducted from the laser spectra of the analysis, and DI (in μm) is given by

$$DI = AR \times T_{IA}/1000$$

where AR is the ablation rate (in μm/s) and $T_{IA}$ is the time of inclusion ablation (in ms).

The time of the inclusion ablation ($T_{IA}$) is evaluated by considering the peak observed on the spectra (Fig. B2) and is given by

$$T_{IA} = T_f - T_i$$

where $T_f$ and $T_i$ are the time (in ms) at the end and at the beginning of the inclusion ablation, respectively. These values are accurately obtained with PlasmaLab software.

## Results of inclusion size estimation

The calculations explained above were carried out for the 30 inclusions observed during the laser ablation of the BMS of the Merensky Reef. The results obtained for the different ablation rates and the different cases are summarized in Table B1. The length of the inclusions calculated varies from ~0·3 to ~12 μm.

To determine whether the size of the inclusions calculated from the laser spectra are realistic and representative of our samples, we compared these results with those obtained from the BSE images analysis of the PGM (described in the text). Both results are in

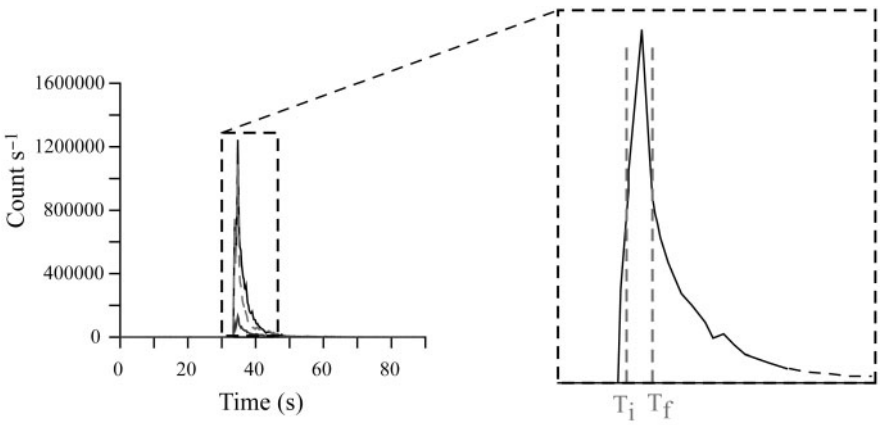


**Fig. B2.** Example of calculation of the time of inclusion ablation.

*Table B1: Results of the calculation of the length of the inclusions observed during the laser ablation of the base-metal sulphides*

| No. | $T_f$ (ms) | $T_i$ (ms) | $T_{IA}$ (ms) | Ablation rate 1·5 μm/s | | | Ablation rate 2·5 μm/s | | | Ablation rate 3·5 μm/s | | | Summary | | |
|---|---|---|---|---|---|---|---|---|---|---|---|---|---|---|---|
| | | | | | Case 1 | Case 2 | | Case 1 | Case 2 | | Case 1 | Case 2 | Length (μm) of inclusion | | |
| | | | | DI (μm) | LI (μm) | LI (μm) | DI (μm) | LI (μm) | LI (μm) | DI (μm) | LI (μm) | LI (μm) | Minimal | Maximal | Average |
| 1 | 35422 | 34635 | 787 | 1·18 | 1·18 | 0·68 | 1·97 | 1·97 | 1·14 | 2·75 | 2·75 | 1·59 | 0·68 | 2·75 | 1·55 |
| 2 | 35029 | 34329 | 700 | 1·05 | 1·05 | 0·61 | 1·75 | 1·75 | 1·01 | 2·45 | 2·45 | 1·41 | 0·61 | 2·45 | 1·38 |
| 3 | 42638 | 41195 | 1443 | 2·16 | 2·16 | 1·25 | 3·61 | 3·61 | 2·08 | 5·05 | 5·05 | 2·92 | 1·25 | 5·05 | 2·85 |
| 4 | 35885 | 34635 | 1250 | 1·88 | 1·88 | 1·08 | 3·13 | 3·13 | 1·80 | 4·38 | 4·38 | 2·53 | 1·08 | 4·38 | 2·46 |
| 5 | 39941 | 39613 | 328 | 0·49 | 0·49 | 0·28 | 0·82 | 0·82 | 0·47 | 1·15 | 1·15 | 0·66 | 0·28 | 1·15 | 0·65 |
| 6 | 35291 | 34766 | 525 | 0·79 | 0·79 | 0·45 | 1·31 | 1·31 | 0·76 | 1·84 | 1·84 | 1·06 | 0·45 | 1·84 | 1·04 |
| 7 | 67303 | 66253 | 1050 | 1·58 | 1·58 | 0·91 | 2·63 | 2·63 | 1·52 | 3·68 | 3·68 | 2·12 | 0·91 | 3·68 | 2·07 |
| 8 | 52740 | 51034 | 1706 | 2·56 | 2·56 | 1·48 | 4·27 | 4·27 | 2·46 | 5·97 | 5·97 | 3·45 | 1·48 | 5·97 | 3·36 |
| 9 | 33848 | 32274 | 1574 | 2·36 | 2·36 | 1·36 | 3·94 | 3·94 | 2·27 | 5·51 | 5·51 | 3·18 | 1·36 | 5·51 | 3·10 |
| 10 | 39358 | 38833 | 525 | 0·79 | 0·79 | 0·45 | 1·31 | 1·31 | 0·76 | 1·84 | 1·84 | 1·06 | 0·45 | 1·84 | 1·04 |
| 11 | 40014 | 39227 | 787 | 1·18 | 1·18 | 0·68 | 1·97 | 1·97 | 1·14 | 2·75 | 2·75 | 1·59 | 0·68 | 2·75 | 1·55 |
| 12 | 53265 | 51428 | 1837 | 2·76 | 2·76 | 1·59 | 4·59 | 4·59 | 2·65 | 6·43 | 6·43 | 3·71 | 1·59 | 6·43 | 3·62 |
| 13 | 43556 | 41720 | 1836 | 2·75 | 2·75 | 1·59 | 4·59 | 4·59 | 2·65 | 6·43 | 6·43 | 3·71 | 1·59 | 6·43 | 3·62 |
| 14 | 34985 | 34460 | 525 | 0·79 | 0·79 | 0·45 | 1·31 | 1·31 | 0·76 | 1·84 | 1·84 | 1·06 | 0·45 | 1·84 | 1·04 |
| 15 | 59956 | 58644 | 1312 | 1·97 | 1·97 | 1·14 | 3·28 | 3·28 | 1·89 | 4·59 | 4·59 | 2·65 | 1·14 | 4·59 | 2·59 |
| 16 | 56807 | 54460 | 2347 | 3·52 | 3·52 | 2·03 | 5·87 | 5·87 | 3·39 | 8·21 | 8·21 | 4·74 | 2·03 | 8·21 | 4·63 |
| 17 | 33192 | 31618 | 1574 | 2·36 | 2·36 | 1·36 | 3·94 | 3·94 | 2·27 | 5·51 | 5·51 | 3·18 | 1·36 | 5·51 | 3·10 |
| 18 | 35160 | 32011 | 3149 | 4·72 | 4·72 | 2·73 | 7·87 | 7·87 | 4·55 | 11·02 | 11·02 | 6·36 | 2·73 | 11·02 | 6·21 |
| 19 | 50379 | 48804 | 1575 | 2·36 | 2·36 | 1·36 | 3·94 | 3·94 | 2·27 | 5·51 | 5·51 | 3·18 | 1·36 | 5·51 | 3·11 |
| 20 | 42769 | 41457 | 1312 | 1·97 | 1·97 | 1·14 | 3·28 | 3·28 | 1·89 | 4·59 | 4·59 | 2·65 | 1·14 | 4·59 | 2·59 |
| 21 | 32142 | 30699 | 1443 | 2·16 | 2·16 | 1·25 | 3·61 | 3·61 | 2·08 | 5·05 | 5·05 | 2·92 | 1·25 | 5·05 | 2·85 |
| 22 | 34897 | 33586 | 1311 | 1·97 | 1·97 | 1·14 | 3·28 | 3·28 | 1·89 | 4·59 | 4·59 | 2·65 | 1·14 | 4·59 | 2·58 |
| 23 | 35816 | 33848 | 1968 | 2·95 | 2·95 | 1·70 | 4·92 | 4·92 | 2·84 | 6·89 | 6·89 | 3·98 | 1·70 | 6·89 | 3·88 |
| 24 | 55364 | 54664 | 700 | 1·05 | 1·05 | 0·61 | 1·75 | 1·75 | 1·01 | 2·45 | 2·45 | 1·41 | 0·61 | 2·45 | 1·38 |
| 25 | 45787 | 43425 | 2362 | 3·54 | 3·54 | 2·05 | 5·91 | 5·91 | 3·41 | 8·27 | 8·27 | 4·77 | 2·05 | 8·27 | 4·66 |
| 26 | 37244 | 36807 | 437 | 0·66 | 0·66 | 0·38 | 1·09 | 1·09 | 0·63 | 1·53 | 1·53 | 0·88 | 0·38 | 1·53 | 0·86 |
| 27 | 38702 | 37645 | 1057 | 1·59 | 1·59 | 0·92 | 2·64 | 2·64 | 1·53 | 3·70 | 3·70 | 2·14 | 0·92 | 3·70 | 2·08 |
| 28 | 46501 | 45699 | 802 | 1·20 | 1·20 | 0·69 | 2·01 | 2·01 | 1·16 | 2·81 | 2·81 | 1·62 | 0·69 | 2·81 | 1·58 |
| 29 | 46705 | 43294 | 3411 | 5·12 | 5·12 | 2·95 | 8·53 | 8·53 | 4·92 | 11·94 | 11·94 | 6·89 | 2·95 | 11·94 | 6·73 |
| 30 | 63498 | 61530 | 1968 | 2·95 | 2·95 | 1·70 | 4·92 | 4·92 | 2·84 | 6·89 | 6·89 | 3·98 | 1·70 | 6·89 | 3·88 |

good agreement (Fig. 13). The distribution of the size of the 222 PGM observed on the BSE images is similar to that calculated from the average laser ablation data (Table B1 and Fig. 13). This implies that the inclusions hit during the laser ablation of the BMS are micron scale in size and are not <100 nm (Ballhaus & Sylvester, 2000).